POLITECNICO DI MILANO

School of Industrial and Information Engineering

Master of Science in Automation and Control Engineering

PREDICTIVE CONTROL SCHEMES FOR FIRE-TUBE STEAM GENERATORS

Supervisor: Prof. Marcello Farina

Co-supervisor: Ing. Stefano Spinelli

Candidate:

Elia Longoni Ident. 899275

Academic Year 2018/2019

CONTENTS

SOMMARIO

La presente tesi tratta problemi di controllo relativi a sistemi di produzione e accumulo di vapore. Sono presentati i modelli matematici di boiler di tipo fire-tube e di accumulatori i cui parametri vengono poi identificati prendendo in considerazione dati estratti da un sistema reale.

Nell'elaborato sono illustrati due diversi schemi di controllo.

Il primo, basato sul controllo predittivo basato su modello (MPC), tratta la regolazione di un sistema composto da un boiler e un accumulatore.

La particolarità di questo sistema è la sua composizione "ibrida". I modelli impiegati per la regolazione e la simulazione sono derivati utilizzando metodi di identificazione differenti:

- il modello del boiler è basato su equazioni fisiche;
- il modello dell'accumulatore è basato su una rete neurale ricorsiva Long Short Term Memory (LSTM). Il motivo di questa scelta è legato al fatto che i modelli di letteratura degli accumulatori risultano essere inadeguati a descrivere con accuratezza l'evoluzione dei dati a disposizione.

L'implementazione dello schema di controllo viene proposta con una tecnica di linearizzazione del sistema lungo le traiettorie degli stati.

Il secondo schema proposto si basa su un'architettura gerarchica e viene impiegato nell'ottimizzazione e nel controllo di un sistema composto da un insieme di boiler che lavorano in parallelo per il raggiungimento di un obiettivo comune. Tale struttura gerarchica è composta da tre livelli:

- alto livello, basato su un ottimizzatore statico, con ha il compito di ripartire la produzione tra i vari componenti dell'insieme;
- medio livello, fondato su schemi di controllo avanzati di tipo MPC, con ha il compito di permettere al sistema di seguire un riferimento tempo variante usando un modello aggregato e centralizzato, il cui ordine non si ridimensiona al variare del numero di sottosistemi;
- basso livello, basato su controllori di tipo Proporzionale/Integrale (PI) decentralizzati, con il compito di stabilizzare la pressione interna dei boiler.

Infine, vengono presentati i risultati delle simulazioni dei due schemi di controllo, eseguite in ambiente MATLAB, per poterne poi valutare prestazioni e potenzialità.

ABSTRACT

This thesis deals with control problems related to steam production units.

Mathematical models of fire-tube boilers and steam accumulators are first presented, whose parameters are then identified using available experimental data.

In this work, two different control schemes are presented.

The first one, based on model predictive control (MPC) deals with the regulation of a system composed of a boiler and an accumulator. The peculiarity of this system is its "hybrid" composition. Indeed, the models used for regulation and simulation are derived using different identification procedures:

- the boiler model is based on the physics of the system;
- the accumulator model is based on a recursive Long Short Term Memory (LSTM) neural network. The reason behind this choice lies in the fact that literature physical-based accumulator models turn out to be not consistent with the available experimental data.

The implementation of the control scheme is proposed with a system linearization along the state trajectories technique.

The second scheme proposed in this thesis is based on a hierarchical architecture and deals with the optimization and control of a system composed of an ensemble of boiler steam generators, which need to sustain jointly a common load. The hierarchical structure is composed of three levels:

- the high-level, based on a static optimizer, computes the optimal shares of production to be allocated to single generators;
- the medium level, based on MPC advanced control schemes, tracks the time-varying demand of the ensemble using a centralized, but aggregate, model, whose order does not scale with the number of subsystems;
- the low level, based on Proportional/Integral (PI) decentralized controllers, regulates the internal pressure of the boilers.

Finally, we present simulation results obtained applying the two control schemes. Simulation tests are obtained in the MATLAB environment. We conclude with the discussion about the performances and the potentiality of the proposed algorithms.

CHAPTER 1

INTRODUCTION

There are three principal forms of energy used in industrial processes: electricity, direct-fired heat, and steam [10, 11]. Electricity is used in many different ways, including mechanical drive, heating, and electrochemical reactions. Direct-fired energy directly transfers the heat of fuel combustion to a process. Steam provides process heating, pressure control, mechanical drive, and component separation, and is a source of water for many process reactions. Steam has many performance advantages that make it an indispensable means of delivering energy. These advantages include low toxicity, ease of transportability, high efficiency, high heat capacity, and low cost with respect to the other alternatives. Since most of the heat content of steam is stored as latent heat, large quantities of heat can be transferred efficiently at a constant temperature, which is a useful attribute in many process heating applications. Steam is generated in a boiler by transferring the heat of combustion gases to water. When water absorbs enough heat, it changes phase from liquid to steam. The distribution system carries steam from the boiler or generator to the points of end-use. Many distribution systems have several take-off lines that operate at different pressures. A properly performing distribution system delivers sufficient quantities of high-quality steam at the right pressures and temperatures to the end uses. Effective distribution system performance requires proper steam pressure balance, complete and optimum insulation, and effective pressure regulation.

The problem discussed in this thesis derived from the European project *Symbioptima*, which aims to improve the process industry efficiency, productivity, service level, and safety while cutting costs, using math-optimization, algorithms, artificial intelligence, and predictive analytics [12].

In this thesis, we discuss steam production systems. We present the model of the fire tube boiler steam generator [4] and the model of a steam accumulator [6, 8]. Boiler and accumulator are widely used together to increase the steam production system efficiency. The derivation and the identification procedure done on these models are based on real plant data. The data provided by sensors are collected by a software, produced in the framework of the *Symbioptima* project, in Excel files.

The first proposed control scheme is a Model Predictive Control (MPC) based scheme to control a system composed of a boiler steam generator and a steam accumulator that work together to supply the user steam demands. The boiler model is identified and linearized from the mathematical equations, while the accumulator one is built using successive linearization of a Long Short Term Memory neural network [13, 14]. The pressure regulation is the main goal of this control scheme. The main advantage of this control scheme is that the controller simultaneously regulates the boiler and the accumulator steam production, maintaining the pressure of the two components within their limits, minimizing the gas consumption and so the production costs.

The second proposed control scheme is a hierarchical scheme for the optimal management of an ensemble of boiler steam generators [1, 3], which need to sustain jointly a common load. The coordination of independent subsystems is provided by a multi-layer control scheme. We have chosen the hierarchical method because it is considered as the best choice for optimal supervision and coordination of the system ensembles. A high-level optimizer computes the optimal shares of production to be allocated to single boilers. At medium level, a robust tube-based MPC is proposed to track the time-varying demand of the ensemble. At low level, decentralized controllers are in place to stabilize the internal boiler pressure.

The thesis is structured as follows:

- *Chapter 2:* we discuss more in detail about steam, its production, and its application. Then, we present the real plant and we describe its components. At the end of the chapter we discuss the available plant data;
- *Chapter 3:* we discuss the boiler and accumulator models, their validation, and the identification procedure;
- *Chapter 4:* we present a theoretical overview of the MPC control algorithms, then we discuss its implementation to control the boiler and accumulator system;
- *Chapter 5:* we show the simulation results related to the control scheme presented in *Chapter 4*;
- *Chapter 6:* we present a theoretical overview of the hierarchical control scheme, then we discuss its implementation for the control of the boiler ensemble;
- *Chapter 7:* we show the simulation results related to the control scheme presented in *Chapter 6;*
- *Chapter 8:* we discuss some conclusions on the presented work;
- *Appendix 1:* we present a short description of the Matlab thermodynamics library used;
- *Appendix 2:* we describe some advanced control schemes used in *Chapter 6;*

CHAPTER 2

STEAM PRODUCTION SYSTEMS AND PLANT DESCRIPTION

2.1 - STEAM

Today, steam systems are part of almost every major industrial process. All major industrial energy users devote significant proportions of their fossil fuels consumption to steam production: food processing (57%), pulp and paper (81%), chemicals (42%), petroleum refining (23%).

Steam is one of the most widely used carriers for transporting energy. From the energy point of view producing steam is economical and efficient. Steam easily transfers its thermal energy to processes. Its temperature is strongly related to its pressure; larger is the pressure, larger the temperature. This property is important because controlling the steam pressure is easy so that it is possible to control the amount of energy transferred to industrial processes. Steam generators, that produce steam, are compact and efficient and can work with a wide variety of fuels.

Boilers dating back in the XVIII century were simple metal containers placed over a charcoal external flame. The smoking pipe system began to be used at the beginning of the XIX century. Thanks to that, boilers became more efficient, because the hot fumes help to heat water. Nevertheless, the system was quite dangerous because there was a large risk of explosion caused by the water large pressure reached inside. In 1867 Babcock and Wilcox created the water pipe boiler. They increased the heat exchange surface so that they could increase the efficiency and, at the same time, avoid the explosion risk. The boilers' evolution continued during the XX century boosted by the evolution of fossil fuels.

Nowadays, steam is used in many different areas. It is widely used to transfer heat from a place to another, as for example in buildings, where steam is used for heating. The steam production systems used for heating are generally composed of:

- a boiler partially filled with water;
- steam outlet tubes that start from the boiler;
- condensate water tubes that return to the boiler;
- a series of radiating plates connecting the steam tubes and the condensate heater tubes.

This is a closed system. The void is created in this kind of system, by extracting air. As soon as the boiler is on, steam formation starts, which is possible even at low temperatures in the void environment. Then steam goes in the tubes and transfers heat to the radiating plates that transfer heat to the environment. Finally, steam condensates and the water returns to the boiler by gravity.

Steam is also widely used in industrial processes [15], as for example heating source for process fluid heat exchangers, where steam raises the temperature of the product by heat transfer. Boilers that are used for these applications have two fluids at different starting temperatures. One flows through the tubes and the other flows outside the tubes but inside the shell. Heat is transferred from one fluid to the other through the tube walls. After heating the fluid inside the tubes, steam condensates and it is discharged through a steam trap. Heat exchangers are used as components of air conditioning and cooling systems or for heating systems. Within industrial plants and factories, heat exchangers are required to keep machinery, chemicals, water gas, and other substances within a safe operating temperature. They may also be used to capture and transfer steam or heat exhaust, that is released for example by combustion processes, so that the steam or heat can be put to better use elsewhere, thereby increasing plant efficiency.

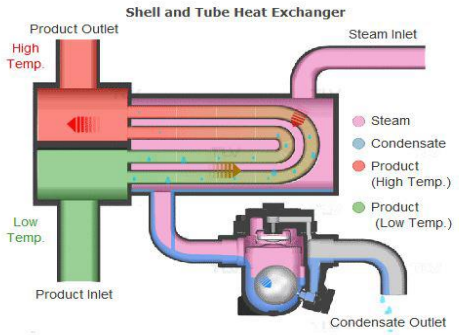

Figure 2.1 – Steam heat exchanger scheme [15]

Large pressure saturated steam can also be used in steam turbines, used for generating electricity in thermal electric power plants. High pressures and temperatures allow to increase the plant efficiency. Superheated steam is used in steam turbines to prevent damage to equipment caused by the inflow of condensate. The driving steam force causes the fins to turn, which causes the rotation of the rotor of the power generator creating electricity. Worldwide, the major part of electric power is produced by steam electric power plants. For example, in the United States, about 80% of the all-electrical production is made using steam turbines. Besides electric power, other typical propulsion applications are turbine-driven compressors or pumps, gas compressors, cooling towers pump, etc.

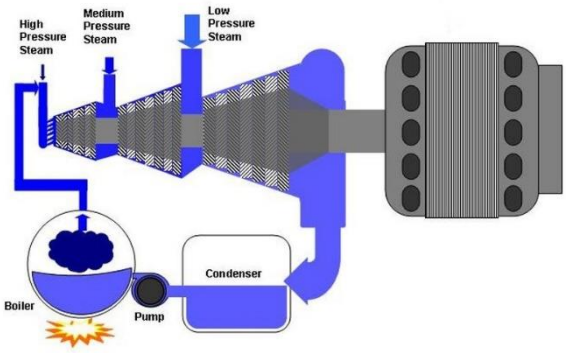

Figure 2.2 – Steam turbine scheme [15]

Steam is also used in atomization processes, where steam is used to mechanically separate a fluid. In some burners, steam is injected into the fuel in order to maximize combustion efficiency and minimize the production of hydrocarbons.

We can also find steam in the food industry and in many activities related to food and beverage processing. In fact, it is used for cooking, drying, warming, cleaning, and sterilization.

2.2 – STEAM PRODUCTION

Nowadays there are many ways to produce steam and many boiler types, depending on one's needs. Steam generators are used wherever a source of steam is required. Shape and size depend on the application. For example, mobile steam engines such as steam locomotives, usually use a smaller boiler integrated in the vehicle. On the other hand, stationary steam engines, as industrial installations and power stations, usually have larger separate steam-generating facilities connected to the point of use by piping. Boilers can be classified into two categories:

- shell boilers;
- once-through boilers.

2.2.1 - SHELL BOILERS

Shell boilers are those in which the heat transfer surfaces are all contained within a steel shell [16]. Shell boilers are also known as fire tube boilers or smoke tube boilers because the hot gases produced by combustion pass through the boilers' tubes transferring heat to the boilers' water. Several different combinations of tube layouts are used in shell boilers, characterized by the number of passes taken by the heat before being discharged. Considering, for example, a two-pass boiler configuration, there exist two new configuration types: a Dry back reversal chamber and a Wet back reversal chamber.

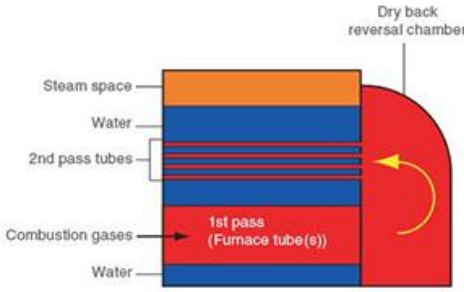

Figure 2.3 – Shell boiler – Dry Back configuration [16]

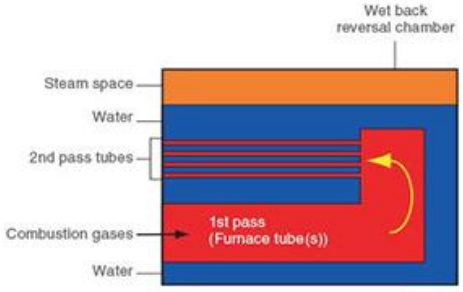

Figure 2.4 – Shell boiler – Wet back configuration [16]

In *Figure* 2.3 in the dry back boiler, the hot gases are reversed by a refractory-lined chamber on the outer planting of the boiler. In *Figure* 2.4 we can see a more efficient method of reversing the hot gases through a wet back boiler configuration. Here the reverse chamber is contained entirely within the boiler. This allows for a greater heat transfer area.

Over the years, many boiler configurations were designed. The economic boilers configurations are the two-pass dry back, the three-pass wet back, and four-pass. Three-pass wet back is considered the standard configuration used today. Four-pass boilers are potentially the most efficient, even if they are subject to higher thermal stresses. In addition, they tend to have low efficiency at low demand operating conditions. For these reasons, four-pass boilers are unusual.

A conventional boiler design variation is the reverse flame (or thimble boiler) shown in *Figure* 2.5. This boiler is limited in both evaporative capacity and its maximum temperature.

This type of boiler is not generally used as a primary steam power generator but as an auxiliary boiler.

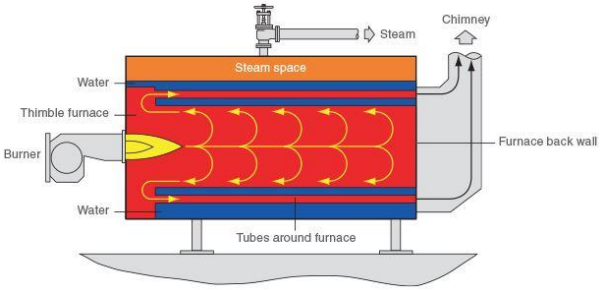

Figure 2.5 – Thimble boiler [16]

2.2.2 - ONCE-THROUGH BOILERS

Once-through boilers have tubes in which water is introduced at the bottom, while steam is produced from the top [16, 18]. They are used for steam production in connection with utility electricity production and they have been the most popular design in Europe for many years.

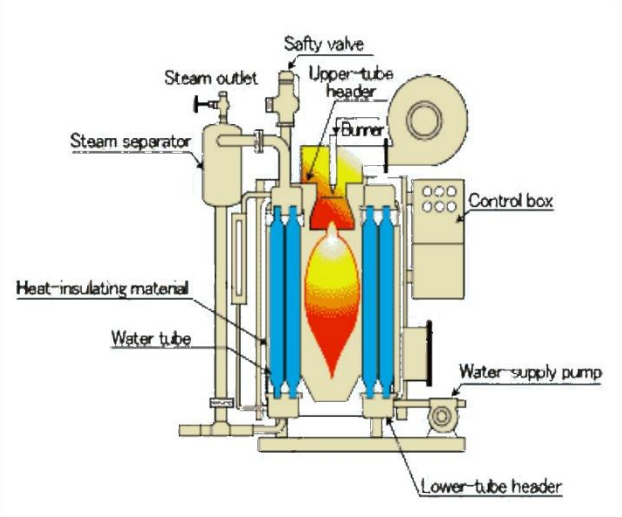

Figure 2.6 – Once through boiler [20]

Once-through boilers incorporate spirally shaped evaporator tubes to form the furnace envelope. Once-through boilers are generally associated with high-pressure operation. Large scale powerplant type once-through boilers normally have 100% conversion of water to steam before it comes out of the boilers. Furnaces may be fired in three ways. Firstly, they can have burners mounted in the front wall. Secondly, they can be fired by opposed firing with burners, normally, in the front and rear walls. Finally, furnaces can be fired by tangential firing achieved by slot-burners mounted in the corners creating a circulating flow, with the advantage of suppressing pollutant formation. Because the water is evaporated to high-quality steam, it is essential to protect the boiler against dryout occurring in high heat flux zones or taking other precautions against burnout. A solution to this problem can be the use rifled-bore tubing. Rifled-bore tubing creates centrifugal forces which allow the liquid phase to mostly remain in contact with the tube wall.

2.3 – PROJECT AND PLANT DESCRIPTION

This thesis project stems from and is inspired by the research carried out in the framework of the European project Symbioptima. The Symbioptima project promotes the interaction of different industries a resource-efficient production at the network level and for a reduction of the adverse environmental impact. This can be made possible thanks to a dynamical optimal management at large-scale, sharing common resources through the coordination of distributed optimization-based controllers.

One of the benchmark case studies of Symbioptima consists of the system depicted in *Figure 2.*8 and whose scheme can be found in *Figure 2.9.* In order to generate steam, in such plant, there are boilers working at different pressure and steam accumulators. The plant's goals are:

1) provide steam at 10 and 60 bar for building heating and for other final users;
2) provide electricity to the premises.

Figure 2.8 – Real plant system

As discussed, the function of the boilers is to heat water and transform it into steam, using heat produced by a burner. There is a dedicated boiler for each level of steam pressure. The role of the accumulators is to store high enthalpy water and convert it into steam helping boilers to reach steam production goals.

Combined Heat and Power (CHP) is another important component of the system. It is composed of a gas engine used for electricity production.

A flow scheme of the connected components in the plant can be:

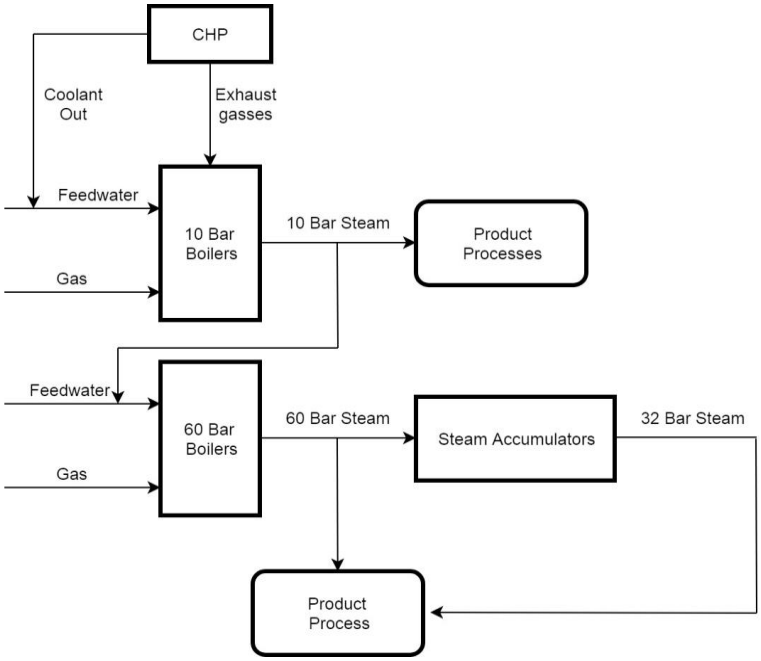

Figure 2.9 – General operating flow scheme

In this work, we consider a particular subsystem composed of 60 bar boilers and steam accumulators. This because in a preceding study the subsystem composed of the CHP and of the 10-bar boiler has been detailed analyzed [2].

In the following sections, a description of all single components of the overall plant will be made, giving also a general description of how they work. Then in the following chapter, only 60-bar boiler and the accumulator will be taken into account

2.4 - 10 BAR BOILERS

The used 10 Bar boilers considered in the Symbioptima project, are Danstoker OPTI shell/tube high-pressure steam boilers with a nominal production rate of 12000 kg/h of saturated steam at 180°C.

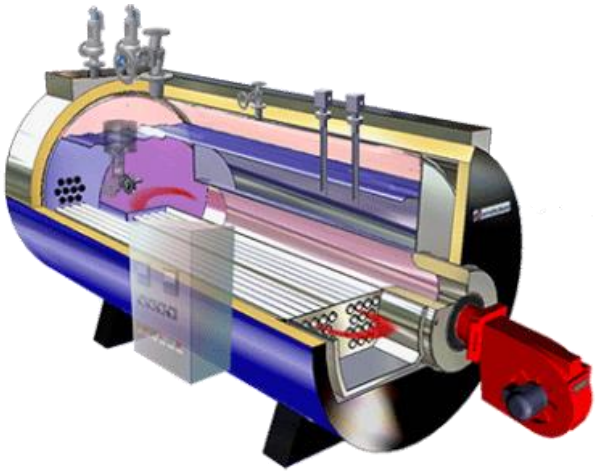

Figure 2.10 - 10 Bar Boiler [21]

The OPTI fire tubes boiler has a 3 – pass wet back design as shown in a schematic way in *Figure* 2.11. The main feature of this design is a reversal chamber that is within the boilers. The reversal chamber is used to direct flue gases from the furnace to the tubes. This system helps heating water and improve efficiency. The tubes are surrounded by water that absorbs burner heat. They are thin and made of metal. Thanks to that, more tubes can be accommodated, a higher heat transfer rate is achievable, and a more compact boilers design can be done.

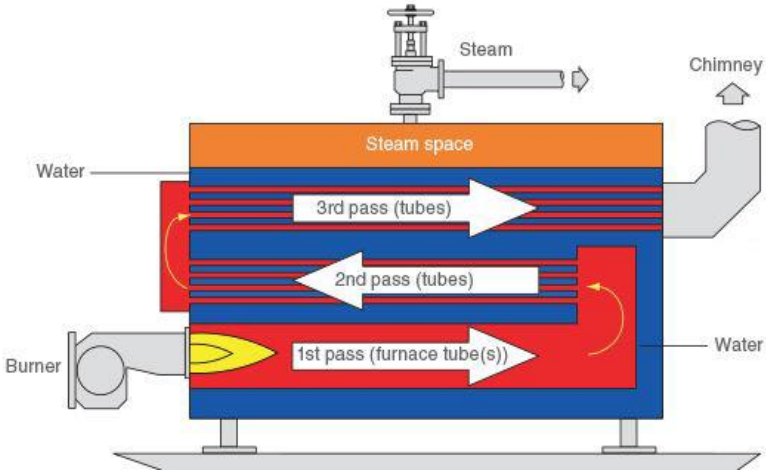

Figure 2.11 – OPTI 3-pass wet back design scheme [16]

In our study plant, we have a Combined Heat and Power (CHP) that is connected to the electric grid. The exhaust gases produced by the CHP are used to help heating the boilers' water. The feedwater is preheated thanks to the heat removed from the CHP by its cooling liquid. This allows achieving higher performance with less power consumption.

2.5 - COMBINED HEAT POWER

Combined heat power systems are heat engines used for the cogeneration of electric and thermal energy. They are engines where the hot water and the hot exhaust gasses are recovered. Using this type of recovery, it is possible to reduce the cost and increase the overall efficiency of used fuel with respect to the separated production of the same amount of electric and thermal energy.

The CHP considered in the Symbioptima project is a TCG 2020 from MWM. It is a high-efficiency gas engine producing 1200kW of electric power at 400V and 50 Hz.

Figure 2.12 – CHP TCG 2020 [24]

It is connected to the electric power grid and its goal is to follow the plant electricity demand. The exhaust gasses of this engine flow inside the 10 Bar boiler helping heating water and so the efficiency of steam production. The water used in the cooling system removes heat from the CHP and then is used to fill the 10 Bar boiler. This also allows to reduce the gas consumption to heat water.

2.6 - 60 BAR BOILER

The 60 Bar boilers considered in this study, are Babcock Wanson coil steam generator Series VPX RR with a nominal production of 5000 kg/h. VPX steam generators are completely packaged coil type once-through forced circulation units. The water is forced by a pump in a helicoidal tube that is the heat transfer surface.

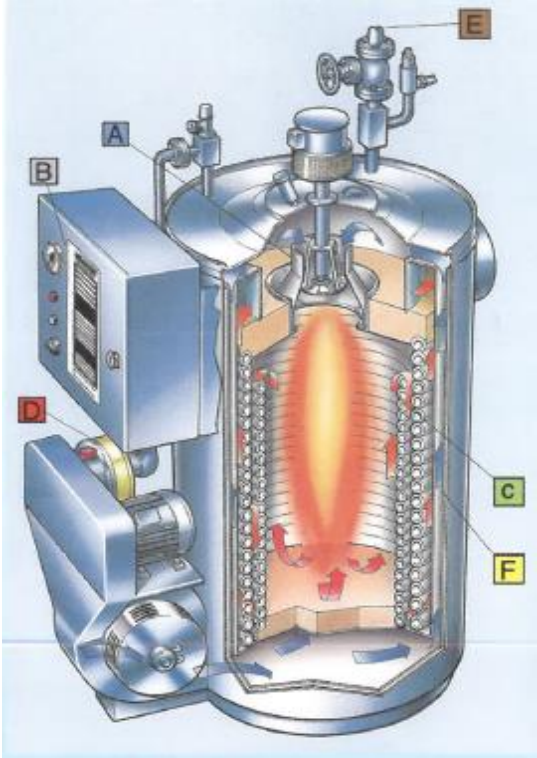

Figure 2.13 - 60 Bar Coil Boiler [22]

Figure 2.12 shows different boiler components:

A) Burner: in the center of the boiler the flame burns, while the coils are placed around the burner.
B) Control cabinet: it contains all electrical and electronic operating equipment for safe automatic operation.
C) Tubular coil construction: it provides high-pressure safety heating surface in compact dimensions. This configuration allows optimal efficiency because of high-velocity convection gas across the heating surface.
D) Feedwater pump.
E) Steam outlet.
F) Thermal insulation.

Boilers with this structure are safer than conventional boiler because the risk of pressure explosion is removed since water and steam flow into thin metal tubes. Another important feature of this design is the reduction of heat losses. This reduction is obtained by minimizing steam distribution and condensate return pipework, which allows for reducing the operating costs. Another important feature of this type of boilers is the use of exhaust gasses produced during the combustion to help heating the helicoidal tubes.
In our study plant, these boilers feed the 60 Bar steam line and the second steam line at 32 bar which is connected to accumulators. They are fed by a 60 bar preheated hot well water by using part of the steam flow from 10 bar boilers.

2.7 - STEAM ACCUMULATOR

Steam accumulators are used in industry and power plants to adjust the differences between steam production and consumption rates. They are applied as buffers between steam generators and consumers. The inputs of steam accumulators are water and steam.

The steam accumulator is:

- charged in periods of lower steam consumption or surplus production, so that the pressure in the accumulator increases and the steam condenses;
- discharged in periods of increased steam consumption (due to the consumers' request) that are not covered with the normal production rate. During the discharging process, the pressure decreases, and the water evaporates.

Steam accumulators, when associated with steam generators, can guarantee better performance and minimum operating costs. In fact, without a steam accumulator, the steam generator must operate at higher power to guarantee large consumption requests. On the other hand, in periods with lower request, the excess steam is discharged since the steam generator usually cannot follow rapid dynamic power changes.

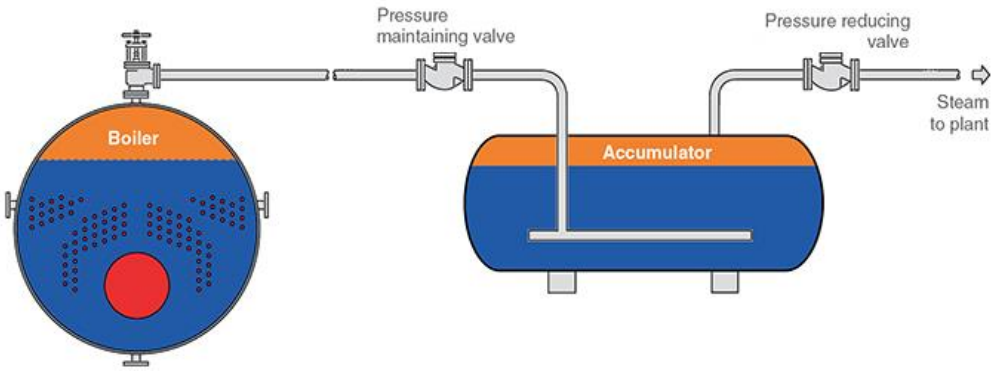

Figure 2.14 – Boiler and steam accumulator general scheme [23]

In our study plant, the accumulator is meant to provide extra capacity when the demand exceeds the boiler maximum continuous rating. That is made, filling the accumulator with saturated steam at boiler pressure. When the boiler cannot cope with the demand, the accumulator pressure starts dropping. The excess energy is released in the form of flashed steam as a result of the pressure reduction. In this way, generating extra steam capacity on top of the incoming steam supply from the boiler. The pressure in the accumulator is allowed to drop only to 36 bar. Then when the excess demand is cut off, the accumulator is allowed to recover its nominal operating pressure, which is about 60 bar.

2.8 – AVAILABLE PLANT DATA

One of the tasks of the Symbioptima project (carried out by other research partners) was also to develop a software tool that collects data from the plant. To achieve this goal, various sensors were mounted on the system. An improvement and an upgrade of these sensors over time have improved data quality. Sensors in the plant collect data regarding most of the physical quantities of the processes. The data are then organized in Excel files, each representing the system operating on a specific day or more days. Sensors are positioned according to the simplified scheme as for as the 60-bar boiler and the accumulator reported in *Figure* 2.15.

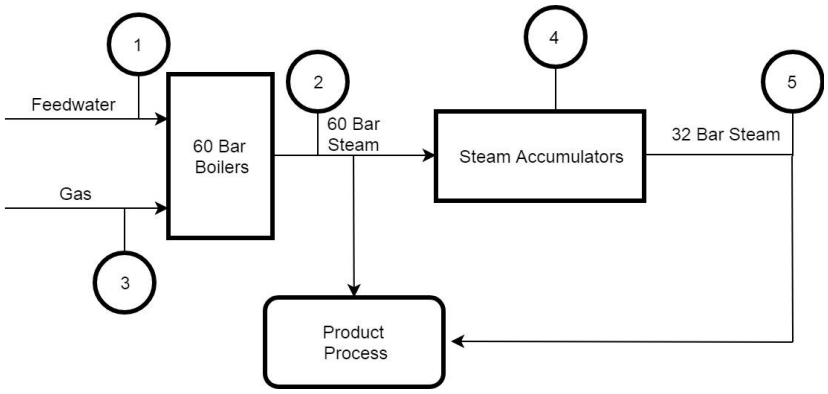

Figure 2.15 – General sensor position scheme

Sensors or multiple sensors, in different locations of the plant, are represented as circles. Note, however, that the exact position of the sensor on the system plants is unknown.

The sensors on this system are listed in *Table 2.1.* They are classified according to their location (from 1 to 5). There will be also information about what they are measuring and what is their basic sampling time.

Sensor position	Physical quantity	Unit of measurement	Sampling Time [s]
1	Boiler inlet water mass flow rate	kg/h	60
1	Boiler inlet water temperature	°C	60
2	Steam mass flow rate in the tube	kg/h	60
2	Steam temperature in the tube	°C	60
2	Steam pressure in the tube	Bar	60
3	Boiler burner gas mass flow rate	kg/h	60
3	Boiler burner power	kW	60
4	Accumulator inflow steam flow rate	kg/h	3 to 8
4	Accumulator water level	%	10
5	Accumulator steam pressure	Bar	1 and 9
5	Accumulator outlet steam	kg/h	1 and 9

Table 2.1 – General sensor description

It is clear, from the list, that some sensors collect data in a somehow counterintuitive way. Sensors related to the accumulator should have a sampling time of 10 seconds but in the Excel files, the data are reported with two different sampling times.

On the other hand, boiler sensors have some inconsistencies due to a non-uniform sampling time (i.e. from time to time the sampling period is 61 seconds).

A selection of useful data is needed since the available Excel files are related to different plant operational periods. In this work data related to the system's start-up and shutdown periods were discarded because nominal operational conditions are mostly considered. A more accurate analysis of data sets allowed to identify some corrupted data and some unphysical data. Corrupted data are those in which physical fundamental data are missing due to one or more sensors malfunction. Unphysical data have non-physical behaviour due to a temporary or permanent sensor malfunction. For that reason, this kind of data was discarded.

CHAPTER 3

MODELLING, IDENTIFICATION AND VALIDATION

In this chapter, we discuss the 60-bar boiler and accumulator modelling phase. Then, we illustrate the system's parameters identification procedure. The last part of the chapter is devoted to the validation of the derived models with the selected parameters.

3.1 – NOTATION

In this section, we list the variables, subscripts, and superscripts used in this thesis.

The system variables are:

- V volume [m^3];
- p pressure [bar];
- l level [%];
- ρ specific density [kg/m^3];
- h specific enthalpy [kj/kg];
- T Temperature [K];
- m mass [kg];
- q flow rate [kg/s];
- Q heat flow rate [kW];
- C specific heat [kj/kgK];
- τ phase change relaxation time [s];
- r phase change latent heat [kj/kg]

The subscripts used for these variables are:

- s steam;
- w water;
- f feedwater;
- m metal;
- tot total system;
- e evaporation;
- c condensation.

The following sub-subscripts are also used:

- sat saturated;
- in input of the physical system;
- out output from the physical system.

Finally, superscripts are also employed, i.e.:

- B Boiler;
- T Steam tube;
- A Accumulator.

3.2– 60 BAR BOILER MODEL AND STEAM TUBE MODEL

In this section, we describe in detail the model of the 60-bar boiler and of the downstream steam tube. In *Figure 3.*1 a picture of a fire-tube 60-bar boiler is depicted, while in *Figure 3.2* we show the corresponding CAD drawing. These two images are taken from the Badcock Wanson UK steam generator series vpx datasheet.

Figure 3.1 – 3D view of the 60 Bar Boiler [22]

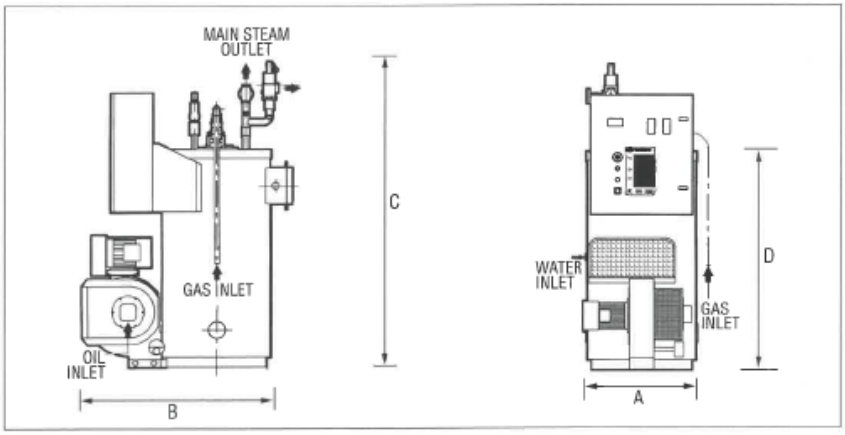

Figure 3.2 – 60 Bar boiler CAD drawing [22]

The plant boiler's geometrical data indicated in *Figure* 3.2 are listed in the following table.

A	2100	mm
B	2950	mm
C	4200	mm
D	3685	mm

Table 3.1 – Boiler geometrical data

The inputs of the systems are:

- Q^{B} the heat flow rate given by the burner to the boiler [kW];
- $q_{\mathrm{f}}^{\mathrm{B}}$ the feedwater mass flow rate [kg/s];

The output of the system is:

- p^{B} the steam pressure [bar].
- $q_{\mathrm{s}}^{\mathrm{B}}$ the outlet steam mass flow rate [kg/s].

The global mass and energy balance equations (that capture the main dynamics of the systems), are the starting point to model the 60 Bar boilers.

3.2.1 – 60 BAR MODEL DERIVATION

The global mass and energy balance equations regarded the boiler are the following [4]:

$$\frac{d}{dt}[\rho_{\mathrm{s}}^{\mathrm{B}} V_{\mathrm{s}}^{\mathrm{B}} + \rho_{\mathrm{w}}^{\mathrm{B}} V_{\mathrm{w}}^{\mathrm{B}}] = q_{\mathrm{f}}^{\mathrm{B}} - q_{\mathrm{s}}^{\mathrm{B}}$$

$$\frac{d}{dt}\left[\rho_{\mathrm{s}}^{\mathrm{B}} h_{\mathrm{s}}^{\mathrm{B}} V_{\mathrm{s}}^{\mathrm{B}} + \rho_{\mathrm{w}}^{\mathrm{B}} h_{\mathrm{w}}^{\mathrm{B}} V_{\mathrm{w}}^{\mathrm{B}} - p^{\mathrm{B}} V_{\mathrm{tot}}^{\mathrm{B}} + m_{\mathrm{tot}}^{\mathrm{B}} C_{\mathrm{p}}^{\mathrm{B}} T_{\mathrm{m}}^{\mathrm{B}}\right] = Q^{\mathrm{B}} + q_{\mathrm{f}}^{\mathrm{B}} h_{\mathrm{f}}^{\mathrm{B}} - q_{\mathrm{s}}^{\mathrm{B}} h_{\mathrm{s}}^{\mathrm{B}}$$

In steady-state conditions, the metal tube temperature is close to the steam saturation temperature. For this reason, the difference between the two is small, so that the metal temperature $T_{\mathrm{m}}^{\mathrm{B}}$ can be expressed as a function of the pressure.

To write the state model we choose as state variables:

- $p_{\mathrm{s}}^{\mathrm{B}}$ that is the pressure of the boiler's outlet steam;
- $V_{\mathrm{w}}^{\mathrm{B}}$ that is the total water volume in the boiler.

Choosing these state variables is convenient because, using the available thermodynamic table, it is possible to define the variables $\rho_{\mathrm{s}}^{\mathrm{B}}, \rho_{\mathrm{w}}^{\mathrm{B}}, h_{\mathrm{s}}^{\mathrm{B}}$, and $h_{\mathrm{w}}^{\mathrm{B}}$ as a function of the steam pressure. In this way we can write the following state equations:

$$e_{11}\frac{dV_{\mathrm{w}}^{\mathrm{B}}}{dt} + e_{12}\frac{dp^{\mathrm{B}}}{dt} = q_{\mathrm{f}}^{\mathrm{B}} - q_{\mathrm{s}}^{\mathrm{B}} \quad (3.1)$$

$$e_{21}\frac{dV_{\mathrm{w}}^{\mathrm{B}}}{dt} + e_{22}\frac{dp^{\mathrm{B}}}{dt} = Q^{\mathrm{B}} + q_{\mathrm{f}}^{\mathrm{B}} h_{\mathrm{f}}^{\mathrm{B}} - q_{\mathrm{s}}^{\mathrm{B}} h_{\mathrm{s}}^{\mathrm{B}} \quad (3.2)$$

where we have defined:

- $e_{11} = \rho_{\mathrm{w}}^{\mathrm{B}} - \rho_{\mathrm{s}}^{\mathrm{B}}$;
- $e_{12} = V_{\mathrm{s}}^{\mathrm{B}}\frac{\delta\rho_{\mathrm{s}}^{\mathrm{B}}}{\delta p^{\mathrm{B}}} + V_{\mathrm{w}}^{\mathrm{B}}\frac{\delta\rho_{\mathrm{w}}^{\mathrm{B}}}{\delta p^{\mathrm{B}}}$;
- $e_{21} = \rho_{\mathrm{w}}^{\mathrm{B}} h_{\mathrm{w}}^{\mathrm{B}} - \rho_{\mathrm{s}}^{\mathrm{B}} h_{\mathrm{s}}^{\mathrm{B}}$;
- $e_{22} = V_{\mathrm{s}}^{\mathrm{B}}\left(h_{\mathrm{s}}^{\mathrm{B}}\frac{\delta\rho_{\mathrm{s}}^{\mathrm{B}}}{\delta p^{\mathrm{B}}} + \rho_{\mathrm{s}}^{\mathrm{B}}\frac{\delta h_{\mathrm{s}}^{\mathrm{B}}}{\delta p^{\mathrm{B}}}\right) + V_{\mathrm{w}}^{\mathrm{B}}\left(h_{\mathrm{w}}^{\mathrm{B}}\frac{\delta\rho_{\mathrm{w}}^{\mathrm{B}}}{\delta p^{\mathrm{B}}} + \rho_{\mathrm{w}}^{\mathrm{B}}\frac{\delta h_{\mathrm{w}}^{\mathrm{B}}}{\delta p^{\mathrm{B}}}\right) - V_{\mathrm{tot}}^{\mathrm{B}} + m_{\mathrm{tot}}^{\mathrm{B}} C_{\mathrm{p}}^{\mathrm{B}}\frac{\delta T_{\mathrm{s}}^{\mathrm{B}}}{\delta p^{\mathrm{B}}}$.

With this set of equations, we can describe the behaviour of pressure changes in input power, feedwater flow rate, and steam flow rate.

We also need to define the efficiency factor of the burner η. This term will multiply the heat term Q, meaning that not all the burner generated heat is transferred to the water in the boiler metal tube.

3.2.2 - STEAM TUBE MODEL DERIVATION

In our system, the pressure sensor is positioned in a tube far from the boiler exit steam valve, as were shown in *Figure 2.9*. For this reason, we introduce other equations to model the steam flow in such a tube, so that we can consider the tube as a dynamical system after the boiler.

The following variables are used. It is worth mentioning that these data are available and will be used for model parameters identification.

- $p_{\mathrm{s}}^{\mathrm{T}}$ that is the pressure measured by the pressure sensor in the tube [bar];
- $q_{\mathrm{s}}^{\mathrm{T}}$ that is the steam flow rate in the tube [kg/s]. This value is measured with a sensor that is in the same position as the pressure sensor of $p_{\mathrm{s}}^{\mathrm{T}}$.

In our framework, the steam flow rate, q_s^{T} will be accounted for as an exogenous variable (i.e. a disturbance when not manipulable), while p_s^{T} will be accounted for a measured output.

We define two parameters A^{B} and A^{T}, that are i.e. the boiler outlet tube's area and the tube's area at the sensor position, respectively. It is possible to write the equation describing the tube pressure.

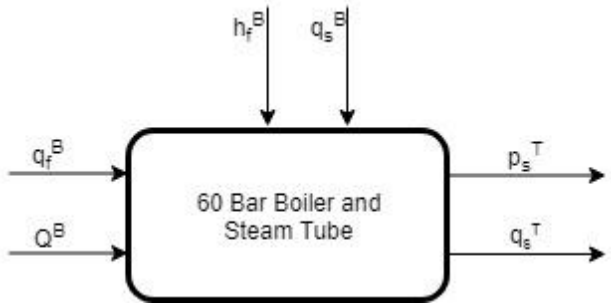

Figure 3.3 – Block diagram: boiler and steam tube

We write the Bernoulli Equations for the tube

$$\frac{q_s^{B2}}{\rho_s^{\mathrm{B}} A^{\mathrm{B}}} + p_s^{\mathrm{B}} = \frac{q_s^{\mathrm{B}2}}{\rho_s^{T} A^{\mathrm{T}}} + p_s^{\mathrm{T}}$$

From the mass balance equation in the tube

$$\frac{dM}{dt} = q_s^{\mathrm{B}} - q_s^{\mathrm{T}}$$

we can compute the steam boiler mass flow rate q_s^{B}

$$q_s^{\mathrm{B}} = V^T \frac{\delta \rho_s^{\mathrm{B}}}{\delta p_s^{\mathrm{B}}} \frac{dp_s^{\mathrm{B}}}{dt} + q_s^{\mathrm{T}} \quad (3.3)$$

where V is the volume of the tube.

Now from the Bernoulli equation, it is possible to write the equation of the pressure measured from the sensor

$$p_s^{\mathrm{T}} = p_s^{\mathrm{B}} + \frac{1}{2}\left(\frac{\left(q_s^{\mathrm{B}}\right)^2}{\rho_s^{\mathrm{B}}(A^{\mathrm{B}})^2}\right) - \frac{1}{2}\left(\frac{\left(q_s^{\mathrm{T}}\right)^2}{\rho_s^{\mathrm{T}}(A^{\mathrm{T}})^2}\right) \quad (3.4)$$

where ρ_s^{T} is the density of the steam at sensor level that can be expressed in function of the pressure p_s^{T} since the steam is saturated.

In this set of equations, we have geometrical parameters like $A_s^{\mathrm{B}}, A_s^{\mathrm{T}}$ and V^{T} that have to be identified. The identification procedure will be described in *Chapter 3.3.3.*

We now slightly modify our theoretical boiler model adding the new equation of the tube and the water $q_{w_{\mathrm{out}}}$ to achieve a better modelling description of our study plant.

3.2.3 – OVERALL MODEL OF THE BOILER AND THE TUBE

As a final step, we need to consider that a water outflow is present. This because the boiler feedwater is not totally converted into steam. This little portion of high enthalpy water must be added to the global mass balance. The reason for this is to have a more realistic model. So, we define the high enthalpy water outflow as the difference of the inlet feedwater and the outlet steam mass flow rate

$$q^{B}_{\mathrm{w_{out}}} = q^{\mathrm{B}}_{\mathrm{f}} - q^{\mathrm{T}}_{\mathrm{s}} \quad (3.5\ )$$

Under this reformulation, the equation (3.1) becomes:

$$e_{11}\frac{dV^{\mathrm{B}}_{\mathrm{w}}}{dt} + e_{12}\frac{dp^{\mathrm{B}}}{dt} = q^{\mathrm{B}}_{\mathrm{f}} - q^{\mathrm{B}}_{\mathrm{s}} - \left(q^{\mathrm{B}}_{\mathrm{f}} - q^{\mathrm{T}}_{\mathrm{s}}\right) \quad (3.6)$$

Replacing (3.6) into equation (3.2) we can compute that

$$e_{11}\frac{dV^{\mathrm{B}}_{\mathrm{w}}}{dt} + e_{12}\frac{dp^{\mathrm{B}}}{dt} = -V^{T}\frac{\delta\rho^{\mathrm{B}}_{\mathrm{s}}}{\delta p^{\mathrm{B}}_{\mathrm{s}}}\frac{dp^{\mathrm{B}}_{\mathrm{s}}}{dt} \quad (3.7)$$

Then, consider equation (3.2) and add the energy term related to the boiler outlet water. Defining h_{w} as its enthalpy, that is found using the thermodynamic water table in functions of the boiler pressure, the equation becomes:

$$e_{21}\frac{dV^{\mathrm{B}}_{\mathrm{w}}}{dt} + e_{22}\frac{dp^{\mathrm{B}}}{dt} = \eta Q^{\mathrm{B}} + q^{\mathrm{B}}_{\mathrm{f}}h^{\mathrm{B}}_{\mathrm{f}} - q^{\mathrm{T}}_{\mathrm{s}}h^{\mathrm{B}}_{\mathrm{s}} - \left(q^{\mathrm{B}}_{\mathrm{f}} - q^{\mathrm{T}}_{\mathrm{s}}\right)h^{\mathrm{B}}_{\mathrm{w}} \quad (3.8)$$

This concludes the boiler and steam tube model derivation.

Overall, the obtained set of equations reads:

$$\begin{cases} e_{11}\dfrac{dV^{\mathrm{B}}_{\mathrm{w}}}{dt} + e_{12}\dfrac{dp^{\mathrm{B}}}{dt} = -V^{T}\dfrac{\delta\rho^{\mathrm{B}}_{\mathrm{s}}}{\delta p^{\mathrm{B}}_{\mathrm{s}}}\dfrac{dp^{\mathrm{B}}_{\mathrm{s}}}{dt} \\ e_{21}\dfrac{dV^{\mathrm{B}}_{\mathrm{w}}}{dt} + e_{22}\dfrac{dp^{\mathrm{B}}}{dt} = \eta Q^{\mathrm{B}} + q^{\mathrm{B}}_{\mathrm{f}}h^{\mathrm{B}}_{\mathrm{f}} - q^{\mathrm{T}}_{\mathrm{s}}h^{\mathrm{B}}_{\mathrm{s}} - \left(q^{\mathrm{B}}_{\mathrm{f}} - q^{\mathrm{T}}_{\mathrm{s}}\right)h^{\mathrm{B}}_{\mathrm{w}} \end{cases} \quad (3.9)$$

It is worth finally recalling that:

- Q^{B} and $q^{\mathrm{B}}_{\mathrm{f}}$ are manipulable input variables;
- $q^{\mathrm{T}}_{\mathrm{s}}$ is a further exogenous variable. It is generally imposed and equal to the users' demand since it represents the steam flowing out of the tube. However, it may be possibly considered as a manipulable variable in case of need since it is controlled through a valve.
- p^{B} and $q^{\mathrm{B}}_{\mathrm{s}}$ are system outputs to be properly regulated at set-point values. The nominal values are, in the plant consider in this thesis, available to the control system. However, they are not available to us for model identification purposes.
- $p^{\mathrm{T}}_{\mathrm{s}}$, expressed as in (3.4), is a measured variable. Its values are currently available and will be used in *Chapter 3.3.3* for parameters tuning.

The validation of the 60 Bar theoretical model and of our modified model will be done in the *validation* sub-chapter.

The model is characterized by a number of parameters, some of which need to be identified or to be subject to fine-tuning.

The known parameter is:

- C^{T}: specific heat of the tube that we set to 0.5 kJ/kgK that correspond to iron steel;

while the ones that will be subject to tuning (in *Chapter 3.3.3)* are listed in the following table:

Name	Variable	Unit of measurement
V^{T}	Total steam tube volume	m^3
A^{B}	Area of the boiler outlet tube	m^2
A^{T}	Area of the steam tube where the sensor is positioned	m^2
m_{tot}	Total metal mass of the boiler	kg
V_{tot}	Total volume of the metal tube inside the boiler	m^3
η	Efficiency factor of the burner	

Table 3.2 – List of parameters to be identified

3.3 – BOILER MODEL VALIDATION AND PARAMETERS IDENTIFICATION

3.3.1 – MODEL VALIDATION WITH RESPECT TO LITERATURE DATA

In this section, we validate the 60 bar boiler presented in *Chapter 3.2* using literature data. For this validation, we consider the boiler parameters used in [4] that are reported in the following table.

Name	Variable	Value
$m_{\text{tot}}^{\text{B}}$	Total metal mass of the boiler	300 000 kg
$V_{\text{tot}}^{\text{B}}$	Total volume of the metal tube inside the boiler	88 m^3

Table 3.3 – Literature boiler parameters

We will do two different tests for the validation:

1) heat Q^{B} changes;
2) steam flow rate q_s^{B} changes.

We remind that here the assumption that the outlet steam mass flow rate is equal to the feedwater mass flow rate is done by [4].

HEAT CHANGES TEST

In this test, we set all the input variables to their steady-state values. At time instant $t = 50$ we do a step of $+10\%$ at the heat Q^{B}. Considering *Figure 3. 4,* we can see that the pressure increases at approximately constant rate because the steam flow remains constant.

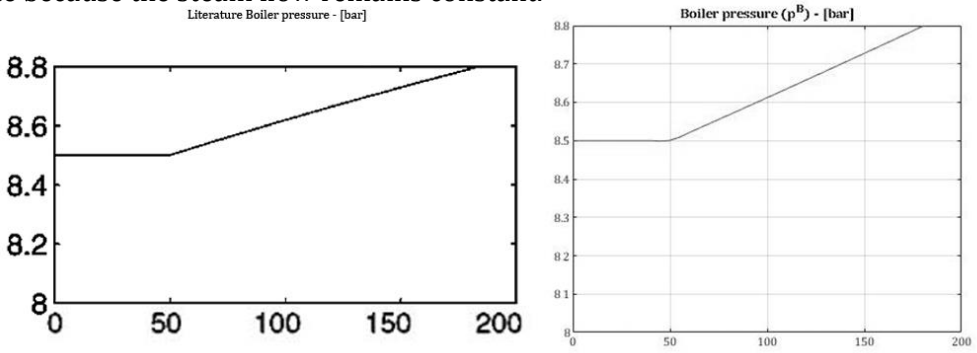

Figure 3.4 – Boiler pressure changes after a +10% heat step

STEAM FLOW RATE CHANGES TEST

For this test, we start setting all the input variables to their steady-state values. At time $t = 50$ we do a step of $+10\%$ at the outlet steam flow rate. For the assumption made at the beginning of this chapter, this is equal to make a step in the feedwater mass flow rate. Considering *Figure 3.5,* we can see that the pressure decreases practically linearly because of the increased steam flow rate.

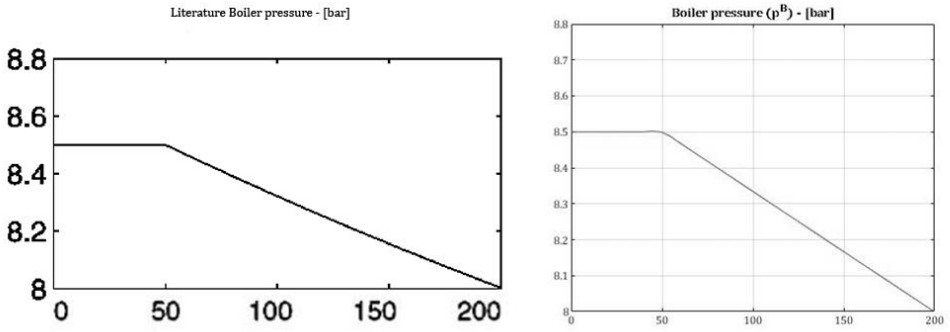

Figure 3.5 – Boiler pressure changes after a +10% feedwater step

3.3.2 – BOILER PARAMETERS AND DATA DESCRIPTION

In this sub-chapter, we will describe the available system data, how we have manipulated them and how they are employed to identify the boiler parameters.

The available data about the system are collected in Excel files. The ones used and they are used to perform simulations and identification procedures. They are summarized in *Table 3.4.*

Data name	Variable	Unit of measurement
p_s^{T}	Pressure measured by the sensor in the tube	Bar
T_f^{B}	Boiler feedwater temperature	°C
q_f^{B}	Boiler feedwater mass flow rate	kg/s
q_s^{T}	Steam mass flow rate in the tube	kg/s
Q^{B}	Burner heat	kW

Table 3.4 – Boiler available data

The boiler model parameters that must be identified are listed in the following table.

Name	Variable	Unit of measurement
V^{T}	Total steam tube volume	m^3
A^{B}	Area of the boiler outlet tube	m^2
A^{T}	Area of the steam tube where the sensor is positioned	m^2
$m_{\mathrm{tot}}^{\mathrm{B}}$	Total metal mass of the boiler	kg
$V_{\mathrm{tot}}^{\mathrm{B}}$	Total volume of the metal tube inside the boiler	m^3
η	Efficiency factor of the burner	

Table 3.5 – List of boiler parameters to be identified

To have a good reconstruction of the real system behaviour in simulation, it is essential to make an accurate choice of these parameters. These six parameters are constitutive of the system, so the main goal is to find the best combination of them that reconstruct in the best way all the real plant data set.

As mentioned in *Chapter* 2.8, since we don't have data about the evolution of the boiler state, we have to identify the initial condition of the boiler state as well. The boiler initial conditions are:

- $p_{s_0}^{B}$ that is the initial pressure of the boiler, measured in bar;
- V_{w_0} that is the initial water volume of the boiler, measured in m^3.

The initial condition of the boiler may be different for each data set since each Excel file is referred to different operating days of the system. For this reason, we identify the initial conditions independently for each data set.

To identify the model parameters, we have used 7 Excel files referring to operating days from January to April 2019. All the selected files have a similar operating condition. We are interested in the operating condition where the pressure in the tube is around 57 Bar. For this reason, all the data about the system's start-up and shutdown were discarded from the available data set.

For simplicity, only two sets of date sequence are shown as example in this chapter. More specifically, the used data set are:

- Boiler data of 18 February 2019 depicted in *Figure 3.6* with a sampling time $T_s = 10\ s$;
- Boiler data of 08 April 2019 depicted in *Figure 3.7* with a sampling time $T_s = 10\ s$.

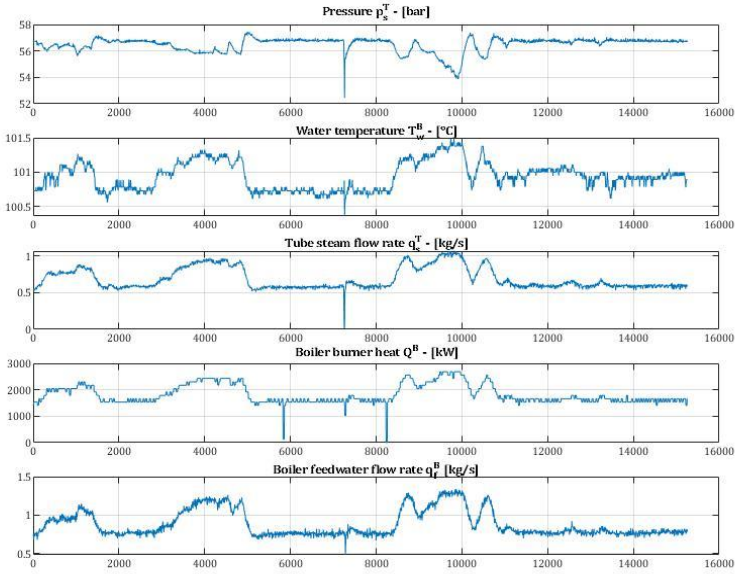

Figure 3.6 - Original signals of file 18 February 2019

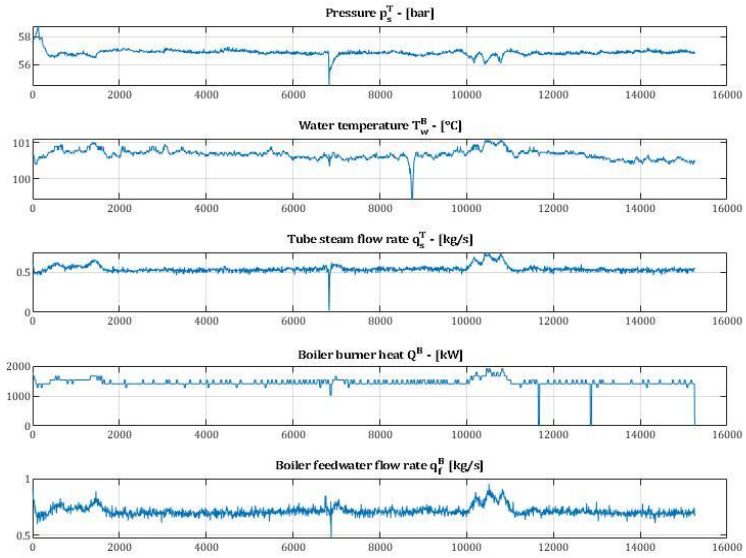

Figure 3.7 - Original signals of file 08 April 2019

The Excel files' original data have different sample times. So, we extracted and resampled all of them to have a more homogenous set of signals with the same new sampling time of 10 seconds. These signals are very noisy, especially the ones related to the mass flow rate. There are also fictitious changes on some signals that are not experienced by the system. For example, the drop (see *Figure 3.6)* in the heat signal to 0kW, at samples 7000, or (see *Figure 3.7)* at samples 12000 and 13000 in. These values are clearly related to missing signals. As such, we classified them as outliers, and we discarded them.

We filtered all the so obtained signals and we removed the outliers. In this way, smoother sets of signals were obtained, and this is pointed out for identification purposes. We decided also to reduce the number of samples of the data sets to have faster computational times. In order to achieve this goal, we have resampled the signals with a 5 minutes sampling time. The result of this filtering is shown in the following figures:

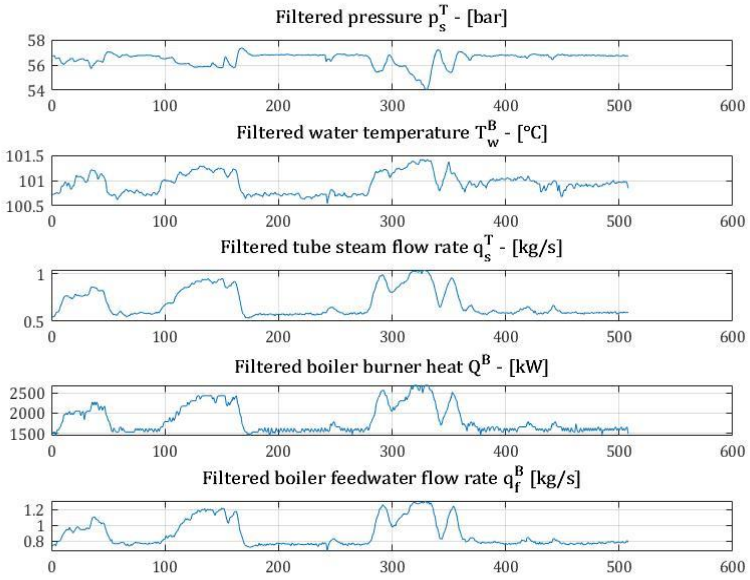

Figure 3.8 - Filtered signals 18 February 2019

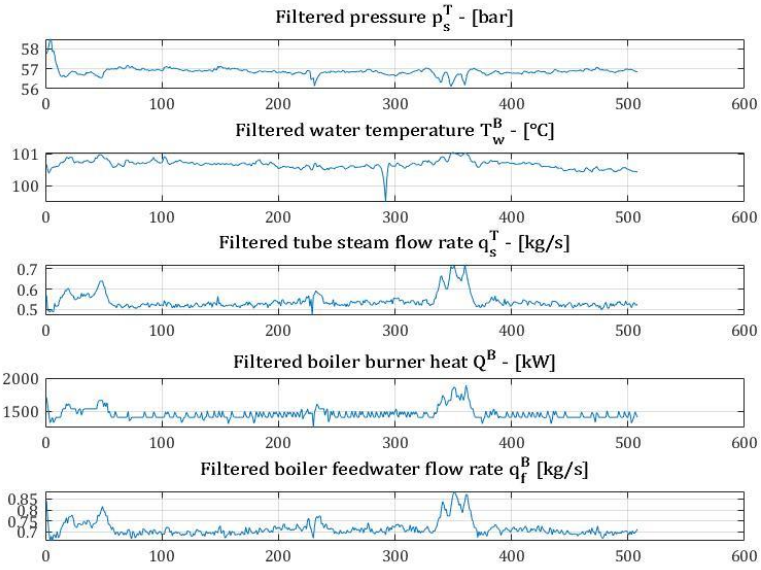

Figure 3.9 - Filtered signals 08 April 2019

The differences between the original and filtered signals are evident. We can, for example, look at *Figure* 3.8 (subplot 5), where the boiler feedwater signal is plotted. We can understand the global signal behaviour, but we can not use this signal for simulation or identification because is too noisy. After the filtering operation, showed in *Figure* 3.9 subplot 5, the signal is improved and displays a more realistic behaviour of what is happening in the real system.

3.3.3 – IDENTIFICATION PROCEDURE

The identification consists of finding the set of parameters that minimize a given objective function. The objective function is defined as the squared error between the pressure measured by the sensor p_s^T and the pressure $p_{s_{Sim}}^T$ obtained as result of the simulation.

The identification is done using a generic MATLAB solver. The used function is *fmincon* that is a nonlinear programming solver. This solver finds the minimum of constrained nonlinear multivariable function. Specifically, it finds the minimum of a problem specified by:

$$\min_x f(x) \text{ such that } Ax \leq b$$

where A is a matrix, b is a vector, $f(x)$ is a function that returns a scalar, and x is a vector.

The first step was the single identification of all the parameters for each file so that the objective function for the boiler file *i* is:

$$\min_{A^{\mathrm{B}},\beta,V^{\mathrm{T}},m^{\mathrm{B}}_{\mathrm{tot}},V^{\mathrm{B}}_{\mathrm{tot}},\eta,p^{\mathrm{B}}_{\mathrm{s}},V^{\mathrm{B}}_{w}} \quad J \quad (3.13)$$

The function *J* for each data set is:

$$J = \sum_{k=1}^{N} \left(p^{\mathrm{T}}_{\mathrm{s}}(k) \; - p^{\mathrm{T}}_{\mathrm{s_{Sim}}}(k) \right)^2$$

where we have that:

- N is the total number of sample points of the data set*;*
- $p^{\mathrm{T}}_{\mathrm{s_{sim}}}$ is the simulated pressure in the tube of the data set, described by the equations (3.5).

The constraints (all lower and upper limits) have been chosen considering the real system, to have the most precise and realistic parameters possible.

We have defined a set of constraint for all parameters:

Name	Variable	Constraint
A^B	Area of the boiler outlet tube	$0.0019 \leq A^{\mathrm{B}} \leq 0.096\ m^2$
β	$A^T = \beta A^{\mathrm{B}}$	$0.3 \leq \beta \leq 3$
V^{T}	Total steam tube volume	$0.0019 \leq V^T \leq 2.4\ m^3$
$m^{\mathrm{B}}_{\mathrm{tot}}$	Total metal mass of the boiler	$2e3 \leq m^{\mathrm{B}}_{\mathrm{tot}} \leq 5.5e3\ \ kg$
$V^{\mathrm{B}}_{\mathrm{tot}}$	Total volume of the metal tube inside the boiler	$0.1 \leq V^{\mathrm{B}}_{\mathrm{tot}} \leq 1.211\ m^3$
η	Efficiency factor of the burner	$0.01 \leq \eta \leq 0.99$
$p^{\mathrm{B}}_{\mathrm{s}}$	Initial pressure of boiler i	$55 \leq pressure_{boiler_i} \leq 61\ Bar$
V^{B}_{w}	Initial water volume of boiler i	$0.1 \leq V^{\mathrm{B}}_{\mathrm{w}_{0_i}} \leq 1.211\ m^3$

Table 3.6 – List of constraint of parameters to be identified

We show the results of this identification for our example data set in the following figures.

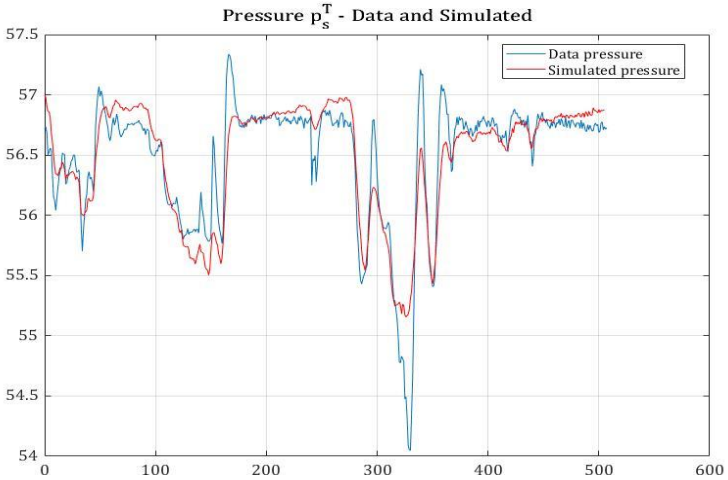

Figure 3.10 - Result of simulated pressure with respect to data for file 18 February 2019

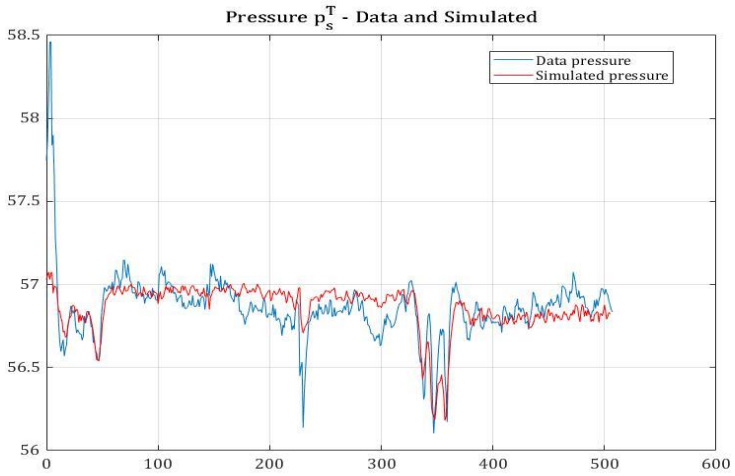

Figure 3.11 - Result of simulated pressure with respect to data for file 08 April 2019

The set of parameters identified for each example data set, reconstruct well the behaviour of the real system pressure. For the example files we are considering, the parameters are listed in the following table:

Name	Data set 18 February 2019	Data set 08 April 2019
A^B	0.0019635 m^2	0.002103 m^2
β	0.1455	0.1135
V^T	2.4052 m^3	2.4046 m^3
m_{tot}^B	5499.9956 kg	5498.9145 kg
V_{tot}^B	1.2109 m^3	1.2108 m^3
η	0.9699	0.9649
p_s^B	57.608 bar	57.7528 bar
V_w^B	1.1109 m^2	1.1106 m^2

Table 3.7 – Two example files' identified parameters

To evaluate and compare the quality of the identification, we compute the value of the objective function divided by the data variance. For this reason, we define parameter K as:

$$K = \frac{var\left(p_{s\ DATA}^T - p_{s\ SIM}^T\right)}{var\left(p_{s\ DATA}^T\right)}$$

For the 18 February 2019 data set we have $K = 0.212$ and for the 08 April 2019 data set we have $K = 0.615$.

At this point, we decided to make an arithmetic mean of all parameters identified from each data set to obtain a single value for each parameter listed in *Table 3.5*. This choice, although very simple, has been found to be more efficient than the solution of a further identification procedure with both data streams.

The new set of mean parameters is listed in *Table* 3.8.

Name	Mean parameters
A^B	0.002 m^2
β	0.1282
V^{T}	2.3345 m^3
$m_{\mathrm{tot}}^{\mathrm{B}}$	5029.2162 kg
$V_{\mathrm{tot}}^{\mathrm{B}}$	1.1618 m^3
η	0.9744

Table 3.8 – Mean parameters

the comparison between real and simulated data (with suitably identified initial conditions), considering the example data sets, are plotted in the following figures:

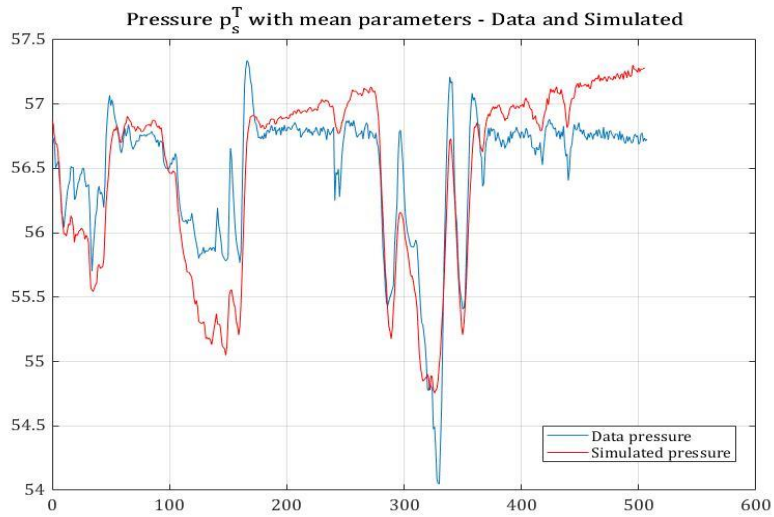

Figure 3.12 - Result of simulated pressure with mean parameters with respect to data for file 18 February 2019

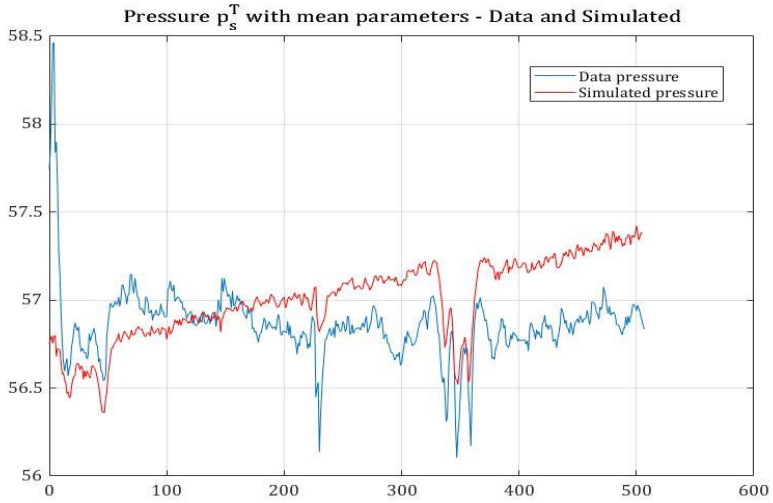

Figure 3.13 - Result of simulated pressure with mean parameters with respect to data for file 08 April 2019

These last results are, as expected, slightly worse than the previous ones because of parameters mean. Now the simulated pressure has a growing trend, but since the original data sets were very noisy, this final error is acceptable. We can also point out that the two example data sets have different variations peaks: the 18 February data set pressure varies from 54 to 57.4 bar, while the 08 April data set has a pressure that is almost constant, and it is between 56.3 to 57.2 bar. With these new parameters set we have a sub-optimal solution to each different data set.

In conclusion, with this set of parameters, we can reconstruct the behaviour of the pressure in the steam tube. We can say that the model of the boiler and the steam tube presented in C*hapter* 3.2 and described by equations (3.9) and (3.4) are validated for the real plant data sets since the error on the data is acceptable.

3.4 STEAM ACCUMULATOR MODEL

A detailed simulation model of a steam accumulator accounts for the dynamics of water and steam masses, water and steam temperatures and pressures [6, 8].

In the literature, models based on the assumption of thermal equilibrium between water and steam have been proposed. Basically, they assume that steam and water are at the same temperature and pressure, and that the evaporation and condensation are instantaneous. This could be a heavy limitation in control design.

In this work, we use a thermal non-equilibrium model that takes into account that water and steam could be at different temperatures and the evaporation and condensation rates are calculated separately. The aim of this model is to have more accurate predictions of the steam accumulator pressure, temperature, and water level during charging and discharging transients.

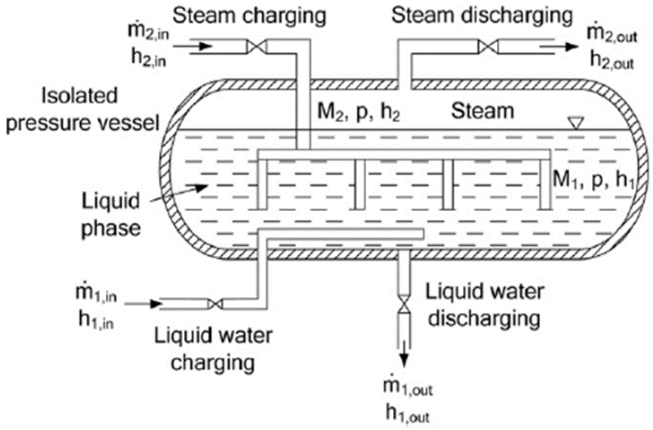

Figure 3.14 – Steam accumulator scheme [6,8]

To develop the model, we start from the mass and energy balance for water and steam. The evaporation and condensation rates are calculated with empirical correlations. The heat transfer rate from the steam to the water is calculated when steam is at a larger temperature than water. The resulting model is a set of five differential equations where the state variables are:

- p^{A} that is the accumulator pressure;
- $m_{\mathrm{w}}^{\mathrm{A}}$ that is the accumulator water mass;
- $m_{\mathrm{s}}^{\mathrm{A}}$ that is the accumulator steam mass;
- $h_{\mathrm{w}}^{\mathrm{A}}$ that is the accumulator water enthalpy;
- $h_{\mathrm{s}}^{\mathrm{A}}$ that is the accumulator steam enthalpy.

The accumulator inputs are:

- $p_{\mathrm{s}}^{\mathrm{T}}$ that is the steam pressure in the tube. This is an accumulator input because the tube starting from the boiler is connected to the accumulator;
- $q_{\mathrm{s}}^{\mathrm{T}}$ that is the steam mass flow rate in the tube.

The outputs are:

- $p_{\mathrm{s}}^{\mathrm{A}}$ that is the accumulator steam pressure;
- $q_{\mathrm{s}}^{\mathrm{A}}$ that is the accumulator outlet steam mass flow rate.

There are computations of derivatives of thermodynamic variables that were solved using the *IAPWS-IF97 MATLAB* library described in *Appendix 1.*

The model equations are:

- Liquid mass balance:

$$\frac{dM_{\mathrm{w}}^{\mathrm{A}}}{dt} = \left(q_{\mathrm{w_{in}}}^{\mathrm{A}} - q_{\mathrm{w_{out}}}^{\mathrm{A}}\right) + (q_{\mathrm{c}} - q_{\mathrm{e}}) \quad (3.14)$$

  where we denote:
  - $\left(q_{\mathrm{w_{in}}}^{\mathrm{A}} - q_{\mathrm{w_{out}}}^{\mathrm{A}}\right) = q_{\mathrm{w}}^{\mathrm{A}}$ the input-output water mass balance;
  - $(q_{\mathrm{c}} - q_{\mathrm{e}}) = q_{\mathrm{w_{ec}}}^{\mathrm{A}}$ the variation mass caused by the vaporization and condensation.

- Steam mass balance

$$\frac{dM_{\mathrm{s}}^{\mathrm{A}}}{dt} = \left(q_{\mathrm{s_{in}}}^{\mathrm{A}} - q_{\mathrm{s_{out}}}^{\mathrm{A}}\right) + (q_{\mathrm{e}} - q_{c}) \quad (3.15)$$

  where we denote:
  - $\left(q_{\mathrm{s_{in}}}^{\mathrm{A}} - q_{\mathrm{s_{out}}}^{\mathrm{A}}\right) = q_{\mathrm{s}}^{\mathrm{A}}$ the input-output steam mass balance;
  - $(q_{\mathrm{e}} - q_{c}) = q_{\mathrm{s_{ec}}}^{\mathrm{A}}$ the variation mass caused by the vaporization and condensation;
  - $q_{\mathrm{e}} = \frac{\left(\rho_{W}^{A} V_{W}^{A} (h_{W}^{A} - {}^{A}_{W_{sat}})\right)}{\tau_{e} r}$ the evaporation rate, that is zero if the water is saturated or subcooled, i.e. $h_{\mathrm{w}}^{\mathrm{A}} \leq h_{\mathrm{w_{sat}}}^{\mathrm{A}}$;
  - $q_{\mathrm{c}} = \frac{\left(\rho_{W}^{A} V_{W}^{A} (h_{W_{sat}}^{A} - h_{W}^{A})\right)}{\tau_{\mathrm{c}} r}$ the condensation rate, that is zero if the water is saturated or superheated, i.e. $h_{\mathrm{w}}^{\mathrm{A}} \geq h_{\mathrm{w_{sat}}}^{\mathrm{A}}$;
  - τ_{e} and τ_{c} the evaporation and condensation relaxation time.

- Liquid specific energy balance

$$\frac{dh_{W}^{A}}{dt} = \frac{1}{M_{W}^{A}} \left[(qh)_{\mathrm{w}} + q_{\mathrm{w_{ec}}}^{\mathrm{A}} h_{s_{sat}}^{A} + Q_{\mathrm{s}\rightarrow\mathrm{w}}^{\mathrm{A}} + M_{\mathrm{w}}^{\mathrm{A}} v_{\mathrm{w}}^{\mathrm{A}} \frac{dp^{\mathrm{A}}}{dt} - h_{\mathrm{w}}^{\mathrm{A}} \frac{dM_{\mathrm{w}}^{\mathrm{A}}}{dt} \right] \quad (3.16)$$

  where:

  - $(qh)_{\mathrm{w}} = q_{\mathrm{w_{in}}}^{\mathrm{A}} \mathrm{h}_{\mathrm{w_{in}}}^{\mathrm{A}} - q_{\mathrm{w_{out}}}^{\mathrm{A}} \mathrm{h}_{\mathrm{w_{out}}}^{\mathrm{A}}$ is the energy balance of the input-output water mass flow;
  - $Q_{\mathrm{s}\rightarrow\mathrm{w}}^{\mathrm{A}} = (ha)_{\mathrm{s}\rightarrow\mathrm{w}} (T_{\mathrm{s}}^{A} - T_{\mathrm{w}}^{A}) V_{\mathrm{w}}^{\mathrm{A}}$ is the heat transfer rate for the heat steam;
  - $(ha)_{\mathrm{s}\rightarrow\mathrm{w}}$ is the product between the heat transfer coefficient and the area contact between water and steam;
  - $V_{\mathrm{w}}^{\mathrm{A}}$ is the water volume;
  - $v_{\mathrm{w}}^{\mathrm{A}}$ is the specific water volume.

- Steam specific energy balance

$$\frac{dh_{\mathrm{s}}^{\mathrm{A}}}{dt} = \frac{1}{M_{\mathrm{s}}^{\mathrm{A}}} \left[(qh)_{\mathrm{s}} + q_{\mathrm{s_{ec}}}^{\mathrm{A}} h_{\mathrm{s_{sat}}}^{\mathrm{A}} - Q_{\mathrm{s}\rightarrow\mathrm{w}}^{\mathrm{A}} + M_{\mathrm{s}}^{\mathrm{A}} v_{\mathrm{s}}^{\mathrm{A}} \frac{dp^{\mathrm{A}}}{dt} - h_{\mathrm{s}}^{\mathrm{A}} \frac{dM_{\mathrm{s}}^{\mathrm{A}}}{dt} \right] \quad (3.17)$$

  where:

  - $(qh)_{\mathrm{s}} = q_{\mathrm{s_{in}}}^{\mathrm{A}} \mathrm{h}_{\mathrm{s_{in}}}^{\mathrm{A}} - q_{\mathrm{s_{out}}}^{\mathrm{A}} \mathrm{h}_{\mathrm{s_{out}}}^{\mathrm{A}}$ is the energy balance of the input-output steam mass flow;
  - $Q_{\mathrm{s}\rightarrow\mathrm{w}}^{\mathrm{A}} = (ha)_{\mathrm{s}\rightarrow\mathrm{w}} (T_{\mathrm{s}}^{A} - T_{\mathrm{w}}^{A}) V_{\mathrm{w}}^{\mathrm{A}}$ is the heat transfer rate for the heat steam.;
  - $(ha)_{\mathrm{s}\rightarrow\mathrm{w}}$ is the product between the heat transfer coefficient and the area contact between water and steam;

- V_s^A is the steam volume;
- v_s^A is the specific steam volume.

- Pressure balance

$$\frac{dp}{dt} = \frac{\left(h_w^A \frac{\partial v_w^A}{\partial h}\Big|_p - v_w^A\right)\frac{dM_w^A}{dt} + \left(h_s^A \frac{\partial v_s^A}{\partial h}\Big|_p - v_s^A\right)\frac{dM_s^A}{dt} - \frac{\partial v_w^A}{\partial h}\Big|_p \left[(qh)_w + q_{wec}^A h_{s_{sat}}^A + Q_{s\to w}^A\right] - \frac{\partial v_s^A}{\partial h}\Big|_p \left[(qh)_s + q_{sec}^A h_{ssat}^A - Q_{s\to w}^A\right]}{\left(\frac{\partial v_w^A}{\partial p}\Big|_h + v_w^A \frac{\partial v_w^A}{\partial h}\Big|_p\right) M_w^A + \left(\frac{\partial v_s^A}{\partial p}\Big|_h + v_s^A \frac{\partial v_s^A}{\partial h}\Big|_p\right) M_s^A} \quad (3.18)$$

These set of five differential equations describe the behaviour of the steam accumulator. This subsystem can be now added to the other part of the systems.

The accumulator subsystem has as input the steam mass flow rate in the tube, and so its enthalpy as a function of the tube pressure.

The output of the subsystem is the accumulator pressure.

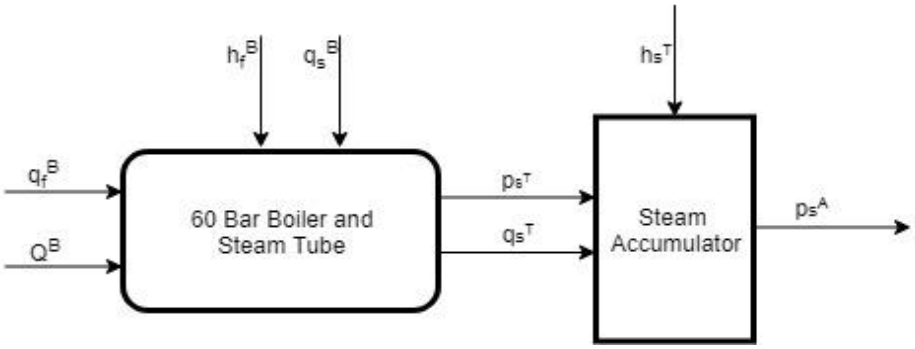

Figure 3.15 – Block diagram of the system plus the accumulator

The accumulator's shape can be easily approximated with a cylinder, so the geometrical parameters of the accumulator in our study plant are reported in the following table.

Name	Variable	Value	Unit of measurement
L	Length	12	m
d	Diameter	2	m
l	Water level		%
$\bar{l}$	Maximum water level	1.8	m

Table 3.9 – Accumulator geometrical data

The accumulator water level is measured starting from a point above the center indicated as "A" in *Figure* 3.16. As we can see this water level has a maximum that is value "B". This is a security feature so that when the water reaches this level it exits from a discharger tube that is in point "C" in *Figure* 3.16.

Besides these parameters, there are other three that will be identified and are: τ_e, τ_c and $(ha)_{s\to w}$. They must be identified from data to have the best fit possible.

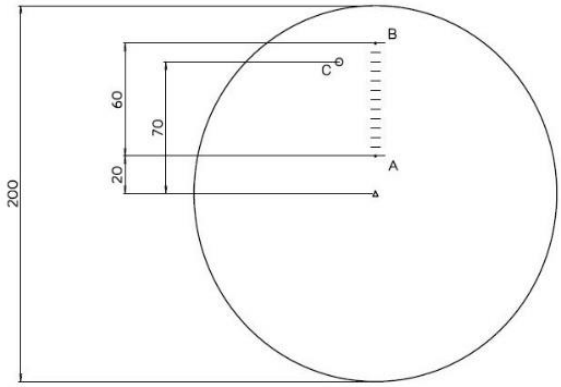

Figure 3.16 – Accumulator front view with dimension in [cm]

3.5 – ACCUMULATOR MODEL VALIDATION

In this section, we put into test the steam accumulator model described in *Chapter 3.4.* first, we will show that such a model is perfectly consistent with other models and data available in the literature. Then, we will show that, using the available data extracted from our plant, a successful model identification procedure has not been possible, due to two possible concurring issue:

1) the accumulator model dynamics shows to be overly sensitive to parameters changes, making the parameters tuning extremely difficult;
2) the model considered in *Chapter 3.4* may not include phenomena or processes that actually occur in the real system, but which are unknown to us.

This will motivate the fact that, in this worth, the physical-based mathematical model shown in *Chapter 3.4* will be eventually discarded, and a neural network will be identified and used in its place for control purposes. The identification procedure of the accumulator parameters will be discussed in *Chapter 3.5.2,* while the identification of the neural network of choice will be discussed in *Chapter 3.5.3.*

3.5.1 – VALIDATION OF THE ACCUMULATOR MODEL USING LITERATURE DATA

Here we show a comparison results of the simulations obtained using the model derived in *Chapter 3.4* with experimental data collected in [7].

Several experiments will be performed in different working conditions to have a complete set of tests, i.e.

- two charging tests at different working condition;
- two discharging tests at different working condition;
- three charging tests with different initial water volume condition;
- three charging tests with different inlet steam mass flow rate;
- three charging tests with different inlet enthalpy.

The steam source's parameters and the initial state of the accumulator are given for each test.

CHARGING TESTS

The charging test can be divided into two conditions: A and B, that are summarized in the following table:

Condition	A	B
Steam pressure [MPa]	0.633	0.8
Steam temperature [°C]	280.2	268.9
Steam enthalpy [kJ/kg]	3019	2991
Steam flow rate [kg/s]	0.2	0.25
Accumulator initial pressure[MPa]	0.484	0.484
Stop pressure [MPa]	0.65	0.65
τ_e and τ_c $[s]$	9.1	8

Table 3.10 - Literature experiments conditions A and B

The *stop pressure* parameter in *Table 3.10* represents the accumulator pressure value that, when reached, induces to the closure of the inlet steam valve. The results of these tests are shown in *Figure 3.17,* where the right panels are the simulated data, while the left ones are from [7].

In these charging tests, we can see the pressure evolution in the steam accumulator indicating a strong non-equilibrium thermodynamics process. The pressure rapidly increases up to the set value. After charging, the valve opens, then the pressure quickly drops as the charging valve closes before finally stabilizing. This phenomenon occurs because part of the inlet steam enters the space filled by the

accumulator steam before there is an enough heat exchange with water. This leads to a quick pressure rise. When the charging valve closes, the water is still unsaturated, thus the steam in the accumulator condenses and transforms into water, which causes the pressure to drop quickly until it reaches a new equilibrium state.

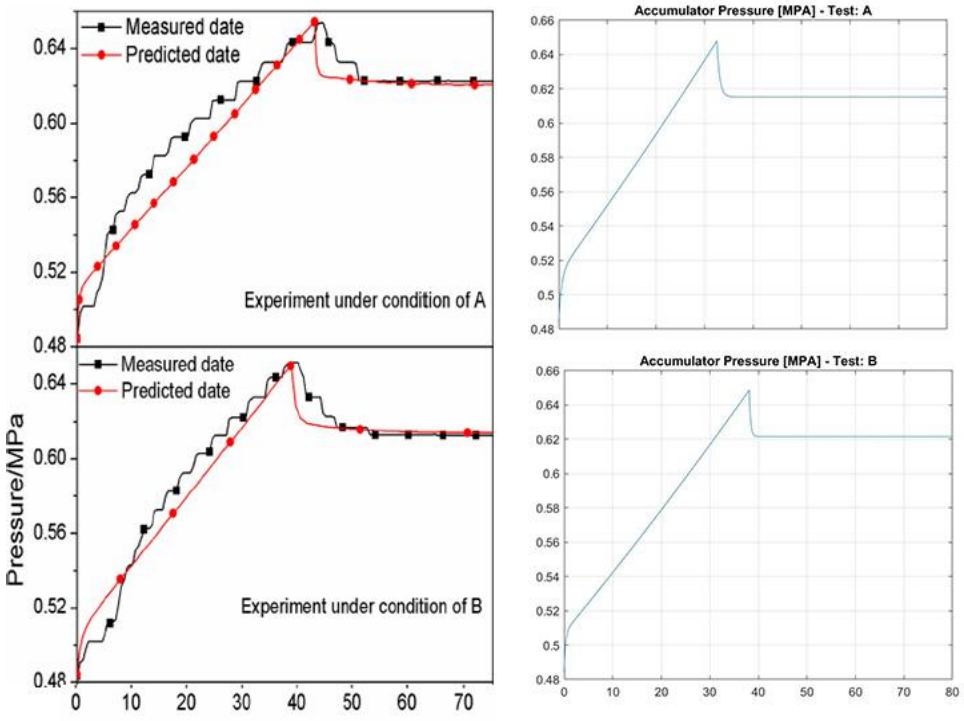

Figure 3.17 - Literature experiments and simulation experiments results for charging

DISCHARGING TESTS

For the discharging process, the two experiments have different initial accumulator pressure. As in the previous tests, there is a *stop pressure* parameter that when is reached induces the closure of the discharging valve.

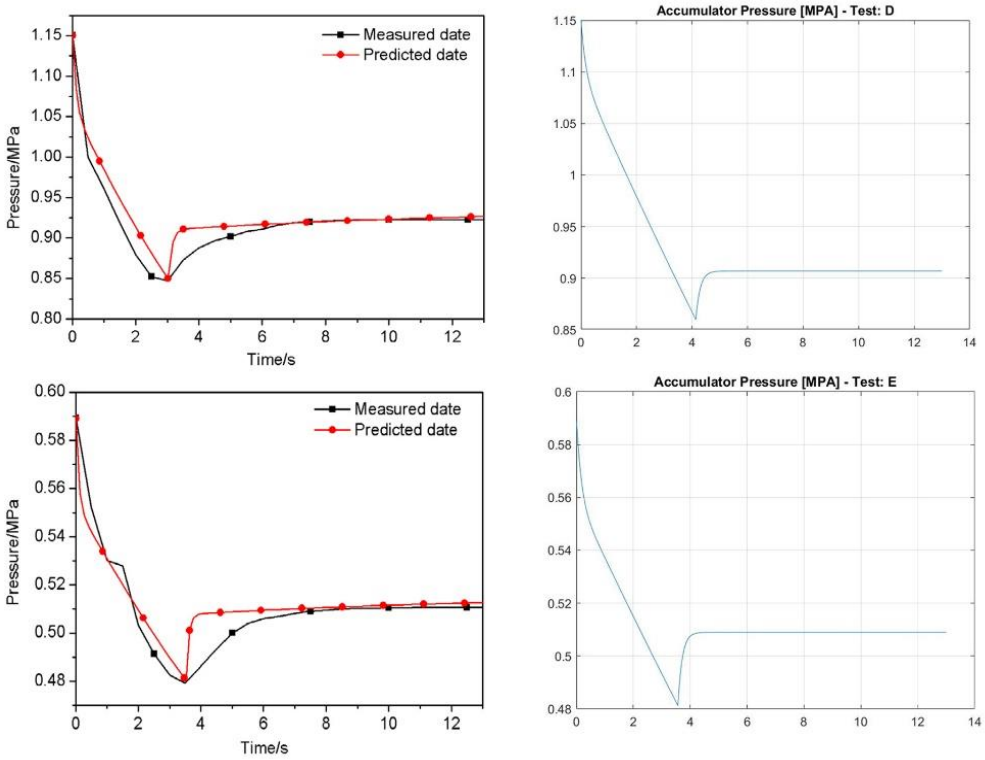

Figure 3.18 - Literature experiments and simulation experiments results for discharging

Also, the pressure, in this case, indicates a strong non-equilibrium thermodynamic process. In *Figure 3.18* we can see the pressure does not maintain stability after the discharge valve is closed, on the contrary slightly increases. The non-equilibrium process mainly occurs because the water is still in a superheated state when the discharge valve closes, due to the extremely short discharging time.

CHARGING TESTS WITH DIFFERENT INITIAL WATER CONDITION

In these tests, we set the initial water filling coefficient to 25%, 40%, and 55% respectively for each test. The water filling coefficient is defined as the ratio of the internal water volume to the total volume of the steam accumulator

$$\alpha = \frac{V_w^A}{V_{\text{tot}}^A} 100\%$$

We also set the charged steam flow rate to 0.25 kg/s, the charged enthalpy to 3000 kJ/kg and the initial pressure and the charging stop pressure to 0.8 and 1.2 MPa. The influence of the initial water volume on the charging process is shown in *Figure 3.19*.

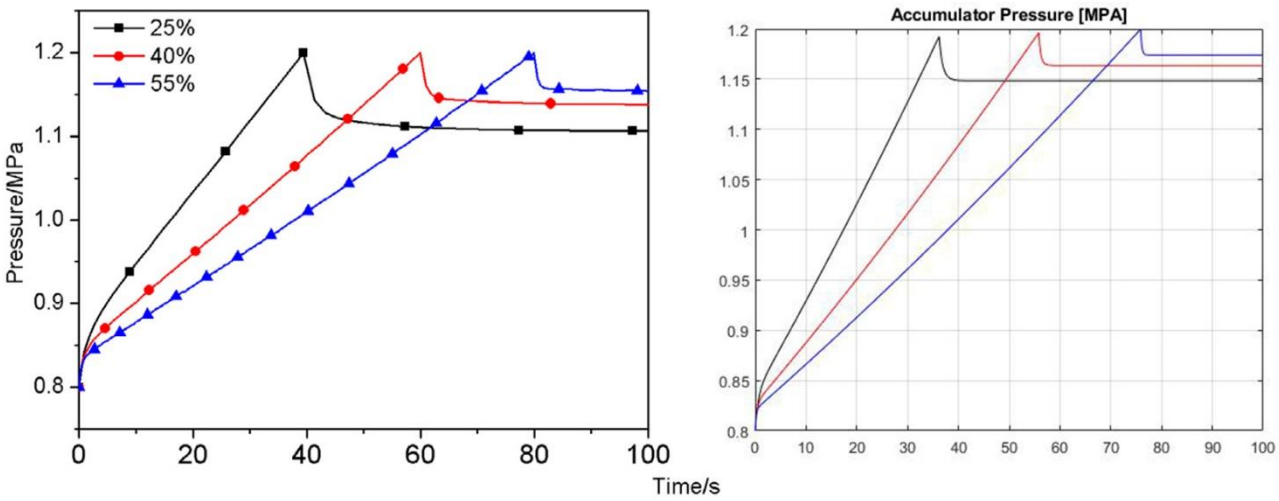

Figure 3.19 - Literature experiments and simulation experiments results for charging with different initial water volume

We can see in *Figure 3.19* that the charging time increases as the water filling coefficient increases. This occurs because a smaller water filling coefficient results in a smaller mass inertia of the system, which makes it easier to change the state of the system. We can also notice that the pressure drop ratio Δp caused by the non-equilibrium thermodynamic process during the charging is different and become smaller when the water filling coefficient becomes higher. This means that the heat transfer becomes more effective between the charged steam and the water with a larger water filling coefficient. So, as the water filling coefficient increases, the heat exchange between the steam and the water increases and there will be more energy to be stored in the water. On the other hand, the steam accumulator requires more steam to maintain the same final pressure. In conclusion, the goal of the steam accumulator to be a heat storage becomes easier to achieve as the water filling coefficient increases. The drawback of having a large water filling coefficient is that the times to reach a given pressure are extended. There could be problems also in the evaporation phase since the steam space height may be insufficient and the evaporation rate cannot be guaranteed.

CHARGING TESTS WITH DIFFERENT INLET STEAM FLOW RATE

For these tests, we set the initial filling water coefficient to 40%, the charged steam enthalpy to 3000 kJ/kg and the initial pressure and the charging stop pressure to 0.8 and 1.2 MPa. The inlet steam mass flow rates are 0.2, 0.25, and 0.3 kg/s respectively.

When the steam enthalpy is constant, the charging time gradually decreases as the charged steam flow rate increases. The pressure drop ratio increases as the charged steam flow increases. The speed of the charging increases and the charging time decreases as the charged steam flow increase, which means that the contact time between the steam and the water inside the steam accumulator decreases as well. More steam turns into water as the charged steam flow decreases, which improves the effective energy storage of the system. Simulation results are shown in *Figure 3.20.*

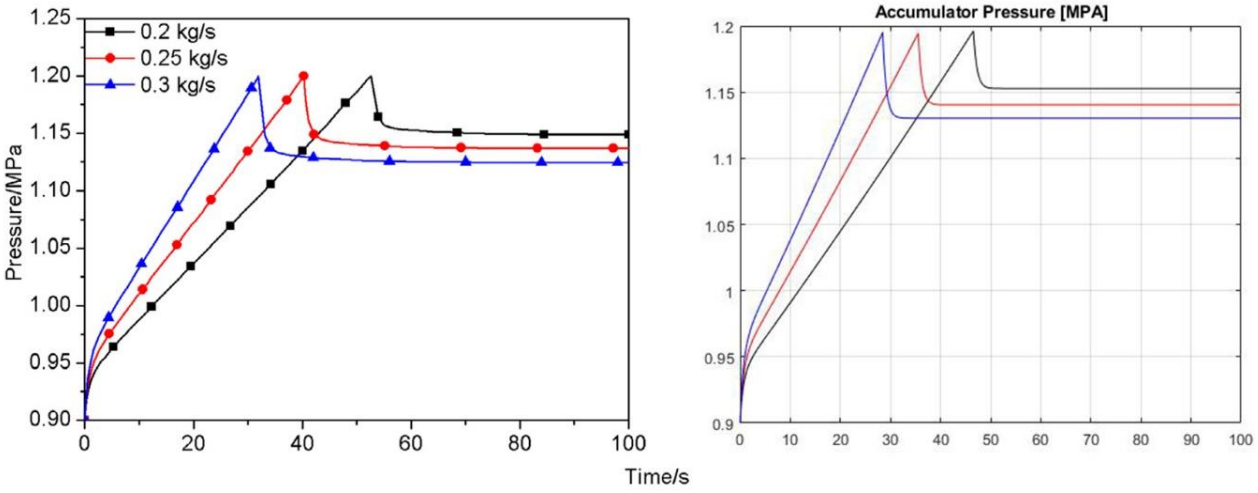

Figure 3.20 - Literature experiments and simulation experiments results for charging with different inlet flow rate

CHARGING TESTS WITH DIFFERENT INLET STEAM ENTHALPY

For these experiments we set the initial water filling coefficient to 40%, the initial pressure and the stop charging pressure to 0.9 and 1.2 MPa, and the charging steam flow rate to 0.25 kg/s. The inlet steam enthalpies are 3050, 3200, 3350 kJ/kg.

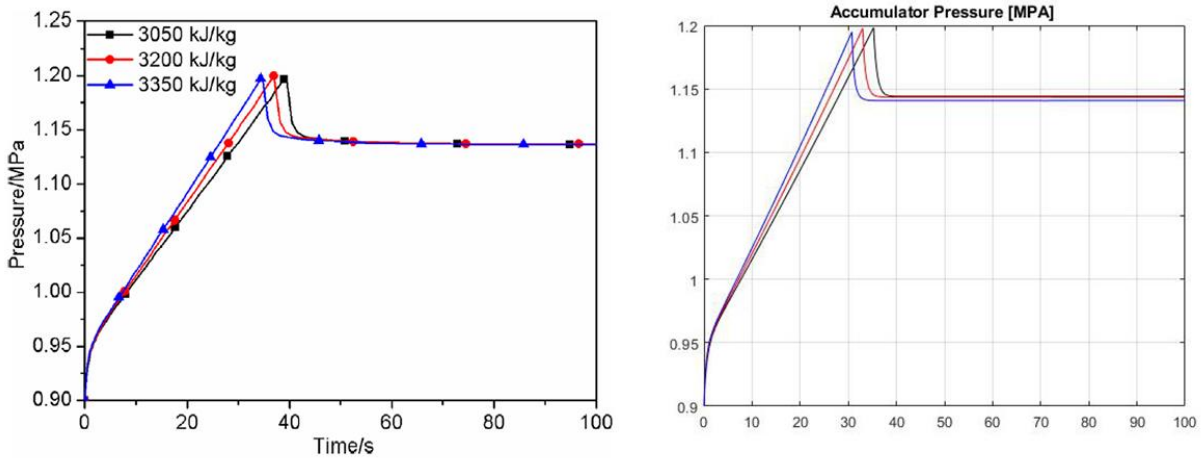

Figure 3.21 - Literature experiments and simulation experiments results for charging with different inlet steam enthaply

In *Figure 3.21* we can see that the pressure in the steam accumulator changes along with the changed steam enthalpy. As the enthalpy increases the charging time gradually increases. Increasing the inlet enthalpy causes the steam accumulator pressure to rise quickly and thus allow the system to achieve a given pressure in a shorter time.

After all these experiments we can say that the non-equilibrium accumulator model is validated with respect to the literature data.

3.5.2 – IDENTIFICATION OF THE ACCUMULATOR PARAMETERS

ACCUMULATOR PARAMETERS AND DATA DESCRIPTION

In this section, we explain the accumulator's parameter identification procedure. As we did for the boiler in *Chapter 3.3.3,* we will describe the available system data, how we have manipulated them and how they are employed to identify the accumulator parameters.

The data we have about the accumulator are collected in Excel files. The data we have used are list in the following table.

Data name	Variable	Unit of measurement
p^{A}	Accumulator pressure	Bar
$T^{A}_{\mathrm{s_{in}}}$	Accumulator inner steam temperature	°C
$l^{\mathrm{A}}_{\mathrm{w}}$	Accumulator water level	%
$q^{A}_{\mathrm{s_{in}}}$	Accumulator inlet steam flow rate	kg/s
$q^{A}_{\mathrm{s_{out}}}$	Accumulator outlet steam flow rate	kg/s

Table 3.11 – Accumulator available data

The accumulator model parameters that must be identified are listed in the following table:

Name	Variable	Unit of measurement
τ_c	Condensation relaxation time	seconds
τ_e	Evaporation relaxation time	seconds
$(ha)_{\mathrm{s\rightarrow w}}$	Product between the heat transfer coefficient and contact area between water and steam	kW/m^3K

Table 3.12 – Accumulator parameters to be identify

The phase change condensation and evaporation relaxation times have a strong influence on the pressure change rate.

We don't need to estimate the initial condition of the accumulator since we have the real data available. To identify the accumulator parameters, we have used 3 Excel files referring to operating days from January to February 2019. As an example, we use the accumulator data set of 07 January 2019, depicted in *Figure 3.22* with a sampling time $T_s = 10\ s$;

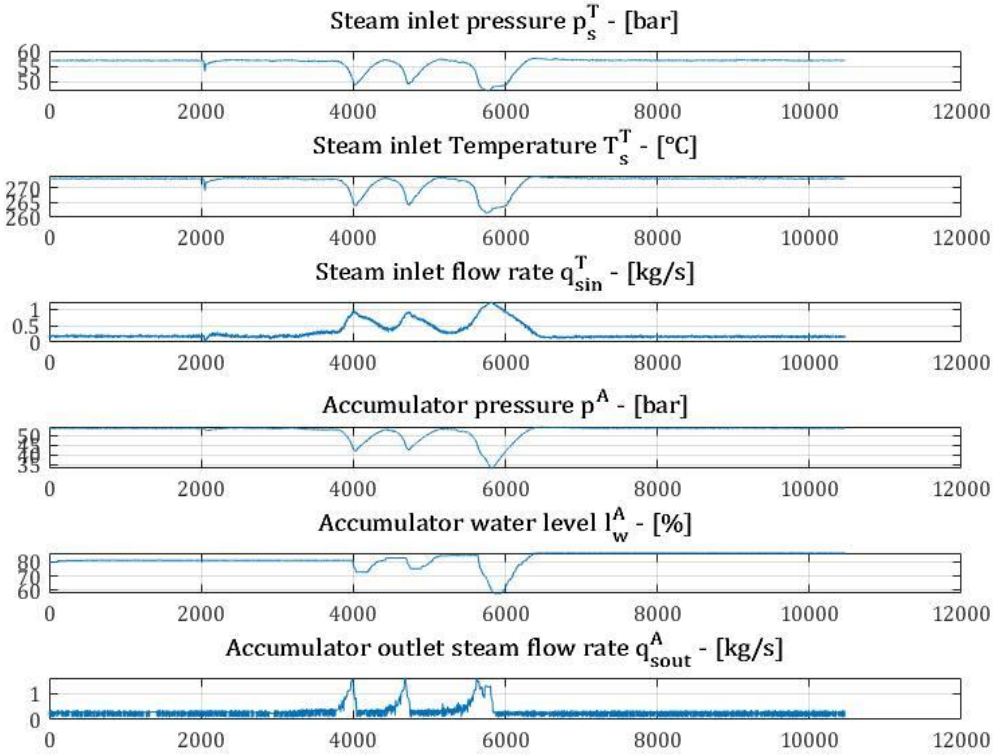

Figure 3.22 – Accumulator data of 7 January 2019

As for the boiler, we extracted and resample the data to have an homogeneous set of signals with the same sampling time of 10 seconds. The noise of these signals is slightly higher than the boiler one. We point out, for example, the outlet steam out mass flow rate $q_{\mathrm{S_{out}}}^{\mathrm{A}}$(see *Figure 3.22 sub-plot 6)* that is the noisiest signal of all data set.

IDENTIFICATION PROCEDURE

The identification consists of finding the set of parameters that minimize a given objective function. The objective function is defined as the squared error between:

- the accumulator measured pressure p^{A} and the simulated pressure $p_{\mathrm{sim}}^{\mathrm{A}}$;
- the accumulator measured water level $l_{\mathrm{w}}^{\mathrm{A}}$ and the simulated level $l_{\mathrm{w_{Sim}}}^{A}$;

The identification is done, as for the boiler, using the Matlab solver function *fmincon.* The objective function for the accumulator is:

$$\min_{\tau_e,\tau_c,(ha)_{\mathrm{s\to w}}} J \quad (3.19)$$

and J is

$$J = \sum_{k=1}^{N} \left(p^{\mathrm{A}}(k) - p_{\mathrm{Sim}}^{\mathrm{A}}(k)\right)^2 + \left(l_{\mathrm{w}}^{\mathrm{A}}(k) - l_{\mathrm{w_{Sim}}}^{\mathrm{A}}(k)\right)^2$$

where we have that:

- *N* is the total number of sample points of the data set.

We have two terms in the cost function because we need that the model reconstructs the pressure and water level behaviour for control purposes.

We do not define strict constraints on the parameters because their value is strongly correlated to the data behaviour. So, we want to give the solver the best range of possible parameter choice to have the best fit possible. Summarizing the parameter constraints are:

$$0.001 \leq [\tau_c; \tau_e] \leq 4000 \text{ seconds}$$

$$0.001 \leq (ha)_{\text{s}\to\text{w}} \leq 4000\ kW/m^3K$$

The optimal parameter values are:

Name	Data set 01 January 2019
τ_c	67 seconds
τ_e	7.5 seconds
$(ha)_{\text{s}\to\text{w}}$	51 kW/m^3K

Table 3.13 – Identified accumulator parameters

We show the results of this identification for our example data set in *Figure 3.23*.

We can immediately notice the steady-state behaviour is reconstructed neither for the pressure nor for the water level. The trends of the downward peaks are also not reconstructed. These errors make this accumulator model impossible to use for controlling purposes. This because the simulated variables are too different with respect to the real ones.

A possible explanation of this result has been proposed at the beginning of *Chapter 3.5*. For these reasons, our study plant accumulator behaviour is not well reconstructed although the model is validated. A solution to this issue is presented in the following chapter: we decided to use a long short-term memory artificial recurrent neural network to reconstruct the accumulator pressure and water level behaviour.

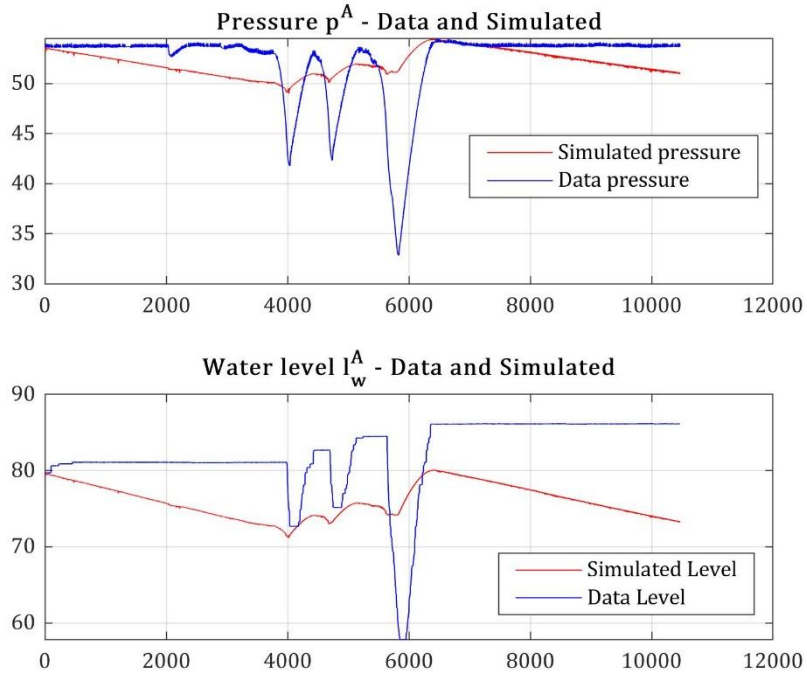

Figure 3.23 – Result of simulated pressure and water level with respect to data file 01

3.5.3 – ACCUMULATOR MODEL IDENTIFICATION WITH LSTM

Here we give the description of the main steps to reconstruct the accumulator model using a Long Short-Term Memory (LSTM) artificial recurrent neural network (RNN).

DATA SELECTION

The first step requires a selection of the data. From all the Excel files, we have selected only the ones that have smooth pressure and water level behaviour. Thus, we discarded all the files where too noisy signals were present. After that, the selected files were divided into two groups. The first group, composed of five files, was used to train the network. The second group, composed of two files, was used to validate the network.

As an example in the following figures are reported two accumulator data set from the five selected for the training:

- Accumulator data of 7 January 2019, depicted in *Figure 3.22* with a sampling time $T_s = 10\ s$;
- Accumulator data of 12 February 2019, depicted in *Figure 3.24* with a sampling time $T_s = 10\ s$;

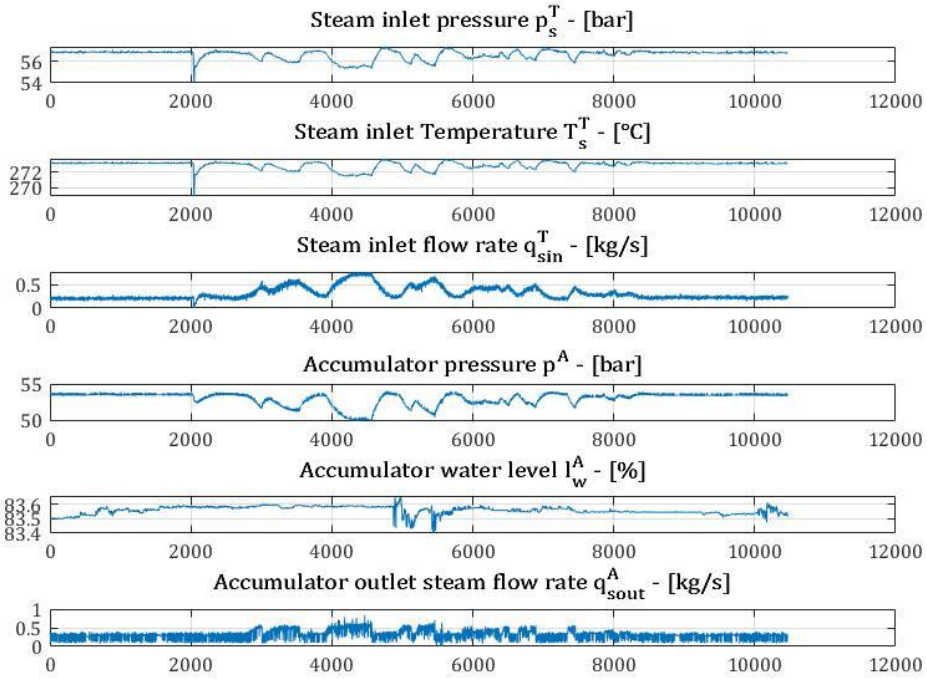

Figure 3.24 – Accumulator data of 12 February 2019

NETWORK SETUP AND TRAINING

Looking at the accumulator data figures, we can see that the data have different ranges. We first normalize them in order to prepare the network to handle this data. This will change the values of the dataset to a common scale, without distorting differences in the ranges of values. The normalization is done with respect to the mean value and the standard deviation of the signal as:

$$x_{\text{Norm}} = \frac{\left(x - \mu(x)\right)}{\sigma(x)}$$

Now that all the signals belong to the same range, we can build up the network features. We select three as feature number, representing the inputs to the system, that are:

- steam inlet enthalpy, calculated with the IAPWS-IF97 (*Appendix 1)* formulation from the inlet steam pressure and temperature;
- steam inlet mass flow rate;
- accumulator steam outlet mass flow rate.

Then we select two responses features, representing the system output:

- accumulator pressure;
- accumulator water level.

So, the system we want to identify with this network is the one sketched in the following figure:

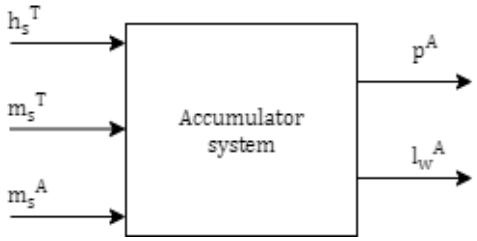

Figure 3.25 – System to be identified

After this, we selected 50 neurons for the network, and we choose 250 as epochs maximum to train the network. in the following figures, we can see the reconstruction of our example data set.

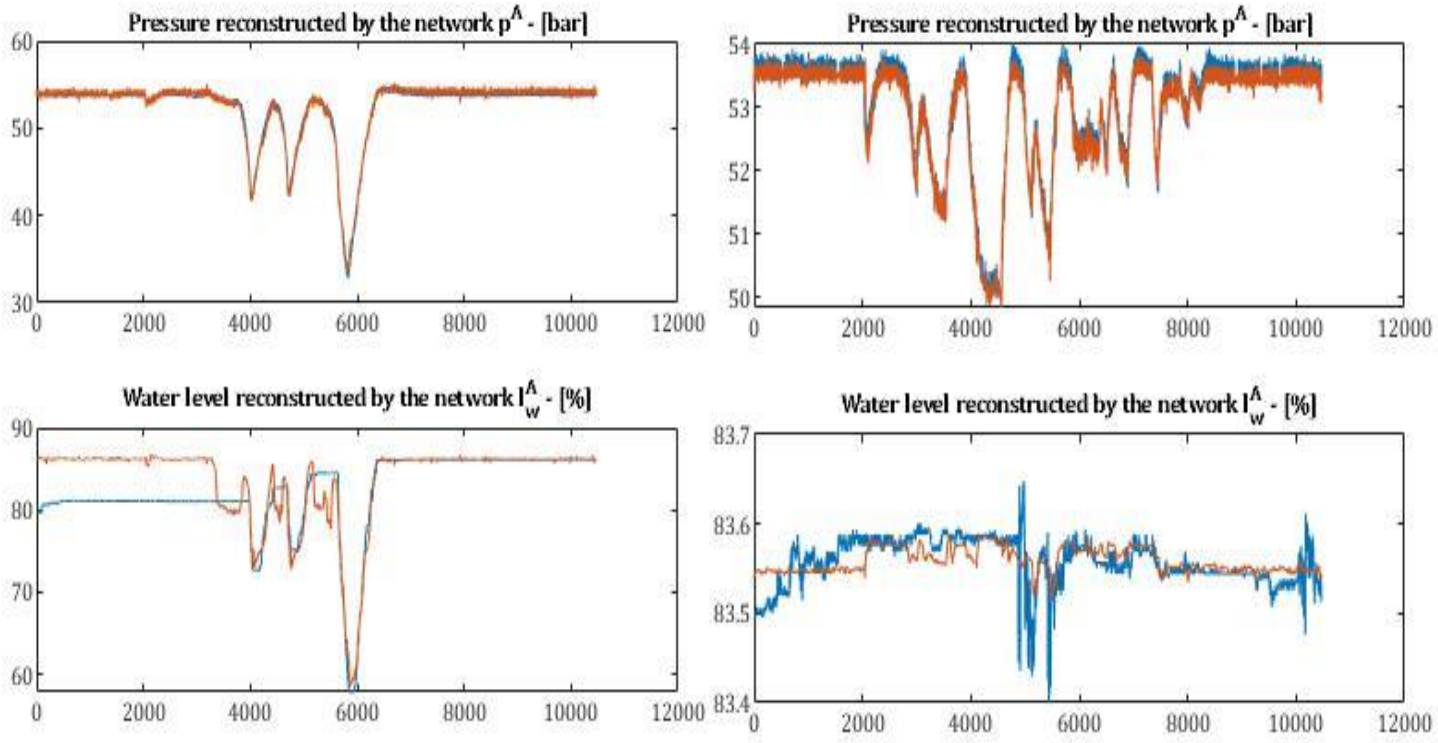

Figure 3.26 and 3.27 – Pressure and water level of accumulator data of 7 January 2019 and data of 12 February 2019 reconstructed by the network

This reconstruction was made on the training data. As expected, the pressure behaviour is reconstructed well. All its dynamics and steady-state trends are good. About the water level, there is not a perfect

match between the original data (blue line) and the reconstructed data (red line). This mainly because of the noise on the signal and a possible malfunction of the sensor. This is evident in the training file on 7 January 2019. Looking at the first 3500 points in *Figure 3.22* we can see that the system is almost in steady-state and the water level is about 80%. After the dynamics behaviour, from point 6500 to the end of the plot the system returns in a steady-state condition that is equal to the first one. But now, the water level has a different equilibrium point that is around 86% that should be impossible. In fact, as mentioned at the end of *Chapter 3.4,* the water level has a security feature that makes the water level stay under 83%. Nevertheless, we take this result as a good reconstruction of the general behaviour of the water level, since we do not have better data to create a more precise model.

VALIDATION ON TESTING DATASETS

Now that the network is trained and it is validated on the training data, we try to validate it with the two data set validation. As validation data sets, we take:

- Accumulator data of 9 January 2019;
- Accumulator data of 13 February 2019;

and they are shown in *Figure 3.28* and *Figure 3.29* respectively, with a sampling time $T_s = 10\ s$;.

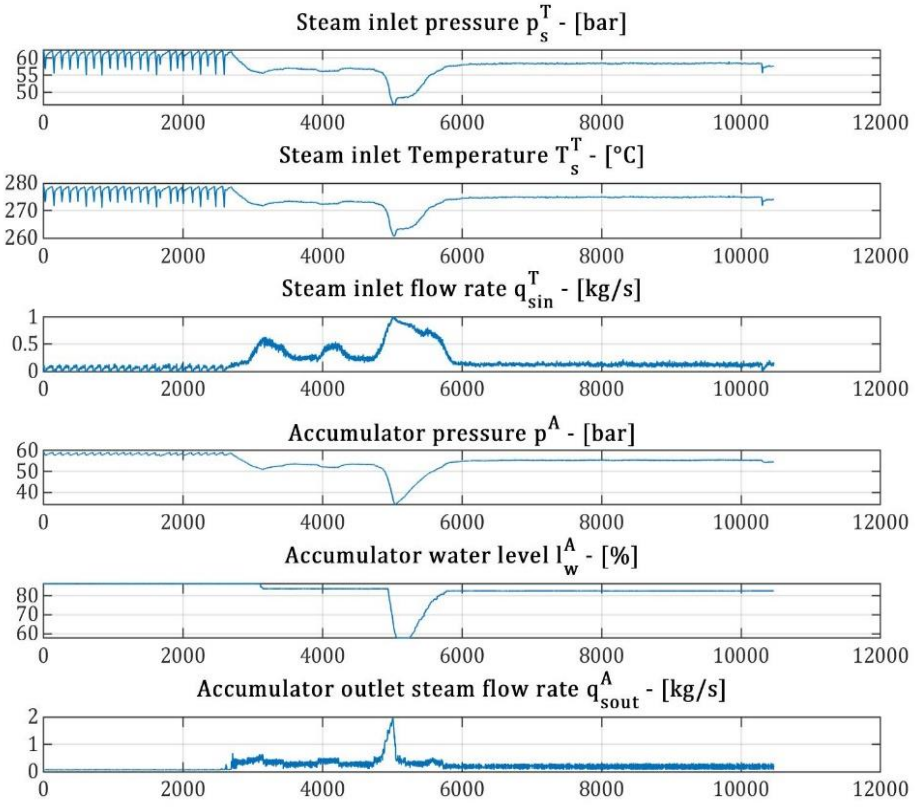

Figure 3.28 – Accumulator data of 9 January 2019

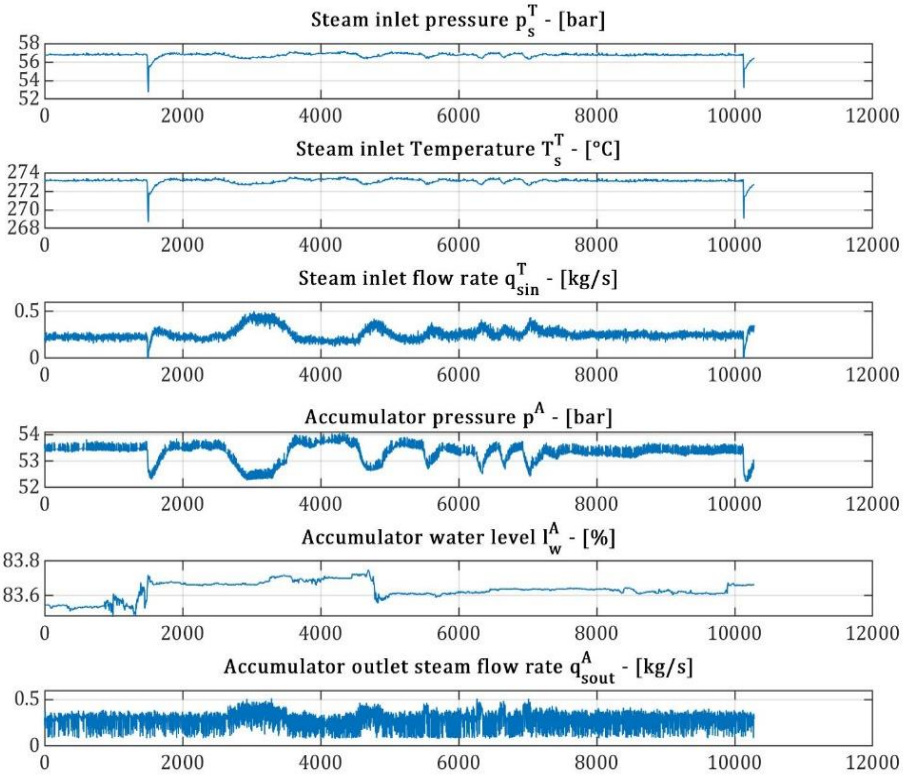

Figure 3.29 – Accumulator data of 13 February 2019

After the simulation of the network on these data sets, the obtained results are shown in the following figures:

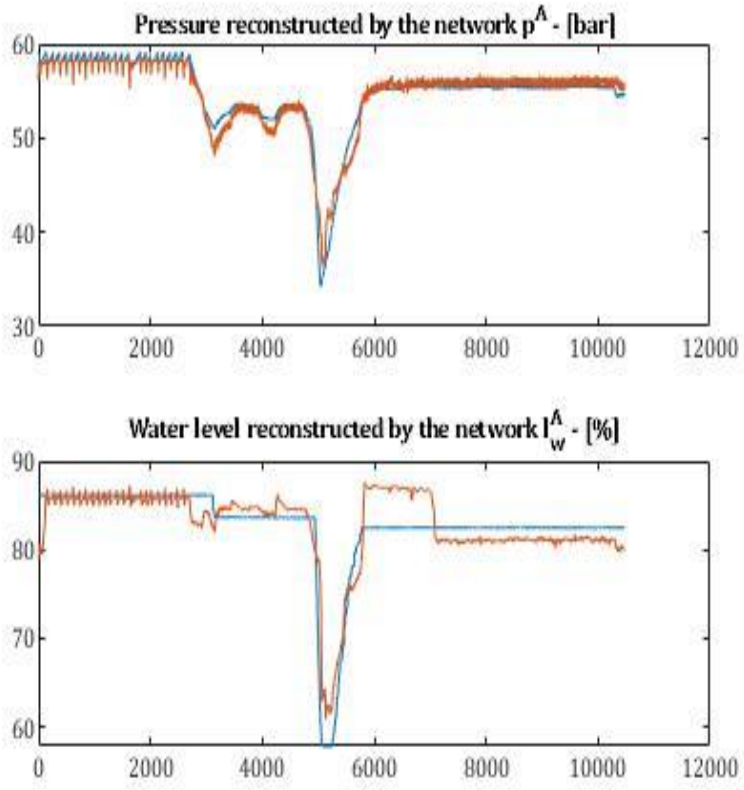

Figure 3.30 – Pressure and water level of accumulator data of 9 January 2019 reconstructed by the network

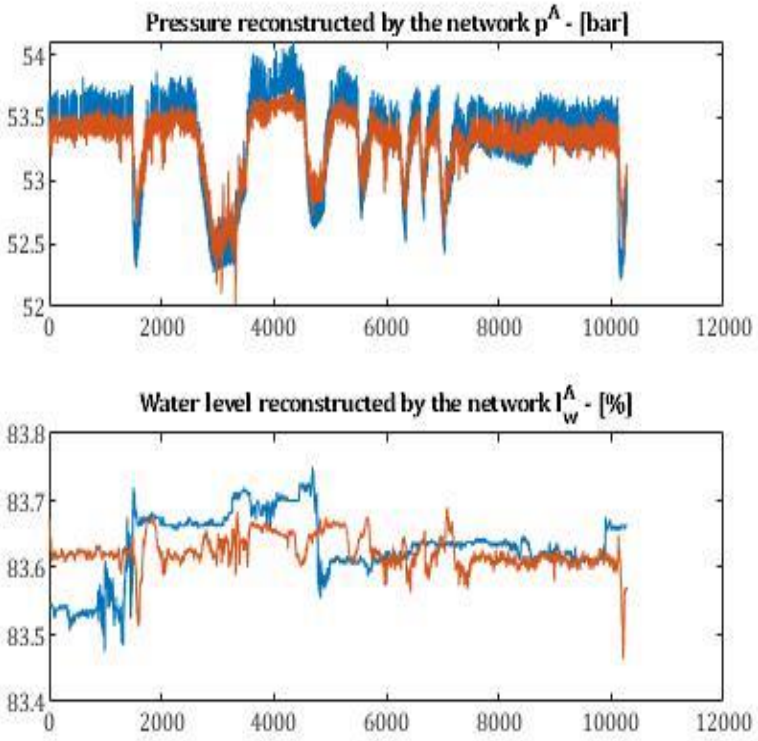

Figure 3.31 – Pressure and water level of accumulator data of 13 February 2019 reconstructed by the network

As we can see the pressure still has good reconstructed behaviour. Also, the level dynamics and general value are good enough to validate the network also on the test data sets.

CHAPTER 4

CENTRALIZED MPC FOR CONTROL OF THE BOILER AND THE ACCUMULATOR

In this chapter the control algorithms, that will be applied to the models described in the previous chapter, are discussed.

4.1 – MODEL PREDICTIVE CONTROL

Model predictive control (MPC) is a family of algorithms that have gained wide popularity because of their widespread diffusion in process control. MPC is the most widely used advanced control methodology in the process industry [9].

The most important characteristics of MPC are the possibility to:

- formulate the control problem as an optimization one, where different goals can be considered;
- explicitly include, in the control problem formulation, state and input constraints;
- synthesize the controller based on the process models.

These characteristics make MPC very flexible and suitable for many applications.

The elements needed to build an MPC controller are:

- a discrete-time process model;
- input, output, and state constraints;
- a cost function J defined, at any time instant k, over a finite horizon $[k, k+N]$;
- an optimization algorithm for computing the future optimal control sequence;

A general scheme of an MPC-based control system is sketched in the following figure.

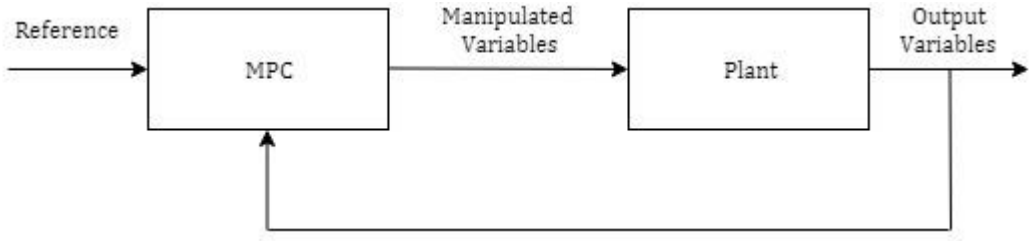

Figure 4.1 – General MPC controlled plant scheme

In the MPC block (*Figure* 4.1) there are two components, that are:

- the plant model;
- the optimizer.

The model used in MPC represents the behaviour of the dynamical system that we want to control. MPC uses the current plant measurements, dynamic states of the process, and the plant model to calculate the future dynamical changes of the system. These changes are calculated to hold the output variables close to the references honouring constraints. So, the essence of MPC is to optimize, suitably using the manipulable inputs, forecasts of process behaviour. For this reason, the model is the essential element of an MPC controller.

MPC is based on the R*eceding Horizon principle:* at any time instant *k,* based on the available process information, solve the optimization problem with respect to the future control sequence $[u(k), \dots, u(k+N-1)]$ and apply only its first element $u^{\circ}(k)$. Then, at the next time instant *k + 1*, a new optimization problem is solved, based on the process information available at time *k + 1,* along the prediction horizon $[k+1, k+N]$. By means of this strategy, a time-invariant feedback control law is obtained even if a finite horizon optimization problem is solved at any time instant.

The rationale of the RH algorithm is represented in *Figure* 4.2.

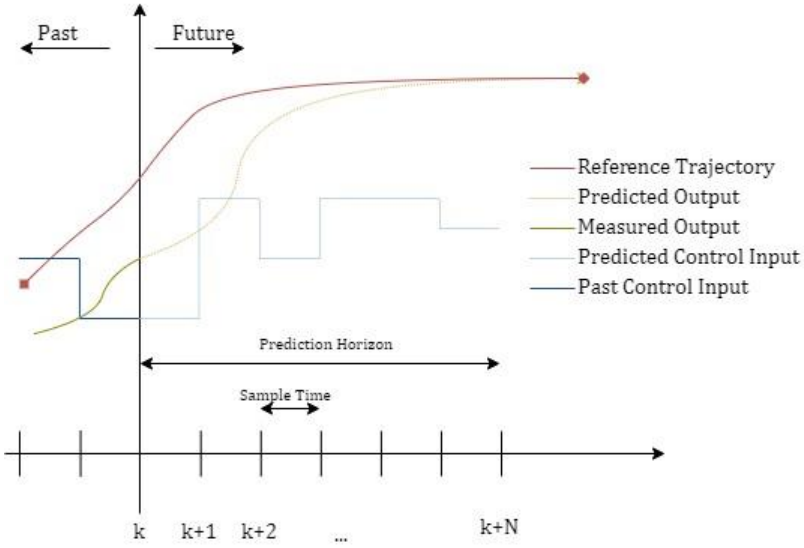

Figure 4.2 – MPC strategy

4.1.1 – LINEAR MPC WITH CONSTRAINS

A typical linear discrete-time model is of the form:

$$\begin{cases} x(k+1) = Ax(k) + Bu(k) \\ y(k) = Cx(k) \end{cases} \quad (4.1)$$

Assuming matrix $D = 0$, we have that $x \in \mathbb{R}^n$ is the state (assumed to be measurable for simplicity), $u \in \mathbb{R}^m$ is the control variable, and $y \in \mathbb{R}^p$ is the output variable. The state-space form has several advantages in MPC control. These advantages are, for example, easy generalization to multivariable systems, ease of analysis of closed-loop properties, and online computation.

The optimization problem consists of computing, at each time instant k, the control sequence $u(k), u(k+1), \dots, u(k+N-1)$ that minimize the finite horizon quadratic cost function:

$$J = \sum_{i=0}^{N-1} \left(||x(k+i)||_Q^2 + ||u(k+i)||_R^2 \right) + ||x(k+N)||_S^2 \quad (4.2)$$

where $Q \in \mathbb{R}^{n \times n}$, $R \in \mathbb{R}^{m \times m}$ and $S \in \mathbb{R}^{n \times n}$ are positive definite matrices. Note that Q and R are free design parameters, while S must be chosen in order to guarantee the properties of the control algorithm. In MPC, the positive integer N is called prediction horizon.

The MPC optimization problem, in general, includes state, input, and output constraints, that take the form:

$$x(k+i) \in \mathcal{X}, \quad i = 0, \dots N$$

$$u(k+i) \in \mathcal{U}, \quad i = 0, \dots N-1$$

$$x(k+N) \in \Omega$$

where $\mathcal{X}$ and $\mathcal{U}$ are convex sets containing the origin and Ω is a convex terminal set containing the origin.

The main properties that can be guaranteed through a proper problem formulation are

- recursive feasibility: if at time instant k the optimization problem is feasible, then it is feasible at every future time instant;
- convergence: the state of the closed-loop system asymptotically converges to the origin.

A general design choice consists of choosing an auxiliary control law $u = Kx$, where $A + BK$ is stable. In this case, to guarantee convergence, S has to be selected in order to satisfy the Lyapunov equality

$$(A+BK)^T S(A+BK) - S = -(Q + K^T SK)$$

The terminal set, to guarantee recursive feasibility, must be chosen such that $\Omega \subseteq \mathcal{X}$, $Kx \in \mathcal{U} \ \forall x \in \Omega$ and $(A+BK)\Omega \subseteq \Omega$, i.e. as a suitable positively invariant set.

4.1.2 – CONSTANT REFERENCE SIGNAL TRACKING

We assume that the reference signal is constant, i.e. $y^{\circ}(k) = y^{\circ}$and that the disturbances are known. Provided that $p \leq m$ and the system does not have any invariant zero $z = 1$, it is possible to compute a steady-state pair $(\bar{x}, \bar{u})$ such that

$$\bar{x} = A\bar{x} + B\bar{u}$$

$$y^{\circ} = C\bar{x}$$

In this case, the cost function can be written as:

$$J = \sum_{i=0}^{N-1} \left(\left|\left| y^{\circ} - y(k+i) \right|\right|_Q^2 + \left|\left| u(k+i) - \bar{u} \right|\right|_R^2 \right) + \left|\left| x(k+N) \right|\right|_S^2$$

so that $J = 0$ for $y(k+i) = y^{\circ}$ and $u(k+i) = \bar{u}$.

4.1.3 – NONLINEAR MPC

Consider now that linear system (4.1) is replaced with a nonlinear system, as in our case, in the form:

$$\begin{cases} x(k+1) = f\big(x(k), u(k)\big) \\ y(k) = g(x) \end{cases} \quad (4.3)$$

The optimization problem and the definition of the ingredients, which formally ensure recursive feasibility and convergence, may become more complex. The adopted solution to this problem is based on the successive linearization of the nonlinear system. This method allows having a problem solution with the same computational load of the linear MPC. This is due to the fact the optimization problem to be solved still a quadratic problem.

Therefore, at each time step, the nonlinear model is linearized around the last available optimal state/input trajectories obtained at the previous step $h-1$.

Assuming that some predicted input/state trajectories $u(k|h-1), x(k|h-1)$ are suitable as the solution to the MPC optimization problem obtained at time $h-1$, the linearized system dynamics at time step h becomes [13, 14].:

$$x(k+1) = A_{\mathrm{k|h-1}} x(k) + B_{\mathrm{k|h-1}} u(k) + d_{\mathrm{k|h-1}} \quad (4.4)$$

where:

$$A_{\mathrm{k|h-1}} = \left.\frac{\delta f\big(x(k),u(k)\big)}{\delta x}\right|_{\substack{x=x(k|h-1)\\u=u(k|h-1)}} \quad (4.5)$$

$$B_{\mathrm{k|h-1}} = \left.\frac{\delta f\big(x(k),u(k)\big)}{\delta u^{\mathrm{A}}}\right|_{\substack{x=x(k-1)\\u=u(k-1)}} \quad (4.6)$$

$$d_{\mathrm{k|h-1}} = -A_{\mathrm{k|h-1}}x(k|h-1) - B_{\mathrm{k|h-1}}u(k|h-1) + f\big(x(k|h-1),u(k|h-1)\big) \quad (4.7)$$

Now we can write the cost function to be minimized at each time instant h as:

$$J = \sum_{k=h}^{h+N}\left(\left|\left|x(k)\right|\right|_Q^2 + \left|\left|u(k)\right|\right|_R^2\right) + \left|\left|x(k+N)\right|\right|_S^2 \quad (4.8)$$

subject to the dynamics given by (4.4) and constraints

$$x(k+i) \in \mathcal{X}, \quad i = 0, \dots N$$
$$u(k+i) \in \mathcal{U}, \quad i = 0, \dots N-1 \quad (4.9)$$
$$x(k+N) \in \Omega$$

where $\mathcal{X}$ and $\mathcal{U}$ are convex sets containing the origin and Ω is a convex terminal set containing the origin [13, 14]. However, in this case, the definition of the terminal set and the terminal weight are non-trivial tasks. So, in this work will not define the terminal constraint. Instead, to guarantee the recursive feasibility, we will use slack variables. Consequently, weighted variables ϵ must be added in the optimization cost function. The weight ρ of this slack variable in the cost function must be selected large enough to guarantee that the optimum is $\epsilon \cong 0$ when a feasible solution exists. Therefore, the cost function can be rewritten as

$$J = \sum_{k=h}^{h+N}\left(\left|\left|x(k)\right|\right|_Q^2 + \left|\left|u(k)\right|\right|_R^2\right) + \rho\epsilon \quad (4.10)$$

subject to:

$$\epsilon \geq 0$$
$$x(k+i) \in \mathcal{X} \oplus \epsilon B(0), \quad i = 0, \dots N \quad (4.11)$$
$$u(k+i) \in \mathcal{U}, \quad i = 0, \dots N-1$$

where $B(0)$ is a ball of unitary radius and centre in the origin.

4.2– MODELS FOR MPC CONTROL

In this section we describe in detail the model used for the MPC control. Specifically, we focus on a boiler model obtained from the nonlinear one described in *Chapter 3.2;*

In the operating condition of interest, the boiler nonlinear model can be linearized with satisfactory results. We choose to identify this linear model and the identification procedure is described in the following sections.

This chapter describes how the linear boiler model is derived. The goal is to obtain a linear model that describes the boiler's pressure behaviour with respect to input changes. As in C*hapter* 3.2, the manipulable inputs are:

- Q^{B} the heat flow rate given by the burner to the boiler [kW];
- $q_{\mathrm{f}}^{\mathrm{B}}$ the feedwater mass flow rate [kg/s].

We also have some non-manipulable inputs that can be considered as disturbances:

- $p_{\mathrm{w_{in}}}^{\mathrm{B}}$ that is the boiler feedwater pressure;
- $T_{\mathrm{w_{in}}}^{\mathrm{B}}$ that is the boiler feedwater temperature;
- $q_{\mathrm{s_{DEM}}}^{\mathrm{B}}$ that is the steam mass flow rate that the boiler should supply to the system.

The boiler feedwater enthalpy $h_{\mathrm{w_{in}}}^{B}$ can be computed based on the first two non-manipulable inputs using the water thermodynamics property. We do not have sensors that measure the feedwater pressure, so it is set to 60 bar. The feedwater pressure is assumed to be constant since small pressure variations have negligible effects with respect to water enthalpy.

In the following, the identification procedure is described.

BOILER DATA CREATION

Firstly, a data set is created. This data set represents the boiler input signals. The data properties are:

- length: 500 samples;
- sampling time: 1 second;

Each signal in the set has a proper variation range. These variation ranges are summarized in *Table* 4.1.

Variable	Nominal value	Variation range
Q^{B}	1600 kW	[1570; 2500] kW
$q_{\mathrm{f}}^{\mathrm{B}}$	0.9 kg/s	[0.85; 1.2] kg/s
$T_{\mathrm{w_{in}}}^{\mathrm{B}}$	100.7 °C	[100.2; 101.7] °C
$q_{\mathrm{s_{DEM}}}^{\mathrm{B}}$	0.58 kg/s	[0.53; 1.08] kg/s

Table 4.1 – Signals nominal values and variation ranges

The variation ranges are within the real plant signals variation range. Steps of different amplitude are applied with an interval of 25 samples. This will allow the identified linear system to be more reactive to input variation. As mentioned before, the feedwater enthalpy is computed based on the water thermodynamics property, described in *Appendix 1*, taking a constant pressure of 60 bar and the generated feedwater temperature signal. The generated data set is used as input of the boiler system to simulate the pressure behaviour. The result is shown in *Figure 4.3*.

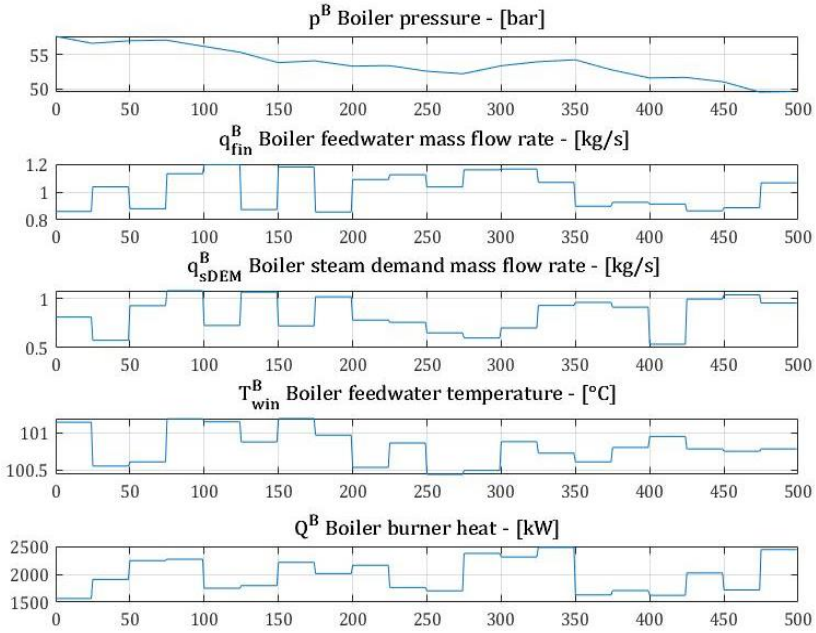

Figure 4.3 – Generated input data set and simulated pressure result

BOILER LINEAR MODEL IDENTIFICATION

The model identification is done using the Matlab toolbox *System Identification,* with the following options*:*

- first-order discrete-time linear state-space model;
- sampling time of 1 second;
- free matrices form and non-including disturbance component;
- subspace N4SID estimation method.
- other settings have been left with their default value.

The so-obtained system matrices and the reconstructed pressure behaviour are shown in the following:

$$A = 0.999862$$

$$B = [-0.03579 \quad 8.79145 \times 10^{-6} \quad 2.1136 \times 10^{-5} \quad -0.01757]$$

$$C = 0.4433$$

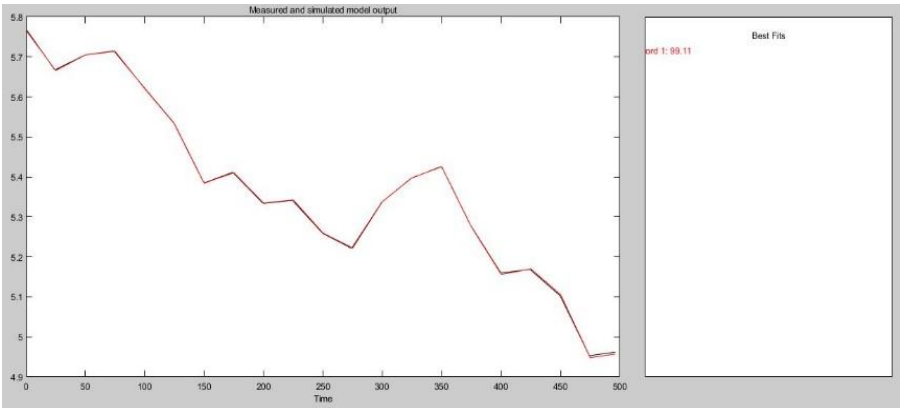

Figure 4.4 – Identified model behavior

Figure 4.4 shows the identified linear boiler pressure behaviour (red line) over the simulated boiler behaviour (black line). It can be noted that they are practically equal, in fact, the data fitting is 99.11%.

BOILER IDENTIFIED LINEAR MODEL VALIDATION

Before using the identified model in MPC control, we want to understand how good it reconstructs the pressure behaviour using other data sets. To do so, other two data sets are generated. After that, the new obtained simulated pressure is used as validation data for the identified model.

The second generated data set and the simulated pressure are shown in *Figure 4.5*.

With this new data set, the simulated boiler pressure has a swinging behaviour with a pick value of 61 bar and a minimum value of 56 bar. This behaviour is different from the one used to identify the model and shown in *Figure* 4.3 subplot 1.

The identified linear model can accurately reconstruct the new pressure behaviour, and the result is showed in *Figure* 4.6. The reconstructed pressure is the blue line, and we can see that we have a data fitting of 93.69%.

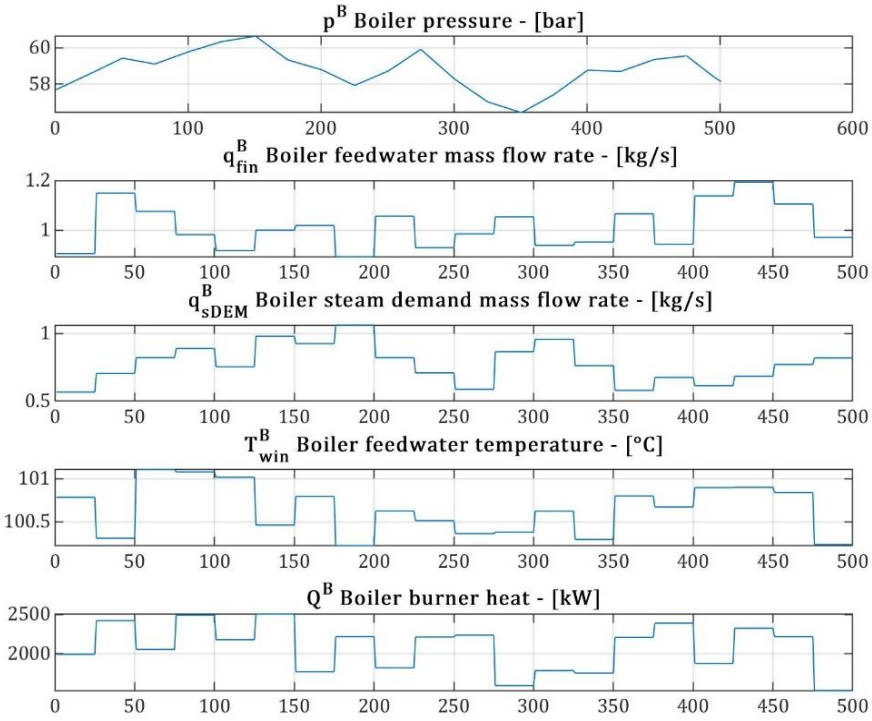

Figure 4.5 – Second generated input data set and simulated pressure result

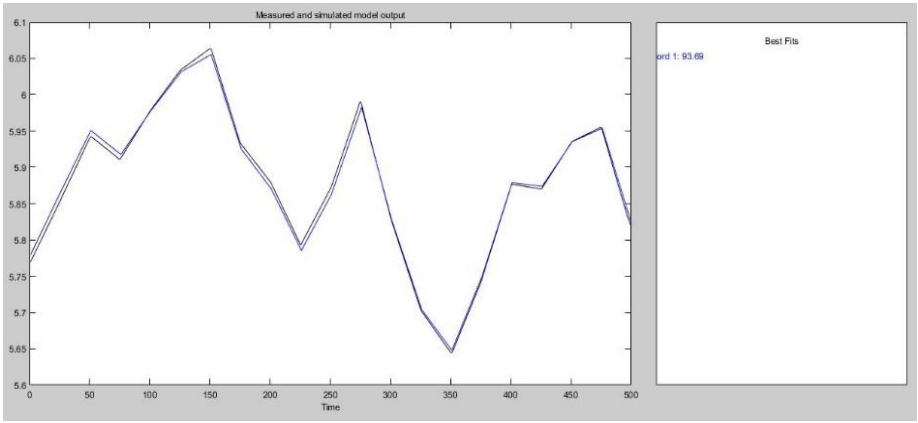

Figure 4.6 – Identified linear model validation with respect the second data set

The third generated data set and the simulated pressure are shown in the next figure.

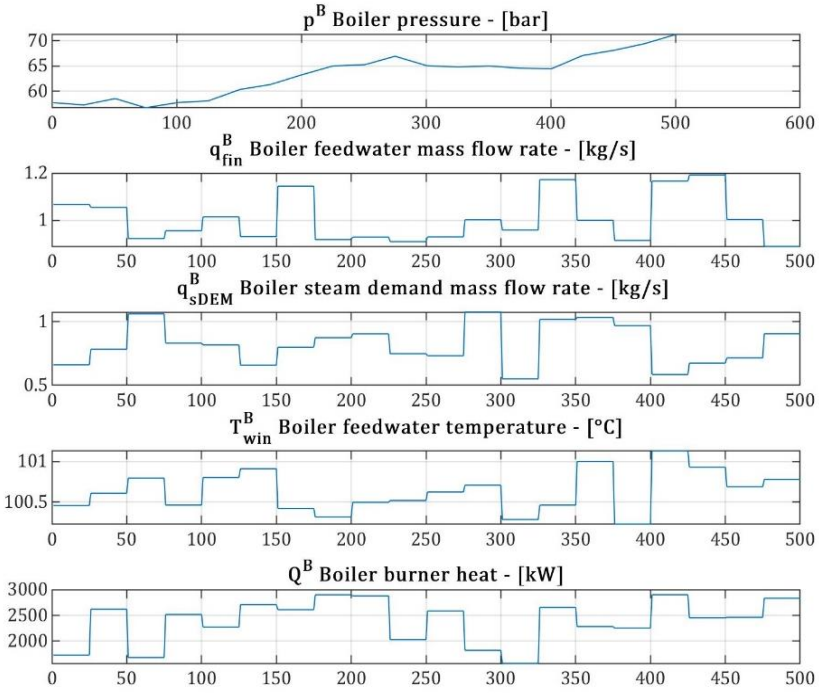

Figure 4.7 – third generated input data set and simulated pressure result

In this data set, we have expanded the signal variation range. The obtained pressure has a growing tendency with a pick value of 70 bar. This value is far from our system operating condition. This validation test is useful because we want to know if the model is able to reconstruct pressure behaviour out of the operating condition range since our final goal is to control the boiler pressure with MPC.

The identified linear model can also accurately reconstruct this new pressure behaviour, and the result is showed in *Figure* 4.8. The reconstructed pressure is the green line, and we can see that we have a data fitting of 90.03%.

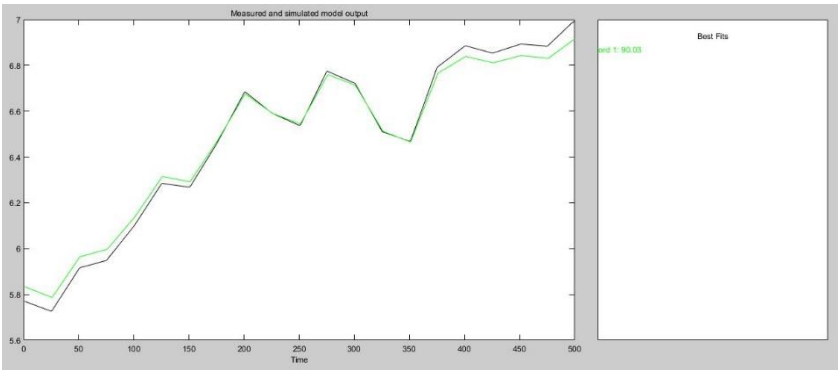

Figure 4.8 – Identified linear model validation with respect the third data set

After these results, we can consider the boiler linear model validated since it can reconstruct different pressure behaviour with a low percentage error.

4.3 – MPC CONTROL OF BOILER AND ACCUMULATOR

In this section, we discuss how the boiler and accumulator MPC control problem is formulated.

Figure 4.9 shows the control scheme idea.

We can see that in the MPC block there are two models that are:

- boiler linear model identified in *Chapter 4.2;*
- accumulator LSTM linear model. This derives from the linearization of the LSTM network;

The "PLANT" group is composed of nonlinear equation models, that are:

- the non-linear 60 bar boiler model is the one presented in *Chapter 3.2.1*;
- the steam tube model is the one presented in *Chapter 3.2.2;*
- the accumulator model is the one represented by the LSTM neural network presented in *Chapter 3.5.3.*

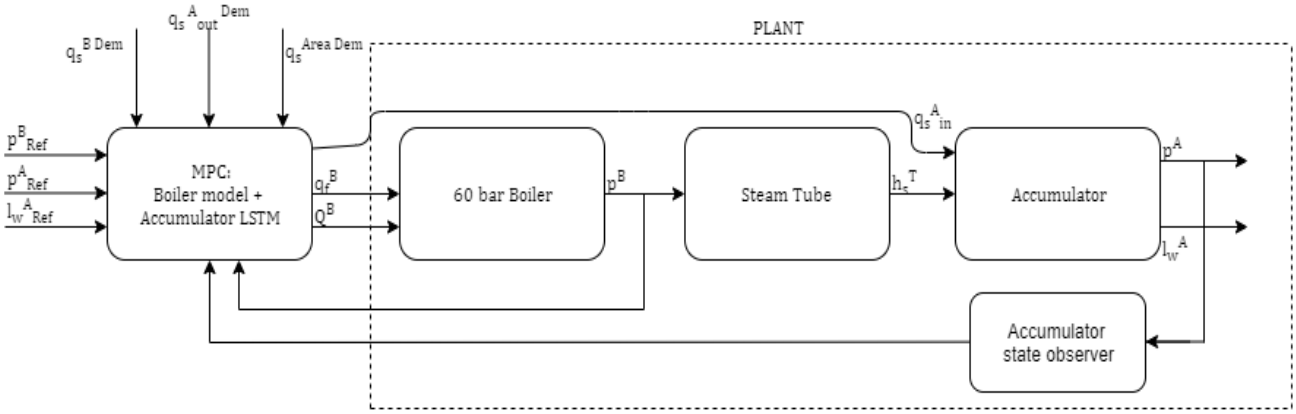

Figure 4.9 – MPC control scheme of boiler and accumulator

More specifically:

- the linear boiler model includes:
  - 1 state;
  - 4 inputs;
  - 1 output;
- the LSTM network includes:
  - 50 neurons, this means that the network states number is 100;
  - 3 inputs;
  - 2 outputs;

The resulting model that is used in the MPC prediction is composed of:

- 104 state, this because the LSTM network linearization matrix A_{LSTM} is a 103x103 matrix.
- 8 inputs;
- 3 outputs.

The main goals of this control are:

- control the boiler pressure p^{B} to a given setpoint $p^{\mathrm{B}}_{\mathrm{set}}$;
- control the accumulator pressure p^{A} to a given setpoint $p^{\mathrm{A}}_{\mathrm{set}}$;
- control the accumulator water level $l^{\mathrm{A}}_{\mathrm{w}}$ to a given setpoint $l^{\mathrm{A}}_{\mathrm{w\,set}}$.

Doing this the system must supply the steam demands from different areas. We have the:

- boiler steam demand $\bar{q}_{\mathrm{s}}^{\mathrm{B\ Dem}}$;
- accumulator steam demand $\bar{q}_{\mathrm{s}}^{\mathrm{A\ Dem}}$;
- 60 bar steam working area request $\bar{q}_{\mathrm{s}}^{\mathrm{Area\ Dem}}$.

The optimization problem is defined as:

$$\min_{p^{\mathrm{B}},p^{\mathrm{A}},l_{\mathrm{w}}^{\mathrm{A}},Q^{\mathrm{B}},q_{\mathrm{f}}^{\mathrm{B}},q_{\mathrm{s_{out}}}^{\mathrm{B}},s^{\mathrm{B}},q_{\mathrm{s_{in}}}^{\mathrm{A}},q_{\mathrm{s_{out}}}^{A}} J\left(p^{\mathrm{B}}, p^{\mathrm{A}}, l_{\mathrm{w}}^{\mathrm{A}}, Q^{\mathrm{B}}, q_{\mathrm{f}}^{\mathrm{B}}, q_{\mathrm{s_{out}}}^{\mathrm{B}}, s^{\mathrm{B}}, q_{\mathrm{s_{in}}}^{\mathrm{A}}, q_{\mathrm{s_{out}}}^{A}\right) \quad (4.12)$$

where

$$J = \sum_{i=0}^{N-1} \left|\left|u(k+i) - u_{\mathrm{SP}}\right|\right|_R^2 + \left|\left|y(k+i) - y_{\mathrm{SP}}\right|\right|_S^2 + \rho s^{\mathrm{B}} \quad (4.13)$$

where $u_{\mathrm{SP}}(k)$ and $y_{\mathrm{SP}}(k)$ are the setpoint vectors, and subject to the constraints:

$$p_{\mathrm{set}}^{\mathrm{B}} - s^{\mathrm{B}} \leq p^{\mathrm{B}} \leq p_{\mathrm{set}}^{\mathrm{B}} + s^{\mathrm{B}} \quad (4.14a)$$

$$p_{\mathrm{min}}^{\mathrm{A}} \leq p^{\mathrm{A}} \leq p_{\mathrm{max}}^{\mathrm{A}} \quad (4.14b)$$

$$l_{w\,\mathrm{min}}^{\mathrm{A}} \leq l_{\mathrm{w}}^{\mathrm{A}} \leq l_{w\,\mathrm{max}}^{\mathrm{A}} \quad (4.14c)$$

$$Q_{\mathrm{min}}^{\mathrm{B}} \leq Q^{\mathrm{B}} \leq Q_{\mathrm{max}}^{\mathrm{B}} \quad (4.14d)$$

$$q_{\mathrm{f\ min}}^{\mathrm{B}} \leq q_{\mathrm{f}}^{\mathrm{B}} \leq q_{\mathrm{f\,max}}^{\mathrm{B}} \quad (4.14e)$$

$$q_{\mathrm{s\ min}}^{\mathrm{B}} \leq q_{\mathrm{s}}^{\mathrm{B}} \leq q_{\mathrm{s\,max}}^{\mathrm{B}} \quad (4.14f)$$

$$q_{\mathrm{s_{in}\,min}}^{\mathrm{A}} \leq q_{\mathrm{s_{in}}}^{A} \leq q_{\mathrm{s_{in}}\,\mathrm{max}}^{\mathrm{A}} \quad (4.14g)$$

$$q_{\mathrm{s_{out}\,min}}^{A} \leq q_{\mathrm{s_{out}}}^{A} \leq q_{\mathrm{s_{out}}\,\mathrm{max}}^{\mathrm{A}} \quad (4.14h)$$

$$s^{\mathrm{B}} \geq 0 \quad (4.14i)$$

$$q_{\mathrm{f}}^{\mathrm{B}} - q_{\mathrm{s}}^{\mathrm{B}} \geq 0 \quad (4.14l)$$

$$q_{\mathrm{s}}^{\mathrm{B}} \geq q_{\mathrm{s_{in}}}^{\mathrm{A}} + q_{\mathrm{s}}^{\mathrm{Area}} \quad (4.14m)$$

The variable s^{B} in (4.14a and 4.14i) is a slack variable used to allow small changes in the boiler pressure with respect to its set-point value.

Constraint (4.14l) is necessary because the difference between the boiler feedwater and the boiler steam production must be greater or equal to zero, to satisfy the mass balance.

Constraint (4.14m) is necessary because the boiler steam production must be greater, or equal to zero, than the sum of the accumulator inlet steam and the 60 bar area steam.

The accumulator pressure and water level would be in given intervals because of their physical behaviour. In fact, to supply the accumulator steam demand, the accumulator must drop its pressure to create more steam and consequently drop the water level. The MPC controller must regulate the accumulator to not violate these bounds.

CHAPTER 5

MPC CONTROL SIMULATION RESULTS

In this chapter, we show the simulation results obtained by applying the MPC controller to the boiler and the accumulator.

We briefly introduce the main steps to build the state observer for the network. Then we will discuss a series of tests on the overall controlled system.

5.1 – OBSERVER DESIGN

In this chapter, we consider the design of the observer for the LSTM network describing the accumulator.

To this purpose, two possible choices can be taken:

1) nonlinear observer;
2) observer-based on the successive linearized models.

In this chapter, we test both solutions. In the following simulation, solution "2" will be preferred due to the reduced convergence speed with respect to the solution "1".

5.1.1 – NONLINEAR TRIVIAL OBSERVER

The design of a nonlinear observer is the first possible choice for the LSTM model. In particular, a simple solution is to use an "open-loop" observer: this consists basically of the LSTM model fed by the actual inputs applied to the system.

This is possible, however, only provided that the identified LSTM model guarantees incremental stability properties.

To empirically prove the existence of such properties, we simulate the network from different initial conditions but with the same (constant) input. The goal is to see if the network converges to the same point. The following table reports the different initial conditions tested (in terms of "external" variables).

Test number	$q^A_{s_{in}}$ [m^3/s]	$q^A_{s_{out}}$ [m^3/s]	$h^A_{s_{in}}$ [kJ/kg]	p^A [Bar]	l^A_w [%]
1	0.15	0.15	2793	53.9	84.1
2	0.106	0.102	2794	54	84.2
3	0.017	0.03	2794	54.1	84.3
4	0.27	0.57	2795	52.8	83.4
5	0.42	0.37	2792	53.5	83.5
6	0.34	0.7	2792	53.2	83

Table 5.1 – Accumulator LSTM network initial conditions

In all these tests we apply the time-varying input depicted in *Figure 5.1.* These input signals are randomly generated, with a sampling time $T_s = 10\ s$. We define as "test 1" the 2-norm state trajectory $||\hat{x}||_2$ as the reference state trajectory of the network for the corresponding inputs. Therefore, at each time instant *k*, we have

$$\left|\left|\hat{x}\ (k)\right|\right|_2 = \left|\left|x_{net}(k)\right|\right|_2$$

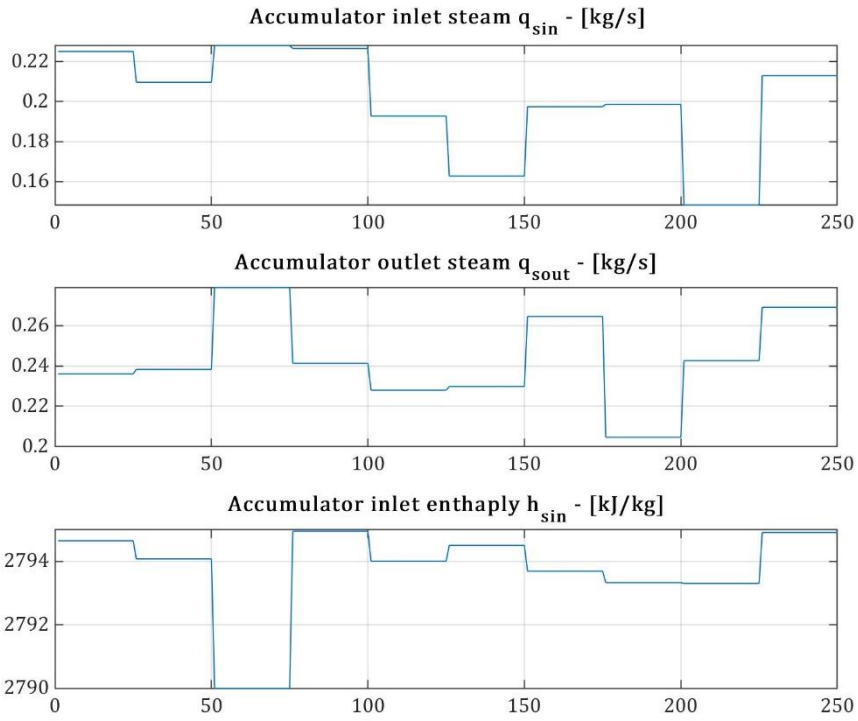

Figure 5.1 – Network time dependent inputs

Then, we define the error between the 2-norm of the other network simulation state trajectory $||x_i||_2$ and the reference state trajectory $||\hat{x}||_2$:

$$err_{i1} = \left|||\hat{x} - x_i||\right|_2$$

where i (from 2 to 6), identifies the number of the performed network simulations. The behaviour of these errors is depicted in the following figure.

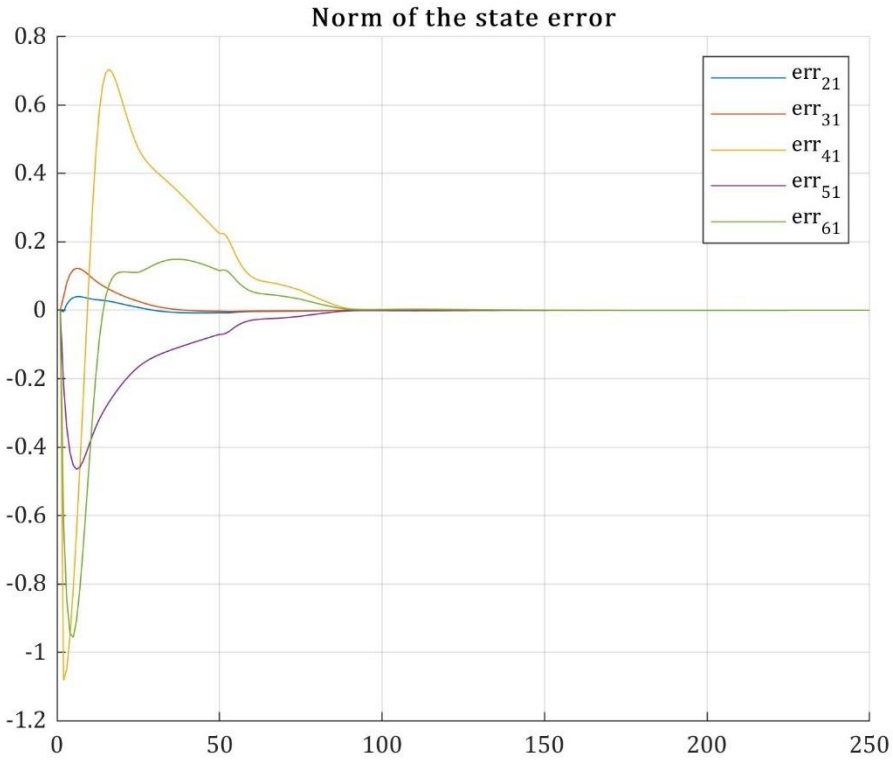

Figure 5.2 – State trajectory error

As we can see from *Figure 5.2,* the error of the state trajectories tend to zero. In view of these results, we can conclude that, in the tested conditions, the identified LSTM network exhibits the required incremental stability property.

In view of this, the trivial nonlinear observer can be employed. However, in view of the fact that the settling time is rather slow, we analyse and design the Kalman filter-based observer, which provides faster settling times, as it is discussed in the following section.

5.1.2 – STATIC KALMAN FILTER IMPLEMENTATION

In this section we design a Kalman type observer derived from the successive linearized models of the LSTM derived in *Chapter 4.1.3.*

As discussed in *Chapter 4.1.3*, the evolution of the system is described by the "local" linearized model:

$$\begin{aligned} x(k+1) &= A_{\mathrm{k|h-1}}x(k) + B_{\mathrm{k|h-1}}u(k) + d_{\mathrm{k|h-1}} \\ y(k) &= Cx(k) \end{aligned} \quad (5.1)$$

where matrices $A_{\mathrm{k|h-1}}, B_{\mathrm{k|h-1}}$, and vector $d_{\mathrm{k|h-1}}$ are defined in *Chapter 4.1.3,* while matrix C is given by:

$$C = [0\ 0\ W_{out}] \quad (5.2)$$

where W_{out} is the output layer of the LSTM network and the *zeros* are needed because this matrix must multiply only the LSTM network controllable state $x(k)$. Therefore, the number of zeros in the matrix are equal to half of the number of states of the network plus the number of inputs of the network.

The corresponding observer is [9]:

$$\hat{x}(k+1) = A_{\mathrm{k|k-1}}\hat{x}(k) + B_{\mathrm{k|k-1}}\hat{u}(k) + d_{\mathrm{k|k-1}} + L_k[y(k) - C\hat{x}(k)] \quad (5.3)$$

where $\hat{x} \in \mathbb{R}^n$ and

$$L_h = A_{\mathrm{k|k-1}}P_kC'(CP_kC' + R)^{-1} \quad (5.4)$$

and where P_h is the solution of the following algebraic Riccati equation:

$$P_k = A_{\mathrm{k|k-1}}P_kA'_{\mathrm{k|k-1}} + Q - A_{\mathrm{k|k-1}}P_kC'(CP_kC' + R)^{-1}CP_kA'_{\mathrm{k|k-1}}$$

The Q and R values are chosen to have a fast observer, so the matrix R is smaller with respect to Q:

$$Q = I_n$$

$$R = 0.01$$

In *Figure 5.3* and *5.4* we can see the convergence of the observer outputs to the ones of the model. By comparing these plots with the ones in *Figure 5.2,* we see that the observer presented in this section enjoys the convergence properties, and will, therefore, be used in the following sections.

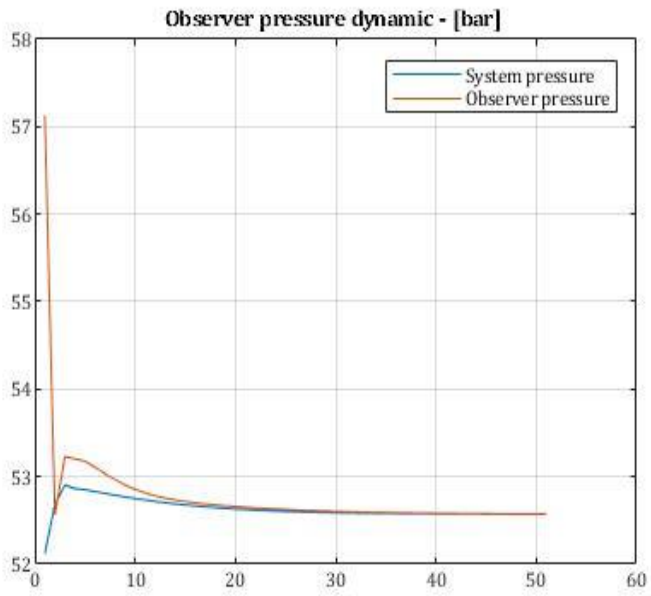

Figure 5.3 – Observer pressure dynamic

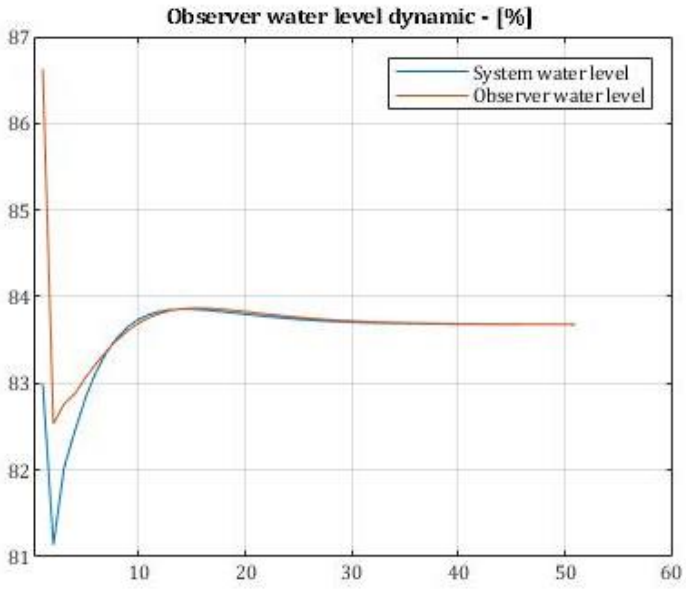

Figure 5.4– Observer water level dynamic

5.2 – WEIGHTS IN THE COST FUNCTION

In our implementation the number of states, inputs, and outputs is reported in the following table:

System variable	Boiler	Accumulator	Total system
State n	1	103	104
Input m	4	3	7
Output p	1	2	3

Table 5.2 – Boiler and accumulator linear system variables

As already discussed:

- the six manipulable inputs are:
  - boiler feedwater mass flow rate $q_{\mathrm{f}}^{\mathrm{B}}$;
  - boiler power Q^{B};
  - boiler outlet steam mass flow rate $q_{\mathrm{s_{out}}}^{B}$;
  - accumulator inlet steam mass flow rate $q_{\mathrm{s_{in}}}^{A}$;
  - accumulator outlet steam mass flow rate $q_{\mathrm{s_{out}}}^{A}$;
- the two non–manipulable inputs are:
  - boiler feedwater enthalpy $h_{\mathrm{f}}^{\mathrm{B}}$;
  - accumulator inlet steam enthalpy $h_{\mathrm{s_{in}}}^{A}$.

The three system's outputs are:

- boiler pressure p^{B};
- accumulator pressure p^{A};
- accumulator water level $l_{\mathrm{w}}^{\mathrm{A}}$.

The weight matrices Q and R of the optimization problem (4.12) are diagonal and are defined in order to achieve the main control goals of the system. Firstly, the boiler pressure must be maintained near its setpoint. Secondly, the boiler and accumulator steam mass flow rate demands must be satisfied. In view of these goals, the weight on these variables must be large. The other variables in the system must change their values to achieve these two primary goals, so they can be different from their setpoint since a lower weight is assigned to them. The weights of all variables are listed in the following table

Variable	Weight
Boiler pressure	10^{10}
Boiler feedwater	10^{11}
Boiler heat	10^{-3}
Boiler outlet steam	10^{8}
Accumulator pressure	10^{0}
Accumulator water level	10^{0}
Accumulator outlet steam	10^{5}

Table 5.3 – Variables' weight

It is worth to remind that the system's constraints are represented by (4.14a to 4.14m). In constraint (4.14a) we have also defined a slack variable to soft the boiler pressure constraint. The weight of such variable is set to 10^{7}.

5.3 – SIMULATION TEST RESULTS

In this chapter we show some significant simulation tests, demonstrating the potentiality of the controller designed in *Chapter 4.*

Note that the feedwater enthalpy in these tests will be considered as a constant non-manipulable input. Note that in all plots, the sampling time is 10 seconds. Moreover, as a legend for the following figures, we defined the following pattern for colours and lines: blue and solid for outputs; red and solid for non-manipulable inputs; green and solid for manipulable inputs; magenta and dotted for profile setpoint.

Some of the constraints defined in (4.14) are specifically given by:

$$57.8 - s^{\mathrm{B}} \leq p^{\mathrm{B}} \leq 57.8 + s^{\mathrm{B}} \ \text{[bar]} \quad (5.5a)$$

$$36 \leq p^{\mathrm{A}} \leq 60 \ \ \text{[bar]} \quad (5.5b)$$

$$0 \leq l_{\mathrm{w}}^{\mathrm{A}} \leq 84 \ \ [\%] \quad (5.5c)$$

$$1410 \leq Q^{\mathrm{B}} \leq 3130 \ \ [k\mathrm{W}] \quad (5.5d)$$

The constraint (5.5a) change dynamically with the evolution of the system. Considering constraint (4.14*f*), the maximum value that the boiler steam production can reach is set to the maximum steam production rate of the boiler, that is 1.4 kg/s. This value is taken directly from the datasheet of the boiler.

$$0 \leq q_{\mathrm{s}}^{\mathrm{B}} \leq 1.4 \ \text{[kg/s]} \quad (5.5e)$$

The constraint for the steam flow rate at the accumulator outlet (4.14*h*) is time-varying with respect to the accumulator steam demand at time step k:

$$0 \leq q_{\mathrm{s_{out}}}^{A} \leq q_{\mathrm{s_{out}}}^{\mathrm{A\,Dem}}(k) \ \ \text{[kg/s]} \quad (5.5f)$$

The boiler feedwater must follow the boiler steam demand profile in order to guarantee that constraint (4.14*l*) is always satisfied.

5.3.1 – BOILER PRESSURE SETPOINT CHANGES

In this first test, the system is subjected to a pressure setpoint step change.

We start the simulation where the boiler setpoint pressure is 57.8 bar. Then we change this setpoint value to 55.8 bar. The next figure shows the simulation results.

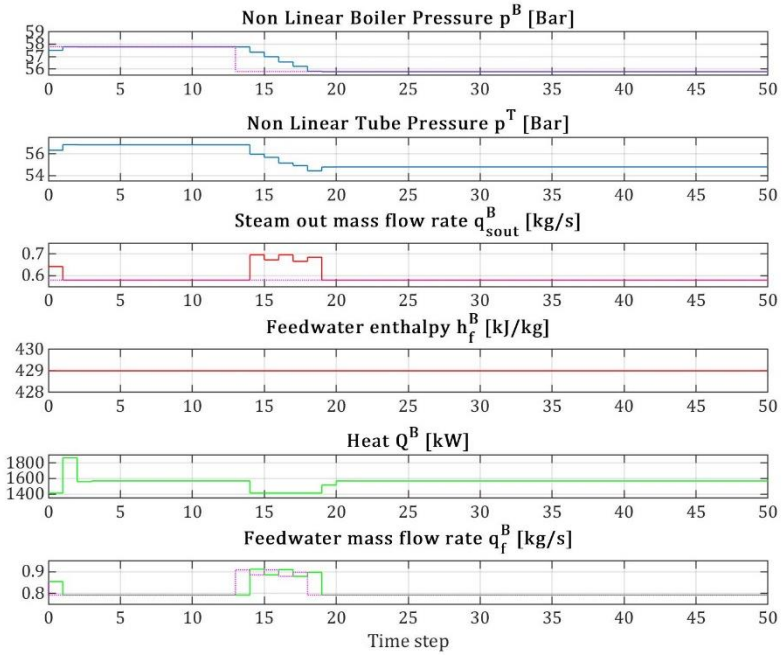

Figure 5.5 – Boiler pressure setpoint change simulation result

We can see from *Figure 5.5* that after reaching the first setpoint, the system stays in steady-state condition until sample 14. After this point, the pressure setpoint changes and we can see that the MPC control increases the inlet water and outlet steam mass flow rate and decrease the power. This decreases the pressure. When the new setpoint is reached the mass flow rates return to their nominal values and the power goes to its new steady-state value. It has to be noticed that, when the step change occurs, the boiler power reaches suddenly the minimum constraint (5.5d). Concurrently, the MPC controller increases the feedwater flow rate since the system leads to a faster

The system chooses this type of control action because it can not further reduce the heat because it has reached already the minimum possible at sample 14. For this reason, to have a fast pressure response, the controller increases the feedwater since this led to a faster pressure drop.

5.3.2 – BOILER STEAM MASS FLOW RATE REQUEST SETPOINT CHANGES

In the second test, the response of the system to a step change of steam demand is presented.

The initial value of the steam demand, 0.58 kg/s, is increased at $\tau = 4$ to 1.16 kg/s and is kept constant for 3 samples and then set back on the original value. *Figure 5.6* shows the simulation result.

At $\tau = 4$ the boiler steam demand rises to the new setpoint value. We can see that the feedwater and the power rise to follow the increased demand. The boiler pressure varies a little from its setpoint. This is allowed by the slack variable used in its constraint (5.5a) permits small pressure changes. This allows the system to be faster in tracking setpoint changes because the constraint on the boiler pressure has been softened. The tube pressure drops due to the augmented steam mass flow rate. Nevertheless, this drop is limited by the boiler pressure rise. After sample 8, the steam demand returns to its nominal value and the system goes back to its steady-state condition.

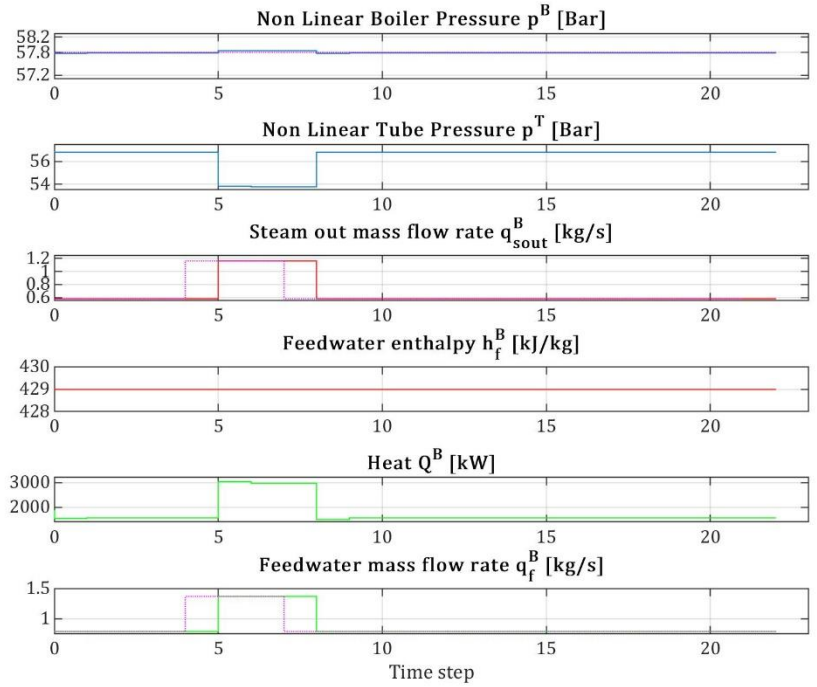

Figure 5.6– Boiler steam demand setpoint change simulation result

In the next figure, we can see the results of the same simulation on accumulator variables.

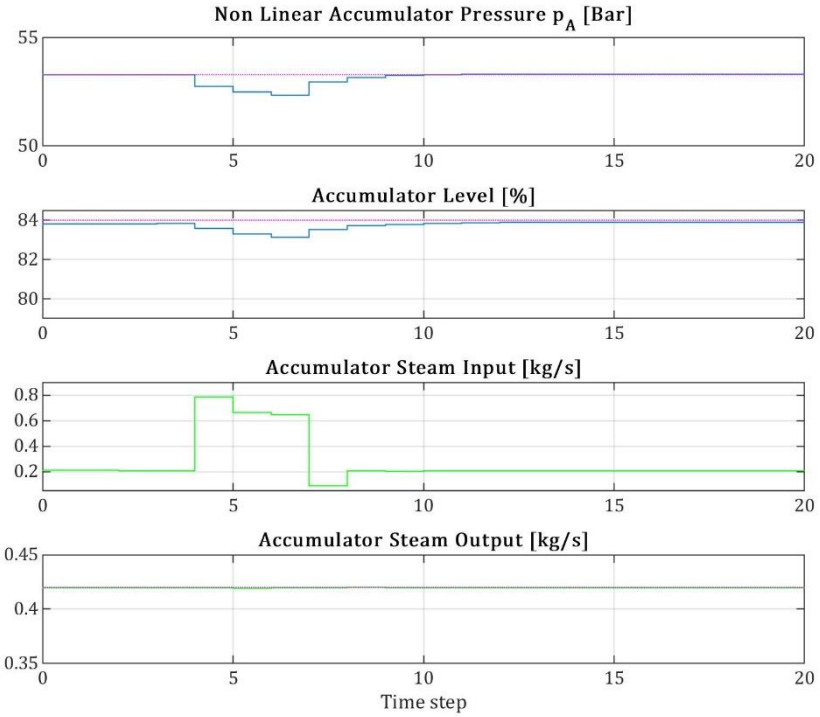

Figure 5.7 – Accumulator simulation result when boiler steam demand changes

From the accumulator point of view, the variation of the boiler steam demand creates no negligible effect. We can notice that the controller decides to charge all the surplus produced boiler steam into the accumulator since we do not have other steam requests. The accumulator pressure drops by a few bars because the inlet steam has lower enthalpy due to the tube pressure drop. This leads to a small drop also of the water level due to a variation of density. When the tube pressure returns at its nominal value, also the accumulator pressure comes back to its nominal value. The water level instead is raised of some

percentage due to the new charged steam. The controller has been designed with low weights on the accumulator pressure and water level since their variation from the nominal values are acceptable.

5.3.3 – ACCUMULATOR OUTLET STEAM DEMAND CHANGES

In the last test, the steam demand at the accumulator outlet is changed, in particular, at $\tau = 2$ the demand is increased to value of 1.26 kg/s. The step demand variation is kept at a high level for 3τ and then it returns to the initial value of 0.42 kg/s. *Figure 5.8* shows the simulation result.

We can see that the system is in steady-state operating condition until sample 4. When the accumulator outlet steam demand changes and we can see that the pressure starts dropping to allow the water to evaporate. This phenomenon causes the drops also of the water level. After the steam demand comes back to its nominal value, the system slowly returns to its steady-state condition. This is explained as follows: when the pressure stops dropping, the water stops evaporating. So, the inlet steam condenses in the water and the level rise, while the outlet steam request is satisfied by the steam already present in the accumulator.

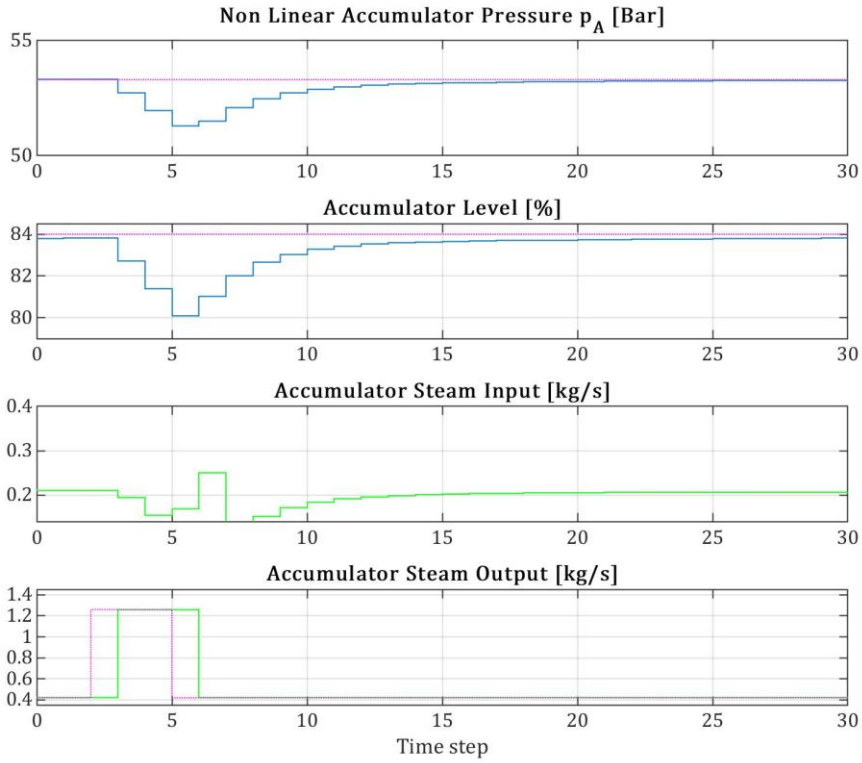

Figure 5.8 – Accumulator outlet steam demand change simulation result

The accumulator results described here and in *Chapter 5.3.2* are consistent with the data used to train the LSTM network presented in *Chapter* 3.5.3. We point out that in our results, and in the plant data, the water level is constant whenever the ratio between the inlet steam and outlet steam is constant. This because the water level mainly depends on the pressure value and so, on the water enthalpy value that is crucial to properly calculate the water density.

5.3.4 – SIMULATION USING REAL PLANT DATA

In this section, we simulate the system using the real plant data set. We take the boiler and the accumulator data set referred to the 07 January 2019. The boiler data set is shown in the following figure with a sampling time $T_s = 10s$, while the accumulator one was already presented in *Figure 3.22.*

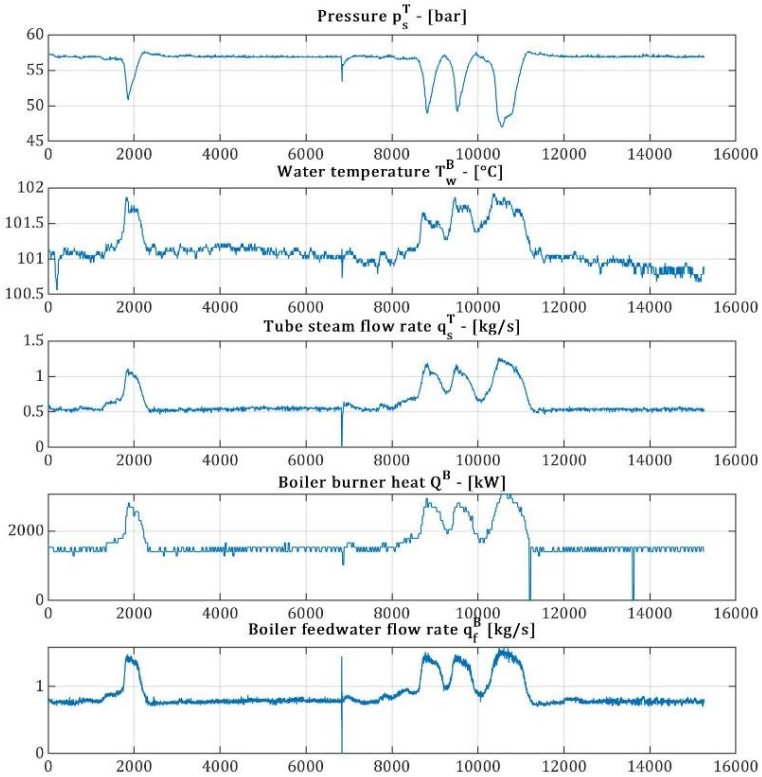

Figure 5.9 – Original signals of file 01 January 2019

In the simulation, we use the following data as input:

- boiler feedwater temperature T_w^B to find the feedwater enthalpy (note that in previous tests, this was assumed constant);
- tube steam flow rate q_s^T, as boiler steam demand;
- accumulator outlet steam mass flow rate $q_{s_{out}}^A$, as accumulator steam demand.

In addition to these data, we create a steam demand from the so-called "60Bar Area", that takes part of the steam flowing in the tube. We arbitrarily create it because the real data is not available to use. We define this steam demand as the difference between the tube steam mass flow rate and the accumulator inlet steam data:

$$q_{s_{60Bar}}^{Dem} = q_s^T - q_{s_{in}}^A$$

The goal of the system is to generate enough steam to satisfy all the steam demands, while the MPC controls that the variables stay in their limits.

The next two figures show the simulation results. We plot the simulation results with the colours defined at the beginning of the chapter and the original plant data as dotted line (where not otherwise specified).

We can see in *Figure 5.10* panel 3 and in *Figure 5.11* panel 4 and 5 that all the three steam requests are successfully satisfied by the system.

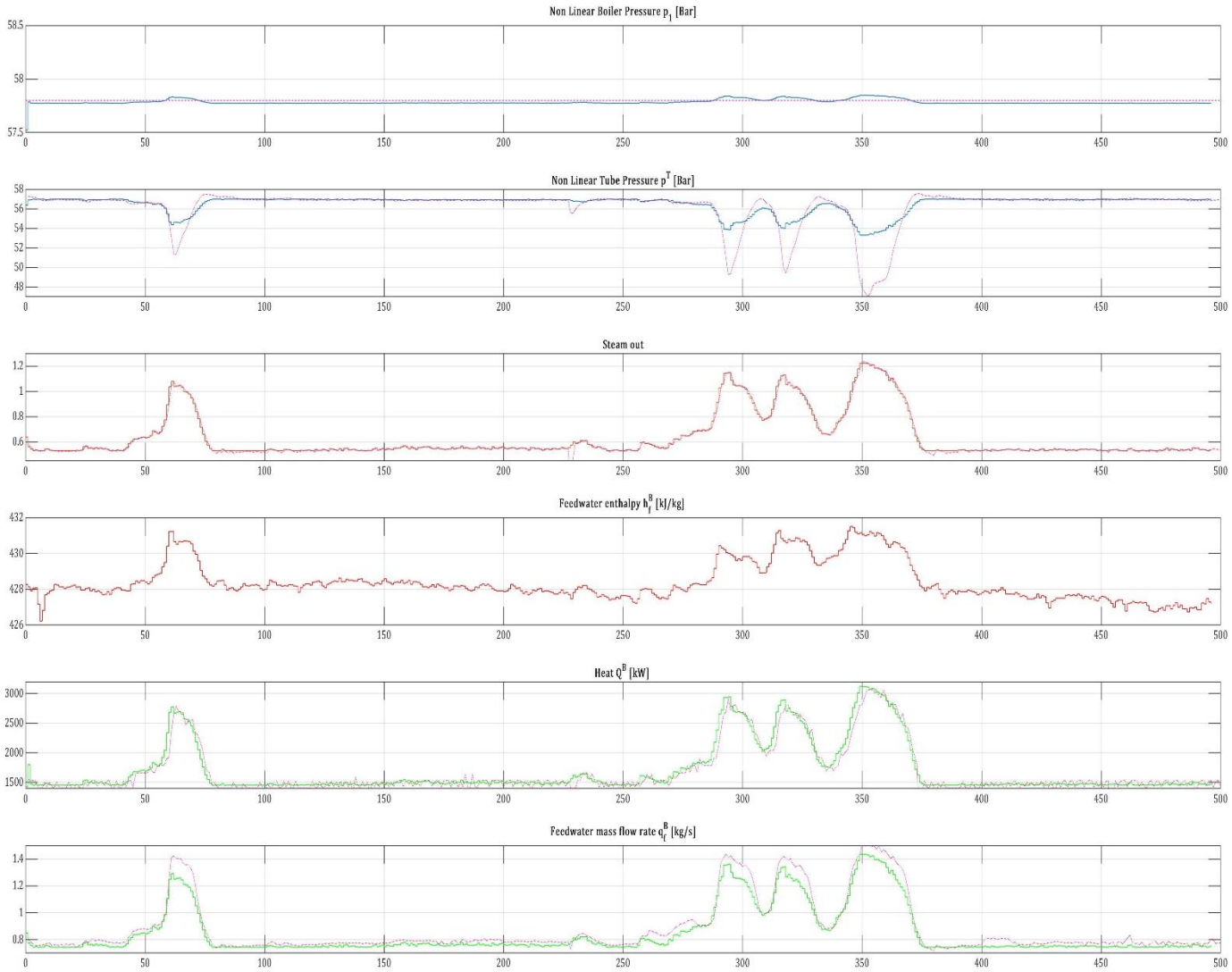

Figure 5.10 – Boiler simulation result

In *Figure 5.10* panel 1 we can see that the boiler pressure is always near its setpoint of 57.8 bar (dotted line). We can notice that when the steam production increases, the pressure slightly increases too. This because the slack variable used in the pressure bound constraint, allows small pressure variation. In panel 2 of the same figure, we can see the tube pressure that has a similar behaviour to the original data, but its drops are smaller. In panel 5 we can see the boiler heat and it is similar to its corresponding original data. It is slightly higher since the pressure constraints are stronger than the real plant ones. Note that the increase in heat made by the MPC controller is in advance with respect to the original plant data. This different control action leads to the small rise of the boiler pressure and to the smaller drops of the tube pressure. The last panel shows the feedwater mass flow rate that must be high enough to produce the requested steam. We notice that the system uses less water to produce the same amount of steam. This is justified by the more efficient use of the heat, that makes the system faster.

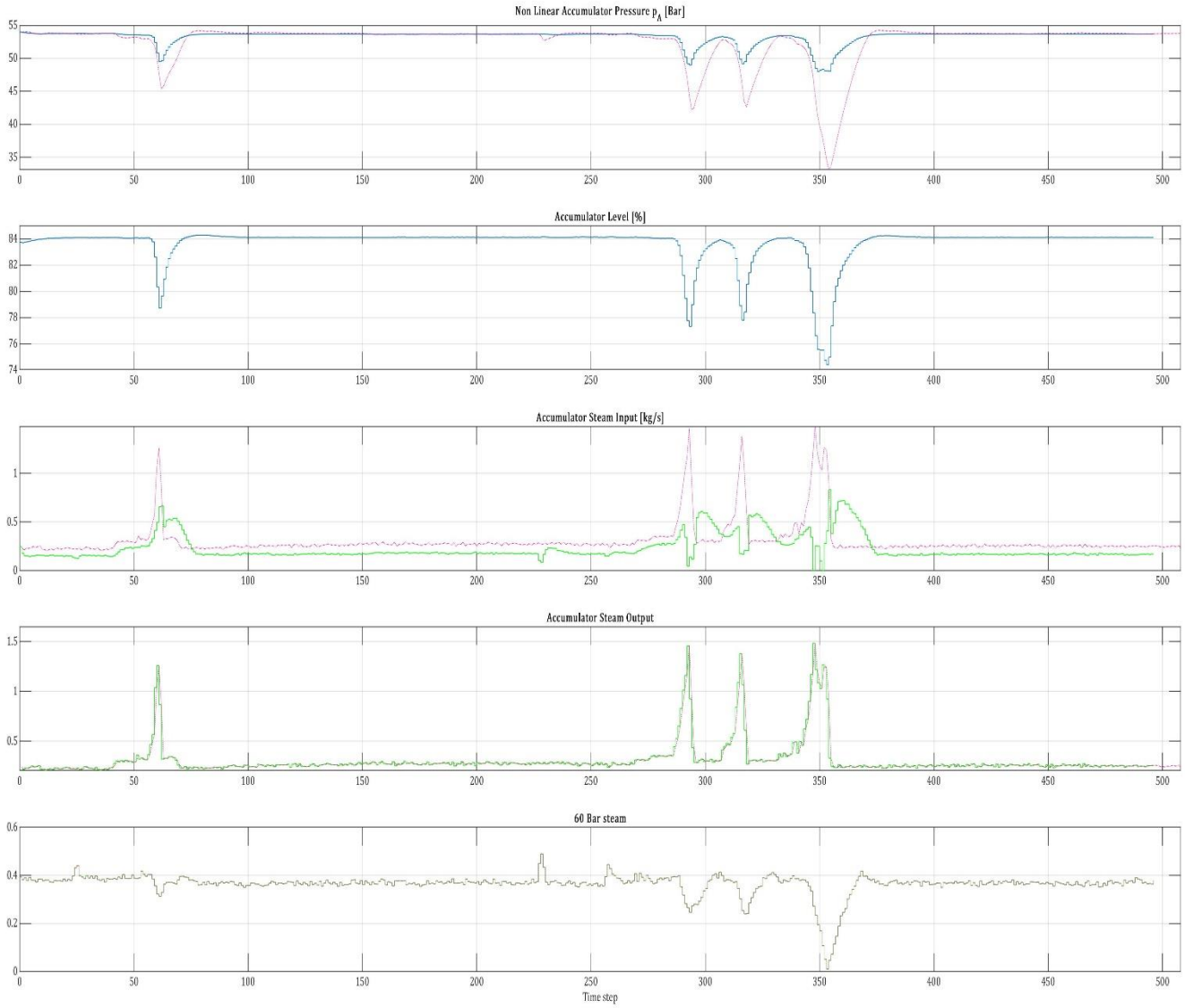

Figure 5.11 – Accumulator simulation result

In *Figure 5.11* panel 1 we show the accumulator pressure. The pressure drops when the accumulator steam demand increases. Compared with the original pressure it follows the same behaviour, but the reductions are smaller. The same consideration can be done for the water level (*Figure 5.11* panel 2). Some different behaviour can be seen for the accumulator inlet steam mass flow rate (*Figure 5.11* panel 3). Here the controller decides to decrease the inlet steam in high-production condition for the outlet steam. We point out that in this condition the tube pressure is lower than the steady-state value, and then the inlet steam enthalpy is lower too. Therefore, a higher inlet steam mass flow rate with this lower enthalpy would have provoked a larger pressure drop.

CHAPTER 6

BOILER ENSEMBLE HIERARCHICAL CONTROL

6.1 – INTRODUCTION

A centralized controller (especially based on optimization-based method like MPC) for large-scale systems is often undesirable and difficult to implement. The dimension of the optimization problem grows with the number of subsystems composing the global process and for a large number of subsystems, the computational demand explodes. Other drawbacks of centralized strategies are their poor flexibility and reliability and the facts that they are not scalable and difficult to maintain. For these reasons other algorithms have been developed for large-scale systems. The most popular ones are:

- Decentralized;
- Distributed;
- Hierarchical.

In decentralized and distributed configurations, the centralized optimization problem is replaced by different parallel local ones in order to achieve global or local objectives. While in decentralized MPC communication between subsystems is not required, in distributed formulations input, state, and output variables can be broadcast to neighbour subsystems to obtain performance comparable with those of centralized controllers or to foster stability.

Hierarchical formulations are widely used in the industrial realm. They are very effective e.g. when controlling systems with separable fast and slow dynamics, and for the coordination of subsystems and when it is desirable to consider different objectives in the same problem. In many hierarchical structures a centralized MPC in used a the high level at a slow time scale to achieve long-term goals, with the possibility to use a simplified model in the design phase, while decentralized or distributed MPC regulators are designed at the low levels at a fast time scale to achieve short-term performance using full orders model.

In recent years many hierarchical control algorithms have been proposed for the optimal control of large-scale systems. Most times these approaches usually have superior short and long term performances compared with distributed methods. They also have many computational advantages with respect to centralized controllers.

Hierarchical MPC methods rely upon different control layers (multilayer structure), also called levels, and are used mainly in two non-exclusive cases:

1) low-level local controllers are used to achieve local goals while a high-level coordinator has the goal to minimize a global performance index and/or satisfy consistency constraints;
2) the high-level controller works at a slow time scale computing the reference signals to be used at the low level, while the low-level controllers solve tracking problems at a fast time scale.

At the upper-layer, Real-Time Optimization (RTO) is often used to compute the steady-state operating points for the low-level controllers according to an economic optimization criterion. Such optimization can be based on a static nonlinear model of the whole system or on a dynamic one, depending on the needs.

At the lower layer, a simpler linear dynamic model of the same system is used to design an MPC regulator that guarantees that the reference values computed and transmitted by the high level are reached satisfying a given set of constraints.

In the next figure, the described structure is represented.

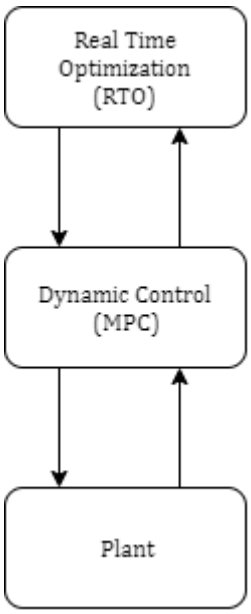

Figure 6.1 – General structure of hierarchical control for plantwide control

In the proposed hierarchical structure, the higher layer (RTO) plays a major role, given the fact that the whole control system relies on the set-points transmitted by it [9]. Some issues must be considered:

- the static model used has to be periodically updated by means of some kind of reconciliations procedure to deal with possible model mismatches and slow disturbances;
- consistency between the models of the upper layer and the lower layer should be ensured;
- an accurate steady-state target optimization must be done to guarantee that the set-points computed by the upper-layer should be reachable by the MPC regulator.

Time-scale separation can be employed when long term-goals such as economic indices have to be achieved with a sampling rate of hours or days, while the short-term behaviour of the actuators should be considered at a much faster sampling interval of minutes or seconds.

6.2 – HIERARCHICAL MPC FOR BOILER ENSEMBLE

Here we discuss the implemented algorithm for the hierarchical control of a boiler steam generator ensemble. The following presented work and results are subjects to the paper submitted for the 21st IFAC World Congress 2020 [1].

More specifically, we consider a group of N_B boiler steam generators that work in a parallel configuration to sustain a cumulative steam demand $\bar{q}_s^{\mathrm{Dem}}$. We aim to fulfil the required steam flow rate, with the minimum amount of fuel gas and optimizing the contribution of each boiler to the overall demand. We assume that the boiler steam generators, although different in dimension, steam, firing rates, and efficiency, are homogeneous dynamical systems, i.e. sets of similar subsystems in terms of input and output.

Subsystem *i* is represented by the boiler presented in *Chapter 3.2.* The single subsystems and the ensemble are subjected to input and output constraints. More specifically, we assume that convex and compact sets $\mathcal{U}_i, \mathcal{Y}_i, \bar{\mathcal{U}}$ and $\mathcal{Y}$ are defined in such a way that

$$q_{\mathrm{s,i}} \in \mathcal{U}_i \quad (6.1a)$$

$$Q_\mathrm{i} \in \mathcal{Y}_i \quad (6.1b)$$

$$\bar{Q} = \sum_{i=1}^{N_\mathrm{B}} Q_\mathrm{i} \in \bar{\mathcal{Y}} \quad (6.1c)$$

$$\bar{q}_\mathrm{s} = \sum_{i=1}^{N_\mathrm{B}} q_{s,i} \in \bar{\mathcal{U}} \quad (6.1d)$$

where $q_{\mathrm{s,i}}$ is the steam mass flow rate generated by boiler *i, Q* is the generated heat, $\bar{Q}$ is the total generated heat, and $\bar{q}_\mathrm{s}$ the total produced steam.

The proposed control scheme consists of three layers.

1) The top layer computes the optimal shares of production to be allocated to each boiler based on the requested profile $\bar{q}_s^{\mathrm{Dem}}$ minimizing the produced heat. This includes the possibility to activate and deactivate boilers in the ensemble. The sharing factors α_i are defined such that

   $$q_{\mathrm{s,i}} = \alpha_\mathrm{i} \bar{q}_\mathrm{s} \quad (6.2)$$

   where $\alpha_i \in [0, 1]$ and

   $$\sum_{i=1}^{N_\mathrm{B}} \alpha_\mathrm{i} = 1 \quad (6.3)$$

   This layer must avoid inconsistencies and constraint violation at the lower levels.

2) At medium control layer, we use an MPC algorithm applied to the aggregate low-order model of the system ensemble to track the overall demand $\bar{q}_\mathrm{s}$. At the same time, the MPC controller determines the local steam request $q_{\mathrm{s,i}}$ for each subsystem.
3) At the lowest layer, we use a decentralized set of proportional-integral (PI) controllers, to track the individual request and regulating the boiler internal pressure. This layer works at faster sampling time τ with respect to the others to improve the performance of the control of the ensemble. We denote with κ the corresponding time index.

In *Figure 6.2*, we can see a schematic view of the system's control layers.

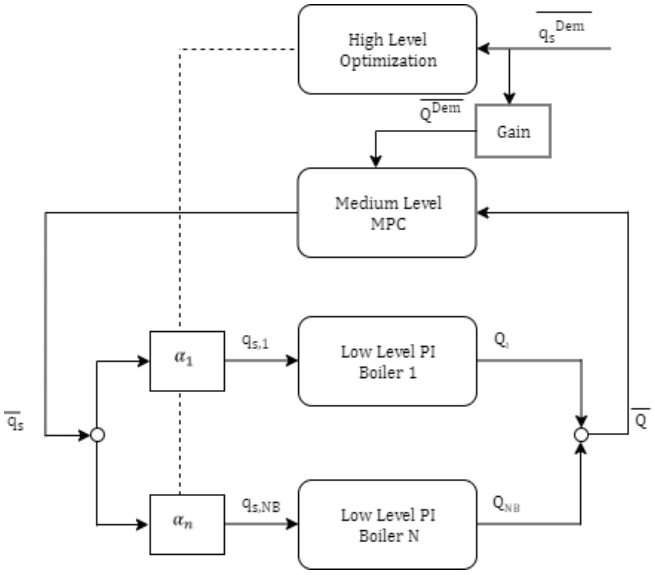

Figure 6.2 – Hierarchical structure

The block "*Gain*" in *Figure 6.2* is used to convert the steam demand $\bar{q}_s^{\mathrm{Dem}}$ into the corresponding numerical value of $\bar{Q}^{\mathrm{Dem}}$ that is needed by MPC as reference.

The ensemble we consider in our study case is composed of five boiler generators. These five components work all at the same pressure, but they are different in size, steam rating, and power efficiency. In the following table, the five boiler parameters are summarized.

Boiler	Total volume [m^3]	Total mass [kg]	Heat efficiency η [%]	Heat equilibrium [kW]	Feedwater equilibrium [m^3/s]
1	1.21	5499	97	1370	0.58
2	1.15	5225	92	1453	0.58
3	1.28	5830	89	1523	0.58
4	1.11	5060	95	1407	0.58
5	1.32	5995	99	1350	0.58

Table 6.1 – Boiler parameters

The parameters of boiler 1 are the ones presented in *Chapter 3.3.3,* while the parameters of the other four boilers are arbitrary.

6.3 – LOW LEVEL CONTROLLERS

As mentioned before, the 60-bar boiler non-linear dynamical system is the one presented in *Chapter 3.2.* In this chapter, for the sake of simplicity of notation, we avoid using the superscript "B" since all the variables are referred to boilers.

6.3.1 – LOW LEVEL CONTROL CONFIGURATION

In this chapter, the low-level controllers are embedded in each subsystem and operate on the local input variables $q_{\mathrm{f,i}}$ and Q_{i} to maintain the pressure at the setpoint level. We assume that a PI regulator R and a disturbance compensator C act on the heat and on the feedwater mass flow rate, respectively, as depicted in the following figure.

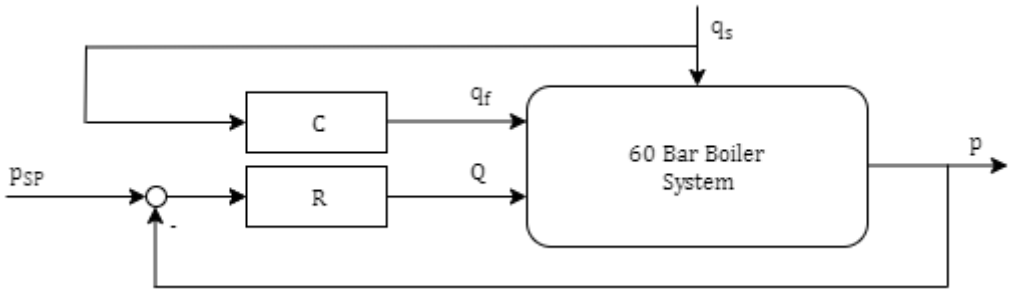

Figure 6.3 – Boiler steam generator closed-loop system

R is a feedback controller regulating the pressure to a setpoint p_{SP}, while the compensator C forces, with an open-loop action, the feedwater to follow the steam demand. As a result, the i-th boiler, controlled at low level, can be described as a nonlinear dynamic model φ_i, denoted as

$$Q_{\mathrm{i}} = \varphi_{\mathrm{i}}(q_{\mathrm{s,i}}) \quad (6.4)$$

The steam mass flow rate can be accounted for as input of the control system, while the heat will be considered as an output. This reverse vision of the boiler, with respect to the actual physical flows of heat and steam, permits to formalize the problem in the framework of hierarchical control of ensemble systems.

6.3.2 - REGULATORS IDENTIFICATION

The parameters of the PI regulator R and of the compensator C were defined in order to reproduce the current available closed-loop plant data. We have built an error vector for the pressure and the feedwater defined as

$$error(i) = Setpoint - Data\_value(i)$$

where i runs from zero to the length of *Data_value, Setpoint* is the actual setpoint of the considered variable. After that, we start the identification of the PI parameters using the Matlab function *fmincon*.

For example, regarding the PI regulator R, the generic control input of the regulator as:

$$u_{\mathrm{gen}} = u_{\mathrm{eq}} + K_p\, err_P + K_I\, err_{\mathrm{I}}$$

where u_{eq} is the equilibrium input value, err_{P} and err_{I} are the proportional and integral error, and K_p and $K_I$are the proportional and integral coefficients that have to be identified. So, we have four parameters to identify since we have two PI regulators. To find these parameters we minimize the cost function defined as:

$$\min_{KP_1,KI_1,KP_2,KI_2} \left(u^1_{\mathrm{gen}} - u^1_{\mathrm{data}}\right)^2 + \left(u^2_{\mathrm{gen}} - u^2_{\mathrm{data}}\right)^2$$

where $u_{\text{gen}}^{\text{j}}$ is the generated input of regulator $j = 1,2$ and $u_{\text{data}}^{\text{j}}$ is the real available plant data.

The transfer function of *R* and *C* result:

$$u_R(k) = \left(0.87 + 0.31\frac{T_s}{z-1}\right)e_R(k)$$

$$u_C(k) = \left(3.54 \text{ x } 10^{-4} + 0.1\frac{T_s}{z-1}\right)e_C(k)$$

where T_s is the sampling time, and $e_R(k), e_C(k)$ are the errors.

These two regulators are used in the Low layer control and they are equal for each boiler.

6.4 – HIGH LEVEL OPTIMIZATION

The high level is devoted to the optimization of the sharing factors α_i, which define the partition of the overall demand among the subsystems of the ensemble. This optimization layer considers the functioning range of each subsystem in the ensemble to ensure the best share resources and the minimization of the associated operating cost. Here a static optimization layer is discussed. In a static environment, we define $g_i = C_i\left(I_{n_i} - A_i\right)^{-1} B_i$.

We assume that $\bar{q}_{\mathrm{s}}^{\mathrm{Dem}}$ is given. Our scope is to compute, at the same time, the corresponding shares α_i and a feasible steady-state overall steam production value $\bar{u}_{ss}$, as close as possible to the demand $\bar{q}_{\mathrm{s}}^{\mathrm{Dem}}$, but which, at the same time, allows to fulfil constraints (6.1a-d) where we have:

$$\mathcal{U}_i = \left[u_{min,i}, u_{max,i}\right]$$

$$\mathcal{Y}_i = \left[y_{min,i}, y_{max,i}\right]$$

$$\bar{\mathcal{U}} = [\bar{u}_{min}, \bar{u}_{max}]$$

$$\bar{\mathcal{Y}} = [\bar{y}_{min}\bar{y}_{max}]$$

A further constraint must be enforced, to guarantee consistency with the medium level controller. More specifically, at medium level, a limitation on the variation of the input value between two consecutive steps is enforced to be lower, in absolute value, than $\Delta\bar{u}$, for all active boilers. In this respect, we introduce the integer variable δ_i, being $\delta_i = 1$ if the boiler *i* is active, while $\delta_i = 0$ otherwise. At higher level, this can be required, for each subsystem, as follows:

$$\left|\alpha_i \bar{u}_{ss} - \delta_i \alpha_i^{\mathrm{old}} \bar{u}_{\mathrm{ss}}^{\mathrm{old}}\right| \leq \Delta\bar{u}$$

where $\alpha_{\mathrm{i}}^{\mathrm{old}}$ and $\bar{u}_{\mathrm{ss}}^{\mathrm{old}}$ are the value of α_i and $\bar{u}_{\mathrm{ss}}$ applied before the optimization is solved.

A mixed-integer program with bilinear inequality constraints is formulated, also allowing for the possibility of having different weights λ_i for each subsystem, e.g. related to the cost of using every single boiler. The optimization problem reads:

$$\min_{\alpha_i, \delta_i, \bar{u}_{\mathrm{ss}}} \sum_{i=1}^{N_{\mathrm{B}}} \lambda_i (g_i \alpha_i \bar{u}_{\mathrm{ss}} + \delta_i \gamma_i) + \bar{\lambda}\left(\bar{u}_{\mathrm{ss}} - \bar{q}_{\mathrm{s}}^{\mathrm{Dem}}\right)^2 \quad (6.5)$$

such that

$$\sum_i \alpha_i = 1$$

$$\bar{u}_{\min} \leq \bar{u}_{\mathrm{ss}} \leq \bar{u}_{max}$$

$$\bar{y}_{min} \leq \sum_{i=1}^{N_{\mathrm{B}}} (g_i \alpha_i \bar{u}_{\mathrm{ss}} + \delta_i \gamma_i) \leq \bar{y}_{max}$$

and for all $i = 1, \ldots, N_{\mathrm{B}}$

$$u_{min,i}\delta_i \leq \alpha_i \bar{u}_{\mathrm{ss}} \leq u_{max,i}\delta_i$$

$$y_{min,i}\delta_i \leq g_i \alpha_i \bar{u}_{\mathrm{ss}} + \delta_i \gamma_i \leq y_{max,i}\delta_i$$

$$-\Delta\bar{u} \leq \alpha_i \bar{u}_{\mathrm{ss}} - \delta_i \alpha_{\mathrm{i}}^{\mathrm{old}} \bar{u}_{\mathrm{ss}}^{\mathrm{old}} \leq \Delta\bar{u}$$

$$0 \leq \alpha_i \leq 1$$

$$\delta_i \in \{0,1\}$$

The high level optimization can be either event-based or cyclically executed. In event-based mode, the triggering can be done when the steam demand varies significantly with respect to the value used in the previous run of the high level itself.

6.5 – MEDIUM-LEVEL CONTROLLER

The medium level controller is based on linear models, derived in the next subchapter.

6.5.1 – LINEAR MODEL OF EACH LOW-LEVEL CONTROLLED BOILER

In the closed-loop configuration presented in *Figure 6.3,* we can consider that the system can be functionally described with the steam demand as input and the heat Q as output. Therefore, we consider N_{B} boiler steam generator, each one described by the closed-loop system model φ_i:

$$Q = \varphi_i(q_{\mathrm{s,i}}) \quad \forall i = 1, \dots, N_{\mathrm{B}}$$

Considering each closed-loop system, φ_i, we propose to identify a linear Output Error model (OE), φ_i, using the controlled nonlinear model φ_i to generate the data-set for the identification. Regarding the single model, φ_i, we propose to approximate the closed-loop dynamics as an OE model in the form:

$$y(\kappa) = \frac{\left(\sum_{j=1}^{N_b}(b_j z^{-j})\right)}{1 + \sum_{j=1}^{N_f}(f_j z^{-j})}\, u(\kappa) + \gamma \quad (6.6)$$

where the auto-regressive polynomial is identified based on the detrended input-output data set and the term γ is the identified bias recovered a posteriori considering $u(k) > 0$.

We present the main steps done for the identification of the output error model of the boiler steam generator. We first generate four sets of signals for q_{s}, each representing a different experiment. The generated signals are different from each other to study different behaviour of the system and have e better identification model.

In *Figure 6.4,* we can see the four q_{s} generated profile used for the identification of the output error model for boiler 1. The other boilers' signals are not shown because they are similar to the one presented.

One by one the experiments are done simulating the real system controlled with the regulators presented in the previous section. After that, the experiments are merged and the OE model is identified.

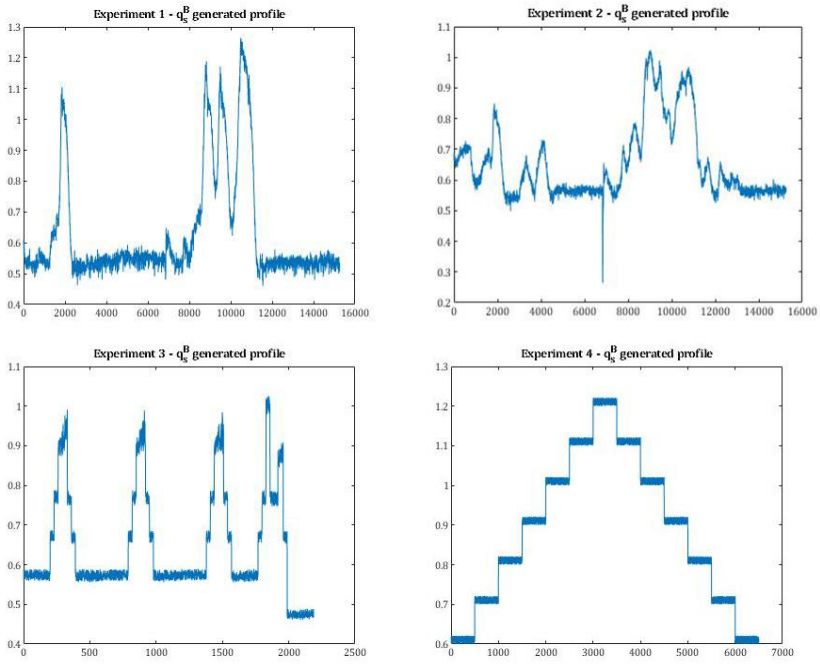

Figure 6.4 – q_s generated profile for each experiment

When the five boiler models are identified, we rewrite them from the OE form (6.6) into state-space form, where *i* runs from one to five:

$$\varphi_i(\kappa): \begin{cases} x_i(\kappa+1) = A_i x_i(\kappa) + B_i u_i(\kappa) \\ y_i(\kappa) = C_i x_i(\kappa) + \gamma_i \end{cases} \quad (6.7)$$

defining, for each subsystem *i,* the state vector as:

$$x(\kappa) = \left[y_\kappa, y_{\kappa-1}, \dots, y_{\kappa-n_f+1}, u_{\kappa-1}, \dots, u_{\kappa-n_b+1}\right] \in \mathbb{R}^n$$

where $n = n_f + n_b - 1$, and matrix A is defined as:

$$A = \left[\begin{array}{cc|cc} -f_1 & \dots \; -f_{n_f-2} \quad -f_{n_f} & b_2 & \dots \; b_{n_b-1} \; b_{n_b} \\ I_{n_f-1} & 0_{(n_f-1)\times 1} & 0_{(n_f-1)\times(n_b-1)} & \\ \hline & & 0_{1\times n_b-2} & 0 \\ 0_{(n_b-1)\times n_f} & & I_{n_b-2} & 0_{(n_b-2)\times 1} \end{array}\right]$$

matrix B is defined as:

$$B = \left[b_1 \; 0_{1x(n_f-1)} \; 1 \; 0_{1x(n_b-2)}\right]$$

and finally, matrix C is defined as

$$C = [1\; 0 \dots 0]$$

All the identified models (6.7) respect the assumption of:

- A_i is Schur stable;
- $m = p$;
- $\det(C_i(I_n - A_i)^{-1}B_i) \neq 0$

In particular, we have that $m = p = 1$.

6.5.2 - SYSTEM REFERENCE MODELS

For control design at medium level, we need to devise a model of the boiler ensemble. To do so, we first define the reference dynamics for each subsystem. In practice we need:

- To define a possibly reduced state of the *i*-th reference model as $\hat{x}_i = \beta_i(x_i)$ where $\beta_i \in \mathbb{R}^{\hat{n}xn_i}$;
- To describe the evolution of the state variable $\hat{x}_i$ using the alternative model [19]

$$\hat{\varphi}_i: \begin{cases} x_i(\kappa+1) = \hat{A}\hat{x}_i(\kappa) + \hat{B}_i u_i(\kappa) + \hat{w}_i(\kappa) \\ y_i(\kappa) = \hat{C}\hat{x}_i(\kappa) + \hat{\gamma}_i \end{cases} \quad (6.8)$$

  where $\hat{w}_i(k)$embeds the error due to the mismatch between model (6.8) and (6.7). if the rate of changes of $\bar{u}$ between consecutive steps is bounded, then it is possible to guarantee that $\hat{w}_i(\kappa)$ is bounded.

We point out that the state and output matrices $\hat{A}$ and $\hat{C}$, respectively, as well as the model order $\hat{n}$, are the same for all subsystems' reference models. On the other hand, matrices $\hat{B}_i$ must be properly selected. The most convenient choice consists of selecting $\hat{A}$, $\hat{B}_i$ and $\hat{C}$ with a similar canonical structure of the ones described in (6.6). In this case, is sufficient to define $\beta_i \in \mathbb{R}^{\hat{n}xn_i}$ as a suitable selection matrix, i.e. whose rows are basis vector of the canonical space and where $\hat{n} \leq n_i$. The reference model (6.7) must satisfy the so-called gain consistency conditions with respect to (6.6), that in this case are verified by sampling setting:

$$\hat{\gamma}_i = \gamma_i \quad (6.9)$$

$$\hat{b}_{(i,1)} = \frac{\sum_{j=1}^{n_b} b_{i,j}}{1+\sum_{j=1}^{n_f} f_{i,j}} \left(1 + \sum_{j=1}^{\widehat{n_f}} \hat{f}_j\right) - \sum_{j=2}^{\widehat{n_b}} \hat{b}_j \quad (6.10)$$

where $b_{i,j}, j = 1, \dots, n_b$ and $f_{i,j}, j = 1, .., n_f$ are the parameters that characterize the *i*-th model (6.8).

The state of the ensemble dynamical model $\hat{\varphi}$ is defined considering the state of the single active boilers, i.e. the ones where $\delta_i = 1$. This is done under the assumption that, when a boiler is switched off, its steam production is inactivated, and the steam produced during the switch off transient is diverted from the ensemble output. Accordingly, $\bar{x} = \sum_i^{N_\mathrm{B}} \delta_i \hat{x}_i$, the input is $\bar{u}$, and the output is $\bar{y} = \sum_i^{N_\mathrm{B}} \delta_i y_i$. Considering the reference model (6.7) we can write:

$$\bar{\varphi}: \begin{cases} \bar{x}(\kappa+1) = \hat{A}\bar{x}(\kappa) + \bar{B}\bar{u}(\kappa) + \bar{w}(\kappa) \\ \bar{y}(\kappa) = \hat{C}\bar{x}(\kappa) + \bar{\gamma} \end{cases} \quad (6.11)$$

where $\bar{B} = \sum_i^{N_B} \alpha_i \hat{B}_i$, $\bar{\gamma} = \sum_i^{N_\mathrm{B}} \delta_i \hat{\gamma}_i$, and $\bar{w} = \sum_i^{N_\mathrm{B}} \delta_i w_i$. We also define the static gain of the ensemble as $\bar{g} = \sum_i^{N_\mathrm{B}} g_i \alpha_i$.

At medium level, the reference tracking controller may operate with a slow sampling time $T = v\tau, v \in \mathbb{N}$. We denote with k the corresponding time index. This requires defining the ensemble variables at the new timescale as follows.

The input is $\bar{u}^{[T]}(k)$, defined such that $\bar{u}(\kappa) = \bar{u}^{[T]}(k)$ for all $\kappa = kv, \dots, (k+1)v$; also, we define $\bar{x}^{[T]}(k) = \bar{x}(kv)$ and $\bar{y}^{[T]}(k) = \bar{y}(kv)$. Accordingly, the system (6.10) is resampled, and its slow timescale dynamics is

$$\bar{\varphi}^{[T]}: \begin{cases} \bar{x}^{[T]}(k+1) = \hat{A}^{[T]}\bar{x}^{[T]}(k) + \bar{B}^{[T]}\bar{u}^{[T]}(k) + \bar{w}^{[T]}(k) \\ \bar{y}^{[T]}(k) = \hat{C}^{[T]}\bar{x}^{[T]}(k) + \bar{\gamma} \end{cases} \quad (6.12)$$

where $\hat{A}^{[T]} = \hat{A}^v$, $\bar{B}^{[T]} = \sum_{j=0}^{v-1} \hat{A}^j \hat{B}$, and $\bar{w}^{[T]}(k)$ is defined consistently.

6.5.3 – MEDIUM LAYER MPC CONTROLLER

The objective of the medium level MPC is to track the global produced heat target $r = \bar{Q}^{\mathrm{Dem}}$, based on the ensemble configuration, defined by the sharing factors optimized at high level.

For all the time steps *k*, the medium level is also committed to enforce the constraints (6.1), i.e.

$$\bar{u}^{[T]}(k) \in \bar{\mathcal{U}} \quad (6.12a)$$

$$\bar{y}^{[T]}(k) \in \bar{\mathcal{Y}} \quad (6.12b)$$

and for all $i = i, \dots, N^{\mathrm{B}}$

$$u_i(kv) = \alpha_i \bar{u}^{[T]}(k) \in \mathcal{U}_i \quad (6.12c)$$

$$y_i(kv) \in \mathcal{Y}_i \quad (6.12d)$$

finally, for consistency we need to ensure that:

$$\bar{u}^{[T]}(k) - \bar{u}^{[T]}(k-1) \in \Delta\bar{\mathcal{U}} \quad (6.12e)$$

To manage this, the medium level MPC is a robust offset-free tracking algorithm [3]. To design the offset-free state-feedback MPC, the ensemble model is augmented and rewritten in the velocity form. This robust MPC algorithm in velocity form, among other things, has the advantage to easily enforce the constraint (6.12e). Furthermore, thanks to the tube-based MPC approach, by tightening opportunely the

constraints, the MPC problem guarantees the feasibility of the actual controller while considering the unperturbed system in the computation of the control action. Finally, the corresponding optimization program to be solved at each time step T is enhanced with the additional optimization variable $\hat{r}$, which is defined as the closest feasible set point to r, to guarantee feasibility when set-point change.

In *Appendix 2*, we look more in details these last concepts, regarding the robust tube-based MPC, the velocity form, and the MPC reference tracking.

CHAPTER 7

BOILER ENSEMBLE HIERARCHICAL CONTROL SIMULATION RESULTS

In this chapter, we show the main simulation result regarding the boiler ensemble hierarchical control presented in *Chapter 6.*

We consider $N_B = 5$ boiler steam generators operating at nominal pressure of 57 bar. These boilers are serving a common load. Some of the boiler parameters are listed in *Table 7.1*, while in the next one we list the production limitations of each boiler and the corresponding cost λ_i of using such boiler.

Boiler	q_s Min [kg/s]	q_s Max [kg/s]	Q Min [kW]	Q Max [kW]	λ
1	0.1	1.264	565	3879	100
2	0.092	1.16	575	3810	130
3	0.089	1.125	584	3820	120
4	0.095	1.20	564	3800	70
5	0.099	1.25	553	3789	80

Table 7.1 – Boiler limitations production

The system is characterized by the global constraints (6.1c-d). In particular, we have that the sets are:

$$\bar{U} = [0.089, 6] \text{ [kg/s]}$$

$$\bar{Y} = [554,19062\ ] \text{ [kW]}$$

We assume that all the systems have the same low-level controllers, that are defined in *Chapter 6.3.1.* the closed-loop nonlinear model is used to generate the data-set for the identification of the discrete-time linear polynomial model (6.6), with sampling time $\tau = 10$ s, $n_f = 3$, $n_b = 2$, and $n_k = 1$. The same setting is used for each boiler, so that system φ_i has the same order n. The comparison of the dynamic response of the nonlinear model φ_i^{NL} and the identified linear one φ_i^L is presented for boiler 1 in the next figure.

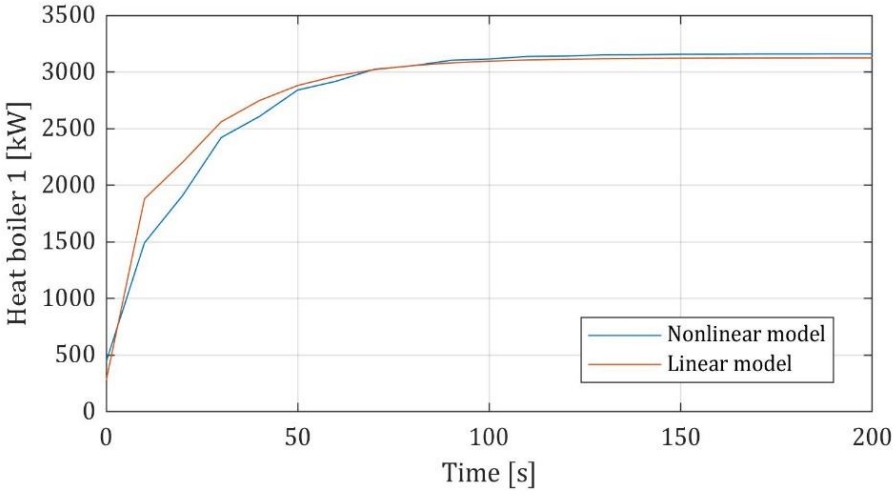

Figure 7.1 – Comparison of step-response of φ_1^{NL} and φ_1^L

The matrices of the first boiler steam generator are chosen for defining the reference model. In *Figure 7.2,* the comparison of the step response of each linear system φ_i^L with its reference model $\hat{\varphi}_i$ is shown: the gain consistency conditions (6.9) and (6.10) guarantee that at steady state the actual and reference model reach the same value.

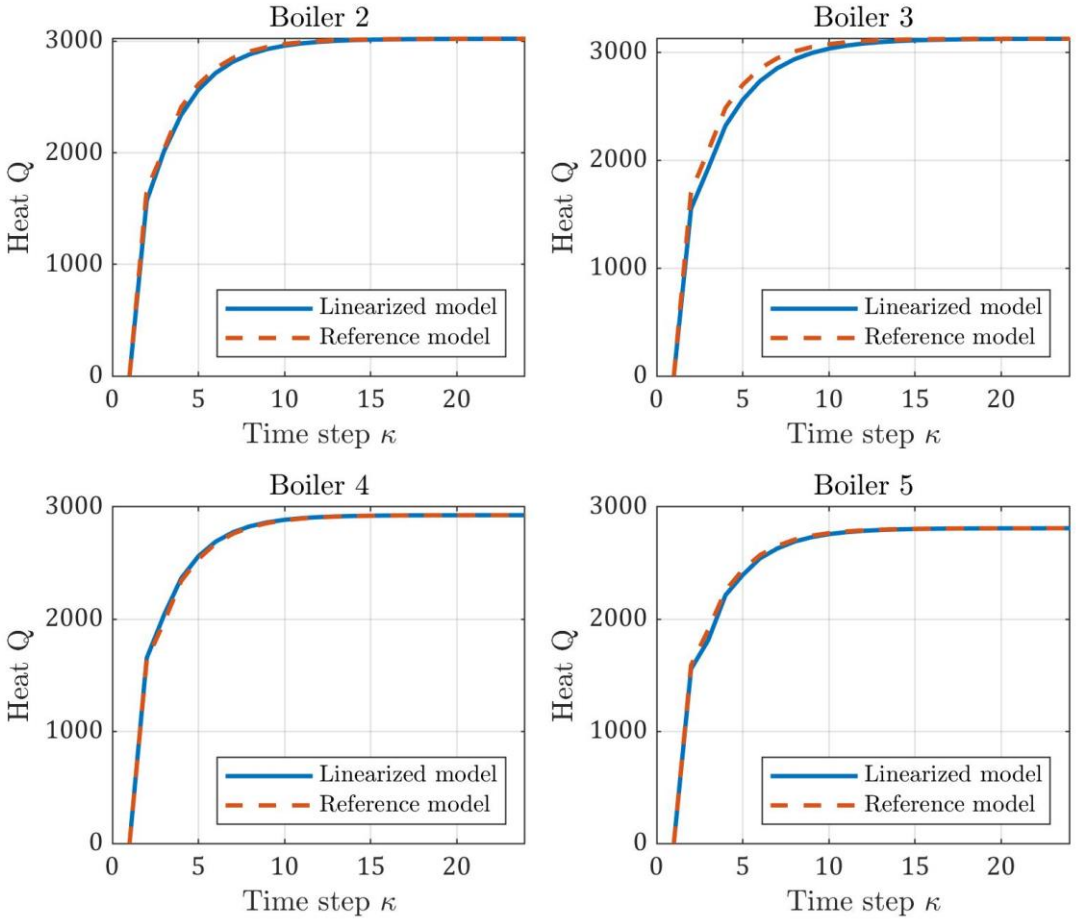

Figure 7.2 – Comparison of step-response of each linear system with its reference

Thanks to the reference models $\hat{\varphi}_i$, the model $\bar{\varphi}$ of the ensemble is derived using (6.12) and re-sampled at the medium-layer time scale, with $T = 30s$.

The robust MPC is designed considering that the disturbance $\bar{w}$ is such that (see *Figure 7.3)*:

$$\left||\bar{w}|\right|_\infty \leq 4 \text{ x } 10^{-2} \ [kg/s]$$

the set $\bar{\mathcal{W}}$ is evaluated by imposing the maximum variation of the input equal to

$$\Delta\bar{u} = 0.5 \ [kg/s]$$

A simulation shows the result of the proposed control architecture when a piece-wise constant demand is given. It is worth noting that, as reported in *Figure 6.2,* the reference trajectory is naturally given in terms of steam demand $\bar{q}_s^{\text{Dem}}$ and converted into an equivalent heat target using the static gain of the ensemble:

$$\bar{Q}^{\text{Dem}} = Gain \, \bar{q}_s^{\text{Dem}} \quad (7.1)$$

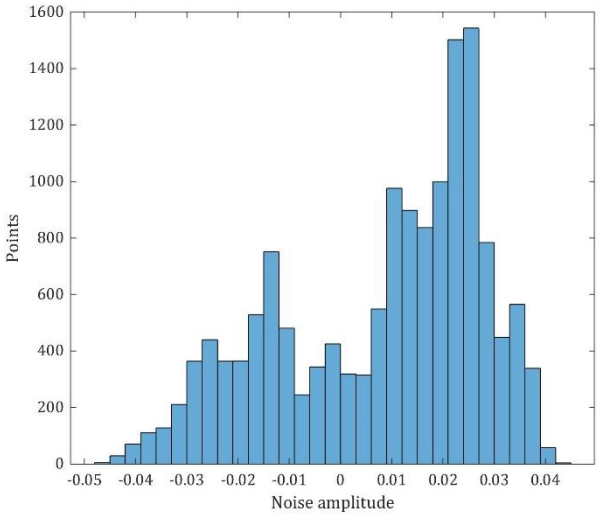

Figure 7.3 – Total disturbance distribution

In *Figure 7.4* it is shown in the top graph the boiler ensemble generated heat $\bar{Q} = \sum_{i=1}^{N^B} Q_i$, in solid red line, that track a time-varying load. The overall heat demand, $\bar{Q}^{\mathrm{Dem}}$ (black line with circles), is directly computed with the static relation (7.1). The actual demand is filtered by the high-level optimization, defined in (6.5), to obtain a feasible steady-state steam production $\bar{u}_{\mathrm{ss}}$, depicted in magenta dotted line. Eventually, at the medium MPC level the reference $\hat{r}$ is further considered as a decision variable (thin blue solid line). In the bottom graph, it can be seen the ensemble steam generation $\bar{q}_{\mathrm{s}} = \sum_{i=1}^{N^B} q_{s,i}$ depicted in ochre solid line) with the time-varying steam demand, $\bar{q}_{\mathrm{s}}^{\mathrm{Dem}}$ in black dotted line.

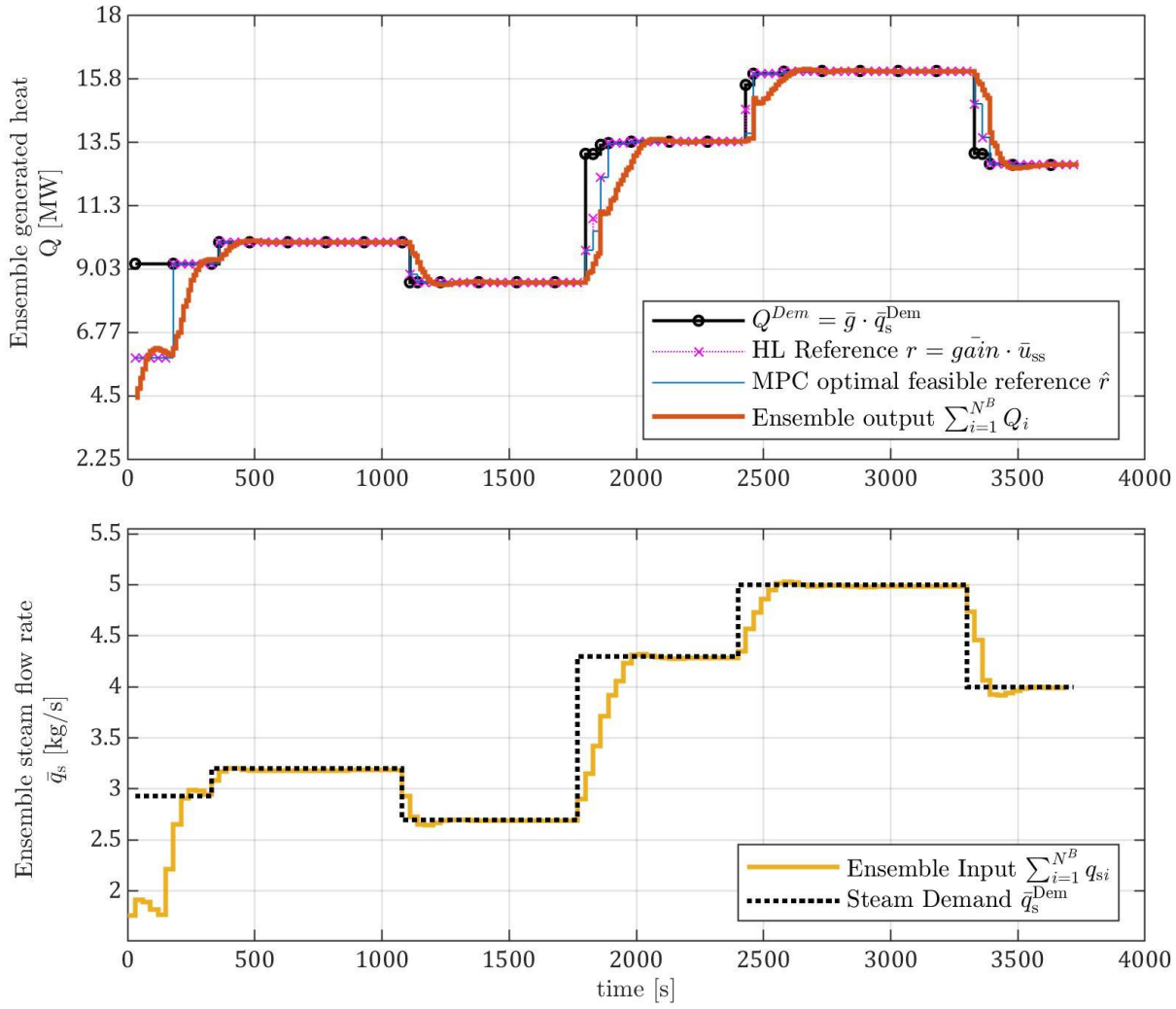

Figure 7.4 – Simulation 1: generated heat and generated steam

As shown in *Figure 7.4,* the reference trajectory for the ensemble is further modulated at high and medium levels: its variation is restrained at high level by considering the implication of the feasibility of the medium predictive controller, as discussed in *Chapter 6.4.* The high-level optimization is executed with a slow cycle time, a multiple of the medium level controller, i.e. $T_{HL} = 5T$. However, the optimization is also triggered when the disturbance from the final target is above a certain threshold, $\Delta\bar{q}_s^{\mathrm{Dem,threshold}} = 3 \times 10^{-2}$. The high level concurrently decides the shares, the activation/deactivation of the generators and the closest reachable steady-state steam value $\bar{u}_{ss}$ used to compute the reference for the lower MPC level, $r = gain\, \bar{u}_{ss}$, to safeguard its feasibility.

As shown in *Figure 7.5*, when the global steam demand rises, the boiler steam generators are added to the ensemble based on the subsystem efficiency rank, but also the associated operating cost λ_i. When the demand slightly changes as in the first half of the simulation, sharing factors are just adapted to improve the ensemble operating efficiency. Instead, a larger increase in the demand, as al $t = 1800\ s$, induces a variation of the ensemble configuration, shown by the activation of the boiler 2. To respond to a further increase of the demand, at $t = 2450\ s$, the boiler 3 is plugged into the ensemble, then when the demand drops again, boiler 2 is unplugged.

When the share factors change or the ensemble configuration is modified by the introduction or removal of a subsystem, the ensemble model is recomputed following (6.12) and the MPC state $\bar{x}^{[T]}$

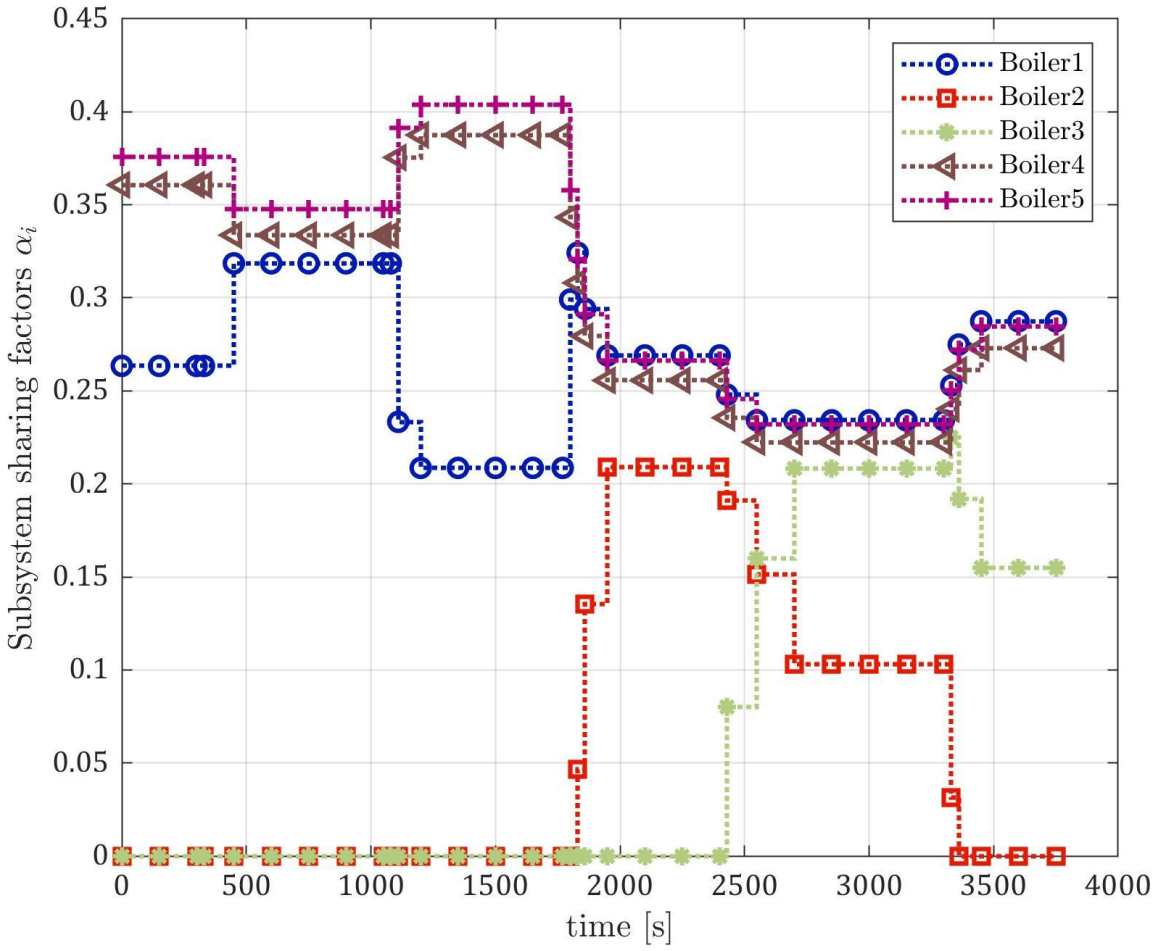

Figure 7.5 – Sharing factors α_i computed from the high-level optimization

and the previous optimal input $\bar{u}_{k-1}^{[T]}$ are reset in order to be consistent with the successive configuration of the ensemble. The optimal steam demand for the ensemble $\bar{q}_s$ is computed by the medium level MPC to track the reference trajectory. Based on the shares given by the high layer, the subsystem steam flow rate $q_{s,i} = \alpha_i \bar{q}_s$ is applied to the boiler nonlinear continuous-time system, described in *Chapter 3.1,* and controlled with sampling time τ.

The next two figures show that for each subsystem the input and output constraints are correctly enforced.

In *Figure 7.6* the steam flow rate $q_{s,i}$ of the single subsystem is shown. When the high-level optimization removes a boiler in the ensemble, the contribution is null, and the steam flow rate is shown below the minimum level with a bold grey line. When the boiler is actively contributing to the ensemble, it is shown that local constraints are always enforced.

In *Figure 7.7* the used heat of the single subsystem is shown. The constraints on the output of the local subsystem are directly imposed at the medium level control of the ensemble. When the boiler is unplugged from the ensemble the corresponding gas flow rate is shown below the minimum level with a bold grey line.

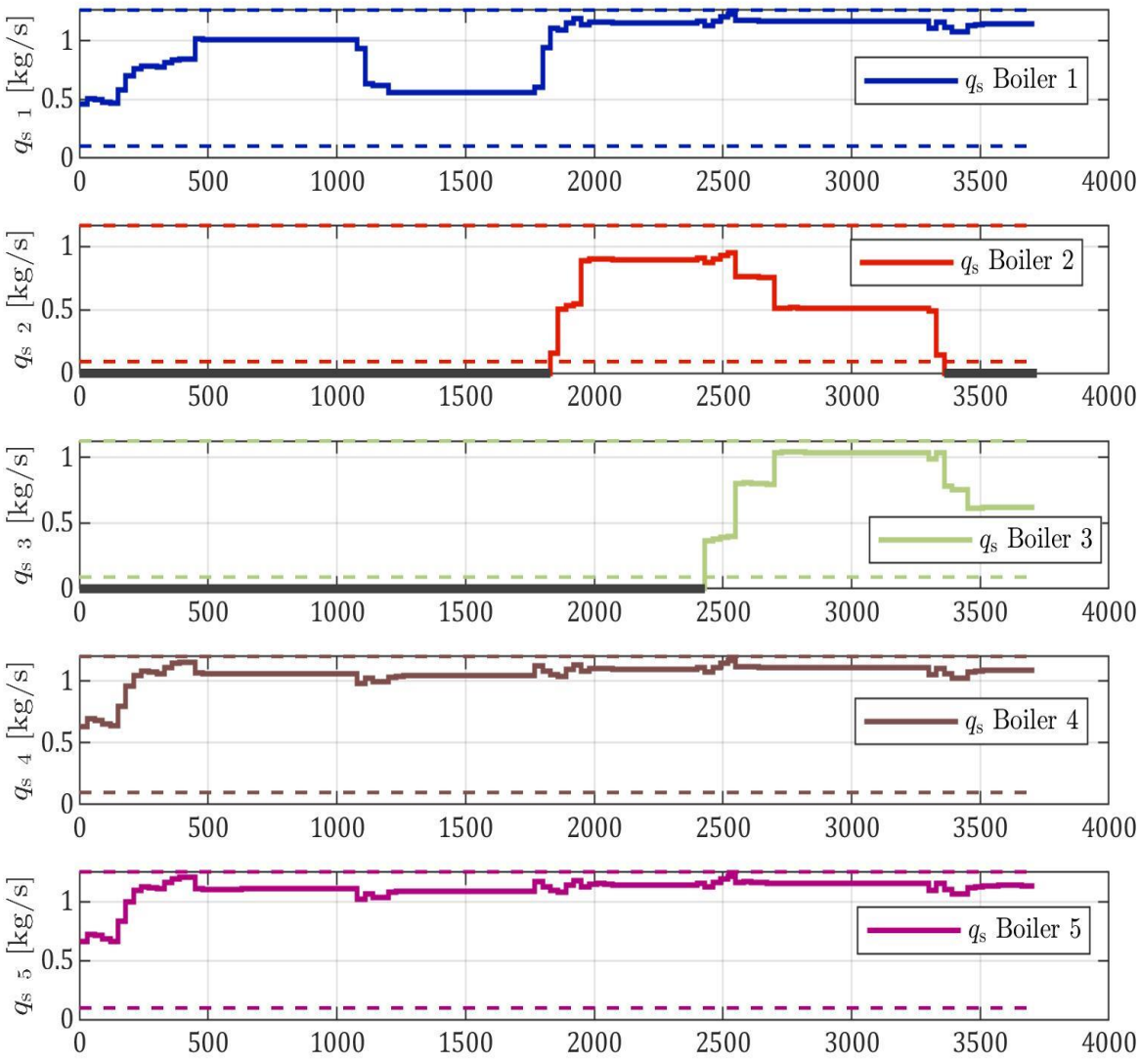

Figure 7.6 –Steam production of each boiler in the ensemble

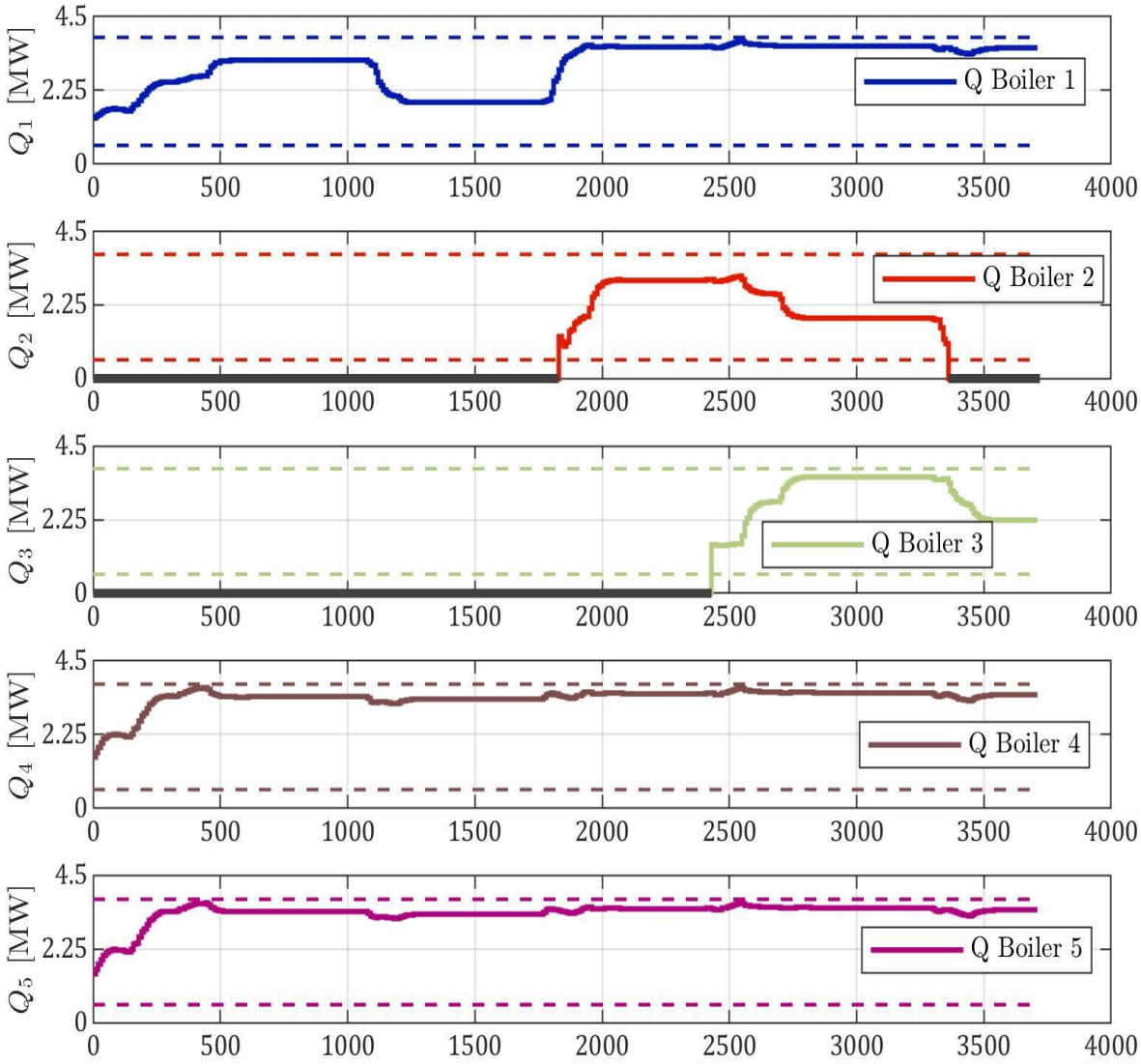

Figure 7.7 – Heat used by each boiler in the ensemble

CHAPTER 8

CONCLUSIONS AND FUTURE WORK

In this thesis we have discussed the importance of steam in the industry processes, we have presented its main properties and how it is produced (*Chapter 2).*

We have derived the boiler physical model and we have shown the identification procedures to detect the set of parameters that best describe the plant real data. (*Chapter 3).* The black box identification of the accumulator using the LSTM was necessary to implement this component in the control problem. The successive linearization technique was powerful and allows use the standard linear MPC algorithms even if we are dealing with a complex nonlinear system.

We have presented two original control schemes that face real application problems i.e. the control of multiple different subsystems (*Chapter 4)* and the control of an ensemble of similar subsystems (*Chapter 6)*. In particular, the hierarchical control algorithm explained in *Chapter 6* can be adapted to any kind of applications that require the coordination of subsystems towards the main goal.

This work can be extended in many possible directions:

First of all, it is case of interest to derive an appropriate model of the accumulator based on the physical equations consistent with the available plant data. This would require further insights on the specific structure and functioning of the accumulator under analysis.

Secondly, as a future step, the hierarchical control architecture will be extended to include accumulators, to improve the system efficiency, especially in transient conditions.

Finally, it could be of great interest to extend the control scheme derived in *Chapter 4* to the control of the boiler in another range of operating conditions, e.g. during start-up and shut down operations.

APPENDIX 1

IAPWS-IF97 GENERAL DESCRIPTION

In 1997, The International Association for the Properties of Water and Steam (IAPWS) [5] adopted a new formulation for the thermodynamics property of water and steam for industrial use. This formulation was designed for much greater computational speed and was an approximation of the previous one.

In this work, we use the MATLAB function related to this formulation [17]. This allows us to calculate all the thermodynamic properties of water and steam given some known parameters. It also allows us to calculate approximately the derivative of certain thermodynamics variables with respect to others and evaluate them at a specific point with very low computational load and low numerical error.

The range of validity of this formulation is:

$$273.15°K \leq T \leq 1073.15K \qquad p \leq 100\ MPa$$
$$1073.15\ K < T \leq 2273.15K \qquad p \leq 50\ MPa$$

and the result error range varies from property to property, but in general, it is in the range of $\pm 0.001\%$ to $\pm 0.3\%$.

The following figure shows five regions into which the entire range of validity of IAPWS-IF97 is divided. It also represents the boundaries of each region.

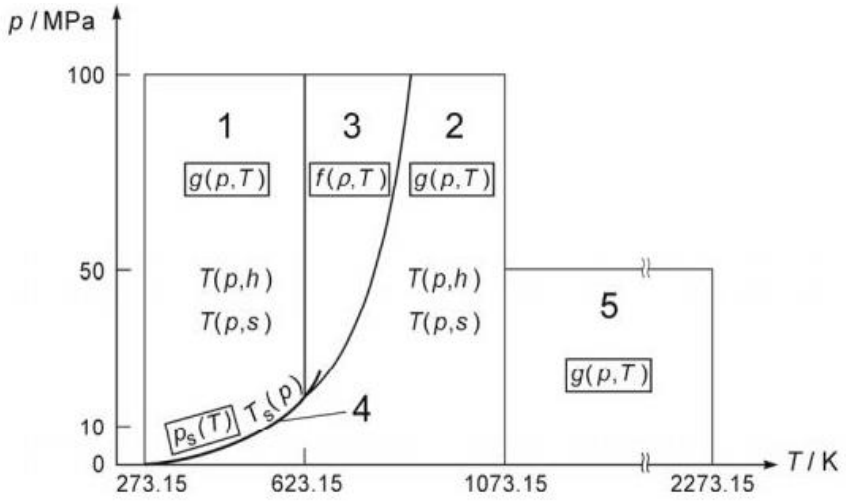

Figure A1.1 – IAPWS range of validity regions

All regions are covered by their respective fundamental equations, that allow calculating the property of water and steam inside the regions.

APPENDIX 2

ADVANCED MPC SCHEMES

In this Appendix, we will consider the three advanced control schemes that combine together allow to define the control problem stated in *Chapter 6.5.3.*

ROBUST TUBE-BASED MPC

If the system to be controlled is affected by an external unknown (but bounded) disturbance, controlling the system neglecting the disturbance, could easily lead to the loss of the stability property and/or to constraint violation. For this reason, the so-called tube-based method has received much attention for its simplicity and in view of the fact that it requires an on-line computational load comparable to that of nominal MPC.

Consider a linear, discrete-time system under control described by:

$$x(k+1) = Ax(k) + Bu(k) + w(k) \quad (A2.1)$$

where $x(k) \in \mathcal{X} \subset \mathbb{R}^n, u(k) \in \mathcal{U} \subset \mathbb{R}^m$ and $w(k) \in \mathcal{W} \subset \mathbb{R}^n$ is an unknown but bounded disturbance. The nominal system corresponding to (A2.1) is.

$$\hat{x}(k+1) = A\hat{x}(k) + B\hat{u}(k) \quad (A2.2)$$

Consider a control gain K selected in such a way that $F = A + BK$ is Schur and the robust positive invariant set $\mathcal{Z}$ verifying $F\mathcal{Z} \oplus \mathbb{W} \subseteq \mathcal{Z}$. It can be proved that if $x(k) - \hat{x}(k) \in \mathcal{Z}$ and if the real system is controlled with

$$u(k) = \hat{u}(k) + K\big(x(k) - \hat{x}(k)\big) \quad (A2.3)$$

then $x(k+1) - \hat{x}(k+1) \in \mathcal{Z}$ for all $w(k) \in \mathcal{W}$. Therefore, the input $u(k)$ to the system $(A2.1)$ is computed as the sum of two terms: by the nominal input $\hat{u}(k)$ obtained as the solution of a standard MPC optimization problem solved considering the nominal model $(A2.2)$ and by the corrective term $K\big(x(k) - \hat{x}(k)\big)$, which has the role of keeping the real system state as close as possible to that of the nominal system. The tube-based MPC considers the nominal system $(A2.2)$ with tighter constraints and its main innovation relies in adding its current state to the set of optimization variables. So, the cost function to be minimized is:

$$J = \sum_{v=0}^{N-1} \left(||\hat{x}(k+v)||_Q^2 + ||\hat{u}(k+v)||_R^2 \right) + ||\hat{x}(k+N)||_S^2$$

where $Q \in \mathbb{R}^{nxn}, R \in \mathbb{R}^{mxm}$ and $S \in \mathbb{R}^{nxn}$ are positive definite matrices. As in the standard MPC case, the simplest choice for parameters *K* and *S* can be done as described in [3].

The optimization problem to be solved at each time step is:

$$min\ J$$

such that

$$x(k) - \hat{x}(k) \in \mathcal{Z}$$

$$\hat{x}(k+v) \in \hat{\mathcal{X}}\ \forall v = 0, .., N-1$$

$$\hat{u}(k+v) \in \hat{\mathcal{U}}\ \forall v = 0, .., N-1$$

$$\hat{x}(k+N) \in \hat{\Omega}$$

$$\hat{x}(k+1) = A\hat{x}(k) + B\hat{u}(k)$$

where $\hat{\mathcal{X}} \subseteq \mathcal{X} \ominus \mathcal{Z}, \hat{\mathcal{U}} \subseteq \mathcal{U} \ominus K\mathcal{Z}$, where $\ominus$ is the Pontryagin difference. $\hat{\Omega}$ is a suitable positive invariant set for the nominal system $(A2.2)$ such that $\hat{\Omega} \subseteq \hat{\mathcal{X}}$, and $K\hat{\Omega} \subseteq \hat{\mathcal{U}}$.

THE VELOCITY FORM

Consider a discrete-time, linear, time-invariant system described by

$$x(k+1) = Ax(k) + Bu(k)$$

$$y(k) = Cx(k) \qquad (A2.4)$$

where $x(k) \in \mathbb{R}^n, u(k) \in \mathbb{R}^m, y(k) \in \mathbb{R}^m$.

In order to solve the tracking problem, the system is enlarged with m integrators and described in velocity-form. Specifically, denoting by $\hat{r}$ a generic tracking target, the corresponding steady-state condition is denoted $(\hat{x}, \hat{u})$. Letting $\delta x(k) = x(k) - x(k-1)$, $\epsilon(k) = y(k) - \hat{r}$, and $\delta u(k) = u(k) - u(k-1)$, the dynamical system $(A2.4)$ can be reformulated as

$$\delta x(k+1) = A\delta x(k) + B\delta u(k)$$

$$\epsilon(k+1) = CA\delta x(k) + \epsilon(k) + Cb\ \delta u(k) \quad (A2.5)$$

Define $\xi(k) = \big(\delta x(k), \epsilon(k)\big)$ and

$$\mathcal{A} = \begin{bmatrix} A & 0 \\ CA & I_m \end{bmatrix} \quad \mathcal{B} = \begin{bmatrix} B \\ CB \end{bmatrix}$$

In this way, the system $(A2.5)$ can be written in compact form as

$$\xi(k+1) = \mathcal{A}\xi(k) + \mathcal{B}\delta u(k) \quad (A2.6)$$

MPC FOR TRACKING PIECEWISE CONSTANT REFERENCES

For practical application purposes, model predictive controllers must be able not only to regulate the system state to zero but also to handle non-zero target steady states which can be provided by the steady-state high-level optimizer. The standard solution to this problem consists of changing the system state coordinates i.e. shifting the state to the desired steady state. Unfortunately, the new target steady state could be unreachable and, moreover, feasibility may not be guaranteed.

An effective MPC algorithm for tracking, that avoid these problems is proposed and its ingredients are:

- the online computation of the actual target to be really tracked at each time instant;
- the penalization of the deviation between the artificial steady state and the desired one at the optimization problem level.

The controller steers the system to any admissible target steady-state while satisfying the system constraints. If the desired target is not admissible, the system is steered to the closet admissible steady state.

If we have to track a generic non admissible target y^d corresponding to $\big(\bar{x}^d, \bar{u}^d\big) = M\bar{y}^d$, possibly non admissible for the system because outside the set $\mathcal{Y}$, the penalization of the distance between admissible

state $\bar{x}^a$ and $\bar{x}^d$ makes the system evolve to an admissible steady state such that its deviation with the desired steady-state $\bar{x}^d$ is minimized.

So, after these considerations, the cost function to be minimized is:

$$J = \sum_{v=0}^{N-1} \left(||x(k+v) - \bar{x}^a||_Q^2 + ||u(k+v) - \bar{u}^a||_R^2 \right) + ||x(k+N) - \bar{x}^a||_S^2 + ||\bar{x}^a - \bar{x}^d||_T^2$$

where $Q \in \mathbb{R}^{nxn}$, $R \in \mathbb{R}^{mxm}$, $S \in \mathbb{R}^{nxn}$ and $T \in \mathbb{R}^{nxn}$ are all assumed to be positive definite. The input sequence over all the prediction horizon N and $\bar{y}^a$ (the target really tracked at time k) are the decision variables, while the current state $x(k)$ and the desired target $\bar{y}^d$ are parameters of the cost function.

BIBLIOGRAPHY

[1] S. Spinelli, E. Longoni, M. Farina, F. Petzke, S. Streif, A. Ballarino, "A Hierarchical Architecture for the Coordination of an Ensemble of Steam Generators", *Submitted to 21st IFAC World Congress, 2020*

[2] S. Spinelli, M. Farina, A. Ballarino, "A hierarchical optimization-based scheme for combined Fire-tube Boiler/CHP generation units", *2018 European Control Conference (ECC),* pp 2362-2367

[3] G. Betti, R. Scattolini, M. Farina, M. Prandini, "Methods and applications of distributed and decentralized model predictive control", *PhD thesis, Politecnico di Milano, 2013*

[4] K.J. Åström, R.D. Bell, "Drum-boiler dynamics", *Automatica, Vol. 36, Issue 3, 2000, pp. 363-378*

[5] W.Wagner, H.J. Kretzschmar, *"International Steam Tables",* Springer, Second edition, 2008

[6] V.D. Stevanovic, B. Maslavaric, S. Prica, "Dynamics of steam accumulation", *Applied Thermal Engineering, Vol. 37, 2012, pp 73-79*

[7] B. Sun, J.Guo, Y. Lei. L. Yang, Y. Li, G. hang, "Simulation and verification of a non-equilibrium thermodynamic model for a steam catapult's steam accumulator", *International Journal of Heat and Mass Transfer, Vol. 85, 2015, pp 88 – 97*

[8] V.D. Stevanovic, M.M. Petrovic, S.M. Maslovaric, B. Maslovaric, "Prediction and Control of Steam Accumulator, *Heat transfer Engineering, Vol. 36, 2015, pp 498-510*

[9] R. Scattolini, L. Magni, *"Advanced and Multivariable Control"*, Pitagora Editrice Bologna, 2014

[10] *"Manufacturing Energy and Carbon Footprint (for Chemical Manufacturing, Forest Products, Petroleum Refining)",* 2010, manufacturing.energy.gov

[11] U.S. Department of Energy, "*Improving Steam System Performance: A Sourcebook for Industry",* Second edition, 2004

[12] "*Symbioptima Project",* https://cordis.europa.eu/project/rcn/198359/factsheet/it

[13] R. Scattolini, E. Terzi, T. Bonetti, D. Saccani, "Modeling and learning-based hybrid predictive control with neural networks of the cooling station of a large business center", *Master Thesis, Politecnico di Milano, 2018*

[14] R. Scattolini, M.Farina, S. Garatti, E. Terzi, "Learning-based Model Predictive Control: Theory and Applications", *PhD thesis, Politecnico di Milano,* 2020, Submitted

[15] *"Principal Applications for Steam"*, https://www.tlv.com/global/TI/steam-theory/principal-applications-for-steam.html

[16] "*Shell Boilers",* https://www.spiraxsarco.com/learn-about-steam/the-boiler-house/shell-boilers

[17] M. Mikofski, IAPWS-IF97, https://www.github.com/mikofski/IAPWS_IF97/, GitHub, 2013. Retrieved May 18, 2019.

[18] A. Chaibakhsh, A. Ghaffari, S. A. Moosavian, "A simulated model for a once-through boiler parameter by adjustment based on genetic algorithms", *Simulation Modelling Practice and Theory, Vol. 15, 2007, pp 1029-1051*

[19] F. Petzke, M. Farina, S. Streif, "A multirate hierarchical mpc scheme for ensemble systems", *Proceedings of the 57th IEEE Conference on Decision and Control (CDC)",* 2018

[20] "*What is MIURA Boiler (Once-Through)?",* "Kang Yong Group", https://www.kyg.co.th/

[21] Danstoker Group, http://danstoker.com/

[22] Babcock Wanson UK Group, https://www.babcock-wanson.com/

[23] "*Steam Accumulators",* https://www.spiraxsarco.com/learn-about-steam/the-boiler-house/steam-accumulators

[24] "*Gas Engine",* https://www.mwm.net/mwm-chp-gas-engines-gensets-cogeneration/gas-engines-power -generators/gas-engine-tcg-2020/